Efficacy of Calcined Layered Double Hydroxide Clays in the Remediation of Phenol from Wastewater

By

Lehlogonolo Shane Tabana

Dissertation submitted in partial fulfilment of the requirements for the degree of

Master of Engineering (Water Utilisation)

In the Faculty of Engineering, Built Environment and Information Technology

University of Pretoria

Pretoria

2021

DECLARATION

I, **Lehlogonolo Shane Tabana, student No. 25154436,** do hereby declare that this research is my original work and that to the best of my knowledge and belief, it has not been previously in its entirety or in part been submitted and is not currently being submitted either in whole or in part at any university for a degree or diploma, and that all references are acknowledged.

SIGNED on this ____10th____ day of ____MAY____ 2021.

Lehlogonolo S. Tabana

Efficacy of Calcined Layered Double Hydroxide Clays in the Remediation of Phenol from Wastewater

Student: Lehlogonolo Shane Tabana

Supervisor: Dr. Shepherd M. Tichapondwa

Co-Supervisor: Prof. Johan Labuschagne

Department: Chemical Engineering

University: University of Pretoria

Degree: Master of Engineering (Water Utilisation)

ABSTRACT

The discharge of poorly treated wastewater containing persistent organic contaminants, such as phenol, into water bodies is a major contributor to water pollution. This is of great concern as it poses health threats to human beings, aquatic species and the ecosystem as a whole. Amongst the water treatment technologies available, adsorption is highly recommended because of its ease of operation, simple design and economic viability. Commercial activated carbon (CAC) has previously been utilised as an adsorbent for remediation of recalcitrant pollutants from wastewater. However, high costs and the complexity of regenerating spent carbon has resulted in the need for economically viable adsorbents.

The current research focused on the use of layered double hydroxide (LDH) clays for removal of phenol from contaminated water. The work is divided into two sections whereby the initial phase focuses on the use of commercial LDH clays, while the second phase is based on the in-house synthesised LDH clays guided by the performance of the commercial clays. Six commercial clays were sourced from different suppliers for the first phase, namely: DHT‑4A and Alcamizer 1 from Kisuma Chemicals (Netherlands), Sorbacid 944, Sorbacid 911 and Hycite 713 from Clariant (Germany) and GF‑450 from Greenfield additives (South Africa). Sorbacid 944 was the only clay which had three metallic constituents, magnesium

(Mg), zinc (Zn) and aluminium (Al) and was quantified to be 100% hydrotalcite; other clays had a substantial amount of impurities, such as calcite, boehmite and silica. Screening tests on the commercial clays were done by contacting 10 g L^{-1} of each clay with 40 mg L^{-1} synthetic phenol solution over 108 h. All the clays produced an adsorption efficiency of less than 10%. However, three clays which showed better adsorption efficiencies, namely: GF‑450 (9%), Sorbacid (6%) and DHT‑4A (3%) were utilised for further assessment. The three clays were thermally treated at 500°C for 4 h to produce mixed metal oxides (MMO), which are known to be good adsorbents. Calcination of the clays resulted in an increase in phenol adsorption efficiency over 24 h on Sorbacid 944 (87%) and DHT‑4A (52%) while GF‑450 remained below 10%.

Having produced a higher adsorption efficiency, Sorbacid 944 was further assessed for optimisation of phenol removal process. The initial pH of the solution was established to have an inverse proportionality relationship with phenol adsorption. Elevated pH resulted in an increase in the concentration of hydroxyl ions (OH^-) which increased the reformation rate of calcined LDH (CLDH) and reduced the adsorption efficiency, while acidic pH was not evaluated as it is known to cause dissolution of LDH. Neutral pH was established to be the optimum pH for phenol adsorption. An increase in operational temperature resulted in a faster phenol adsorption rate from $2 \times 10^{-4} \text{ g mg}^{-1}\text{min}^{-1}$ at 25 °C to $3.8 \times 10^{-3} \text{ g mg}^{-1}\text{min}^{-1}$ at 65 °C. The optimum clay loading was 10 g L^{-1} and the clay proved to be effective over three cycles. The Freundlich equilibrium isotherm best fitted the phenol adsorption equilibrium data, with a maximum adsorption capacity of 16.6 mg g^{-1}. The change in enthalpy of the adsorption process was determined to be *ca.*20 kJ mol^{-1} indicating an endothermic process dominated by physical adsorption. The changes in Gibbs free energy over the evaluated temperatures ranged between -12 kJ mol^{-1} and -16 kJ mol^{-1}. This showed that the adsorption process was spontaneous irrespective of the operating temperature.

The second phase of the study involved the synthesis of eight LDH clays containing varying compositions of Mg, Zn and Al with a carbonate interlayer anion. The clay which contained molar ratios of Mg (60%), Zn (20%) and Al (20%) ($Mg_{0.6}Zn_{0.2}Al_{0.2}$) was found to possess higher adsorption efficiencies upon calcination at 450 °C for 4 h. Clays which had a Zn/Mg molar ratio greater than 1, $Mg_{0.4}Zn_{0.4}Al_{0.2}$, $Mg_{0.25}Zn_{0.5}Al_{0.25}$ and $Zn_{0.75}Al_{0.25}$ showed lower phenol adsorption efficiencies of 63%, 65% and 50% respectively. Clays with a Zn/Mg ratio less than 1, $Mg_{0.6}Zn_{0.2}Al_{0.2}$ and $Mg_{0.5}Zn_{0.25}Al_{0.25}$ showed optimal ratio of acidic and basic

sites hence higher phenol adsorption efficiencies of 89% and 80% respectively. A higher aluminium content in the clay increased the spinel content ($MgAl_2O_4$) upon calcination resulting in a decrease in phenol adsorption. Phenol adsorption equilibrium data and kinetics for clay $Mg_{0.6}Zn_{0.2}Al_{0.2}$ were comparable with those of Sorbacid 944.

Column reactor configurations should be investigated for industrial applications. Furthermore, real wastewater matrices containing multi-contaminants should be used instead of synthetic wastewater with a few pollutants. This will provide insight in the applicability of LDH for impurity removal from wastewater on an industrial scale.

Keywords: hydrotalcite; water treatment; phenol; adsorption capacity; adsorption model.

ACKNOWLEDGEMENTS

DEDICATION

This work is dedicated to:
Ntakaneng, Ngaletjane, Makala and their respective families.

TABLE OF CONTENTS

LIST OF FIGURES

LIST OF TABLES

ABBREVIATIONS

AOP	Advanced Oxidation Process
ATR	Attenuation Total Reflectance
BET	Brunauer-Emmet-Teller
BPA	Bisphenol A
CAC	Commercial Activated Carbon
CLDH	Calcined Layered Double Hydroxide
DTG	Derivative Thermogravimetric
FTIR	Fourier Transform Infrared
GC	Gas Chromatography
HPLC	High-Performance Liquid Chromatography
ICSD	Inorganic Crystal Structure Database
LDH	Layered Double Hydroxide
LDO	Layered Double Oxide
LLE	Liquid Liquid Extraction
MMO	Mixed Metal Oxide
NF	Nanofiltration
PDA	Photo Diode Array
RO	Reverse Osmosis
SEM	Scanning Electron Microscopy
SDG	Sustainable Development Goals
TGA	Thermogravimetric Analysis
TOC	Total Organic Carbon
UN	United Nations
UNDESA	United Nations Department of Economic and Social Affairs
USEPA	United States Environmental Protection Agency
UV	Ultraviolet
WHO	World Health Organization
XRD	X‑Ray Diffraction
XRF	X‑Ray Fluorescence

LIST OF SYMBOLS

α	Initial sorption rate constant for Elovich kinetics model (mg g^{-1}min^{-1})
β	Line broadening at half maximum (FWHM) of the diffraction peak (°)
β_E	Extent of surface coverage and activation energy for chemisorption (g mg^{-1})
λ	Wavelength (Å)
θ	Angle of incidence (°)
γ	Activity coefficient
A_T	Equilibrium binding constant corresponding to the maximum binding energy (L g^{-1})
a	Density of metal-ion stacking (Å)
b_T	Temkin constant related to heat of sorption (dimensionless)
c	Layer thickness (Å)
C_{ads}°	Standard adsorbate concentration (1 mol L^{-1})
C_e	Equilibrium concentration of adsorbate (mg L^{-1})
d_{003}	Layer distance at plane (003) (Å)
ΔG°	Change in Gibbs free energy (kJ mol^{-1})
ΔH°	Change in enthalpy (kJ mol^{-1})
K_1	Lagergren rate constant (min^{-1})
K_2	Pseudo second order rate constant (g mg^{-1}min^{-1})
K_a	Thermodynamic equilibrium constant (dimensionless)
K_F	Freundlich equilibrium constant (L g^{-1})
K_I	Equilibrium constant depending on the best isotherm model fitted (L mg^{-1})
K_L	Langmuir equilibrium constant (L mg^{-1})
L_{003}	Crystallite size in the direction parallel to plane (003) (Å)
MM_{ads}	Molar mass of adsorbate (g mol^{-1})
n	Adsorption intensity
N	Order of the spectrum (dimensionless)
q_e	Equilibrium adsorption capacity (mg g^{-1})
q_m	Maximum adsorption capacity (mg g^{-1})
R	Universal gas constant (8.314 J mol^{-1}K^{-1})
ΔS°	Change in entropy (kJ mol^{-1}K^{-1})
t	Time (min)
T	Temperature (°C or K)

PUBLICATIONS

Peer Reviewed Articles

Tabana, L., Tichapondwa, S., Labuschagne, F. and Chirwa, E., 2020. Adsorption of Phenol from Wastewater Using Calcined Magnesium-Zinc-Aluminium Layered Double Hydroxide Clay. *Sustainability*, *12*(10), p.4273.(https://doi.org/10.3390/su12104273).

Tabana L.S., Labuschagne F.J.W.J., Tichapondwa S.M., 2020, The Effect of Metallic Composition of Layered Double Hydroxide Clay on the Removal of Phenol from Aqueous Solution, Chemical Engineering Transactions, 81, 193-198 (https://doi.org/10.3303/CET2081033).

Tabana L.S., Ledikwa R.P., Tichapondwa S.M., 2019, Adsorption of Phenol from Wastewater Using Modified Layered Double Hydroxide Clay, Chemical Engineering Transactions, 76, 1267-1272 (https://doi.org/10.3303/CET1976212).

Conference Presentations

The Effect of Metallic Composition of Layered Double Hydroxide Clay on the Removal of Phenol from Aqueous Solution, 23rd Conference on Process Integration, Modelling, and Optimisation for Energy Saving and Pollution Reduction (PRES'20) 17th - 21st August 2020, Xi'an, China (oral virtual presentation).

Adsorption of phenol from wastewater using modified layered double hydroxide clay. 22nd conference on Process Integration, Modelling and Optimisation for Energy Saving and Pollution Reduction, 20th - 23rd October 2019, Agios Nikolaos, Greece. (oral presentation).

1 INTRODUCTION

1.1 Background

The build-up of enormous amounts of hazardous wastes in the environment has caused numerous global problems, including water pollution. In order to sustain life on the planet, fresh water is required; however, the quality and quantity of freshwater across the globe continues to drop as more wastewater is generated. Concerns on potable water arise daily due to increasing needs for food production, utilisations in agriculture, industry and power plants, and poor water management (Pandey *et al.*, 2009).

Anthropogenic activities arising from household, industrial, transportation, mining and agricultural processes are the main sources of various waste materials and pollutants, which are dumped in the environment (Salih, 2018). These waste materials are continuously generated while there has not been development of proper sustainable and effective treatment technologies. The Division for Sustainable Development at the United Nations Department of Economic and Social Affairs (UNDESA) has stated that the handling of quality potable water and retaining contaminant-free water should be prioritised to prevent diseases and ensure that the environment is conserved (Adeel *et al.*, 2014). Globally, there are agreements about the shortfalls regarding the treatment of contaminated water for an imperishable future. Mulligan *et al.* (2001) reported that polluted water may cause temporary and permanent adverse effects to the environment. There has been the development of international policies and regulations, such as the International Kyoto protocol in order to prevent problems caused by wastewater (Böhringer, 2003). The United Nations (UN) Sustainable Development Goal 6 addresses the inclusion of principles of sustainable development into countries' strategies and policies to ensure protection of natural resources and providing every human being with access to safe drinking water and improved hygiene conditions (Salih, 2018). Crini (2006) stated that attempts should be made to minimise pollutants through reclamation procedures as part of sustainable development and waste management programmes. This can lead to a reduction in the utilisation of raw materials, operational costs, quantities of waste production and their environmental impact.

1.2   Problem statement

The degradation of recalcitrant organic pollutants in water is a universal problem (Rodgher, 2012). Kalló (2001) reported that wastewater collected from municipalities, communities and industries requires extensive treatment prior to returning to aquatic systems. Studies by Kukadiya (2016) showed that phenol is one of the organic pollutants found in effluents arising from industries, such as oil refineries, paper mills, wood processing, coal gasification, textile, resins production and agro-industrial waste. Drinking of phenol-contaminated water has been reported to cause protein degeneration, tissue erosion, paralysis of the central nervous system and damage to the kidneys, liver and pancreas in the human body (Geyikci & Coruh, 2013). The World Health Organization (WHO) recommends that the allowable concentration of phenols in potable water should be 1 mg L^{-1} (WHO, 1996). The regulations by the United States Environmental Protection Agency (USEPA) call for the reduction of phenols in wastewaters to be less than 1 mg L^{-1} (Anku *et al*., 2017).

Water contaminated with phenols should be remediated prior to disposal into the aquatic systems (Salih, 2018). Process technologies which can be used to treat polluted water, include physical, biological and chemical processes. A treatment technology can be implemented on its own or with other technologies. The choice of a treatment process depends on the type of pollutant, initial and targeted residual concentration and volume of the effluent stream. Bioremediation processes are known to be economically viable compared to the other two technologies. They include microbial degradation and enzymatic treatment methods. According to Ahmaruzzaman (2008) and Crini (2006), biological treatment processes are less favoured as they require large operational sites (land), are sensitive toward diurnal variation and toxicity of chemicals, and are less flexible in design and operation. The current conventional biodegradation processes, which are widely applied across the world are incapable of removing phenol to allowable concentrations, due to toxicity effects of pollutants to microbes (Kim *et al*., 2009; Kumar, 2010; Salih, 2018). Chemical oxidation, electrochemical removal and advanced oxidation processes (AOPs) are some of the chemical processes used in the remediation of phenols (Audino, 2019; Villegas *et al*., 2016; Zhang *et al*., 2013). These techniques are capable of mineralising phenol to less toxic compounds, such as water (H_2O) and carbon dioxide (CO_2). However, they tend to be expensive, create sludge build-up and require excessive use of chemicals, which can lead to secondary pollution (Ahmaruzzaman, 2008).

2

Physical processes that are widely used for wastewater treatment, include membrane filtration, ion exchange and adsorption (Alexandratos, 2009; Lakherwal, 2014; Villegas *et al*., 2016). The adsorption process is favoured for water decontamination over other processes due to its economic viability, insensitivity, ease of operation, flexibility and simplicity of design (Dichiara *et al*., 2015; Lakherwal, 2014). Commercial activated carbon (CAC) has been the most popular adsorbent for removal of pollutants from contaminated water (Babel & Kurniawan, 2003; Crini & Lichtfouse, 2018; Derbyshire *et al*., 2001). The disadvantages of using CAC for water remediation are related to the regeneration of saturated carbon as the process is expensive, complex and often leads to depletion of the adsorbent (Babel & Kurniawan, 2003; Crini, 2006). The use of costly materials for pollution control is also unjustified (Streat *et al*., 1995). This prompted many researchers to explore and evaluate more economical adsorbents, such as clays for pollutant remediation from wastewater (Babel & Kurniawan, 2002; Ahmaruzzman, 2008, Ali *et al.*, 2012, Mallakpour & Hatami, 2019).

Clay minerals can be divided into three categories according to their ion exchange property, namely nonionic, cationic and anionic clays (Russell & Wilson, 1987). All three categories have been found to be good adsorbents for various impurities in wastewater. For example, Cavallaro *et al*. (2019) reported that halloysite, a nonionic clay, efficiently removed dyes from aqueous solutions, while vermiculite, a cationic clay, was able to remove chromium from tannery effluent (Jayabalakrishnan & Raja, 2007). Layered double hydroxide (LDH), which is an anionic clay, has been reported to have removed both organic and inorganic contaminants. The organic pollutants included 2-chlorophenol (Chuang *et al.*, 2008), methyl orange (Chen, *et al.*, 2011) and nitrobenzene (Kameda *et al.*, 2010), while inorganic pollutants included rare earth elements (Iftekhar *et al*., 2018), antimony and flouride (Bessaies *et al*., 2021), and phosphate and sulphate (Rizescu, *et al*., 2020). The current study focuses on the use of LDH clays in phenol removal from wastewater.

1.3   Hypothesis

Layered double hydroxide clays can be used to remove phenol from contaminated water. Their capability is fortified by several mechanisms that are applicable when utilised in water purification. These mechanisms include surface adsorption, anion exchange, adsolubilisation of organics into organo-modified LDH and reconstruction of calcined clays. The performance of LDH clays is expected to be comparable to that of other low-cost adsorbents, such as natural clays.

3

1.4 Aims and objectives

This study aimed to evaluate the ability of selected commercial LDH clays in removing phenol from wastewater and to synthesise LDH clays that can remove phenol from synthetic wastewater. The main parameters that influence LDH clay's adsorption abilities were considered with regard to phenol removal, therefore, the main objectives of this work were to:

- Establish the physical and chemical properties of both the commercial and synthesised clays using several characterisation techniques.
- Investigate the effect of metallic compositions on the adsorption capacity of the clays.
- Establish the phenol adsorption mechanism with the aid of equilibrium isotherms.
- Study the kinetics and thermodynamics of the adsorption process.
- Establish the regeneration capabilities and reusability of the clays.
- Compare the performance of the two types of clays (commercial and in-house synthesised).

1.5 Outline of dissertation

Chapter 1

This chapter provides background on water pollution mainly by phenolic pollutants, which have been found to be recalcitrant. It also provides a brief overview on the technologies available for removal of organic contaminants from wastewater and why adsorption is favoured over others. LDHs are defined together with the overall aims and objectives of the study.

Chapter 2

This chapter presents the literature study for this work. It is divided into three sections, which focus on: 1. the pollutant (phenol), 2. the adsorbent (LDH clay) and 3. the process (adsorption).

Chapter 3

This chapter outlines the materials, experimental procedures, methods, characterisation techniques and the analytical techniques used in this work. It is divided into two sections with

the first section focusing on materials and methods for commercial clays, while the second section focuses on the materials and methods used for in-house synthesised clays.

Chapter 4

This chapter provides the characterisation and phenol adsorption results based on commercial clays. Characterisation results include crystallinity and phase identification, elemental analysis chemical bonds identification, BET surface area and morphologies of the commercial clays. Adsorption results include the effect of various process parameters, such as initial pH, operating temperature, clay loading, equilibrium, kinetics and thermodynamics studies.

Chapter 5

This chapter presents both characterisation and phenol adsorption studies based on synthesised clays. The results are compared to those of commercial clays in Chapter 4.

Chapter 6
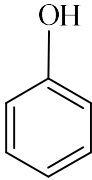
Final conclusions are drawn based on the results from Chapter 4 and Chapter 5.

2 LITERATURE REVIEW

2.1 Phenol

Phenol is a solid at ambient temperature and atmospheric pressure, it is made-up of white crystals that turn pink or red when exposed to air and light (Swearingen, 2002). It has a burning taste and a distinctive odour. Its solubility in water is limited to 6.7 g/100 mL and is soluble in most organic solvents (Gross & Seybold, 2001; World Health Organization, 1994). Its melting point of 43°C gets lowered by the addition of water to the extent that a 90% mixture of phenol in water is liquid at room temperature. Chemically, the compound is a weak acid. The pH of its aqueous solution is approximately neutral. It exists in nature and can be synthesised commercially with a purity of at least 98%. Gas chromatography (GC) and high-performance liquid chromatography (HPLC) with an ultraviolet (UV) detector are among the most common types of methods that are used to detect and quantify phenol. Table 2-1 summarises the chemical and physical properties of phenol.

Table 2-1: Phenol's chemical and physical data (National Centre for Biotechnology Information, 2021)

Name	Phenol
Molecular formula	C_6H_6O
Molecular weight	94.1
Structure	OH
Density (25 °C)	1072.2 g L^{-1}
Boiling point	181.7°C
Melting point	40.5°C
pKa	9.9
LogK$_{ow}$	1.5

2.1.1 Environmental fate and uses of phenol

Phenol and its derivatives find their applications in various industries including the health sector, automotive industry and agriculture. For example, Bisphenol A (BPA) which is synthesised from a condensation reaction of phenol and acetone with hydrogen chloride, an acid catalyst and methyl mercaptan is used in making plastics or resins (Gardziella *et al*., 2013). High purity BPA is used to make polycarbonate plastics while lower purity BPA is used to make epoxy resin (Vandenberg *et al*., 2007). According to Pilato (2010), the production of phenolic resins with formaldehyde has been confirmed to be the largest consumer of phenol. Phenolic resins have a variety of applications such as adhesives, laminating, moulding binders and surface coatings.

2.1.2 Sources of phenolic compounds in water

Natural and anthropogenic activities contribute to the prevalence of phenolic compounds in water. Dead plants and animals are the natural sources of phenolic compounds, while anthropogenic activities include municipal, domestic, agricultural and industrial waste.

2.1.2.1 Natural sources

Run-offs of decomposing materials from land to aquatic systems lead to the deposition of phenols into water bodies. Anku *et al*. (2017) reported that phenolic derivates are constituents of numerous plant species and that phenolic compounds can be formed from amino acids present in hemicelluloses of some plants under UV light irradiation. Human and animal bodies produce phenol without any external exposure; the produced phenol is eventually excreted (Senturk *et al*., 2009). Therefore, metabolic waste products of human beings and animals contain phenol (Anku *et al*., 2017).

2.1.2.2 Anthropogenic sources

Industrial waste

There is a broad application of phenol in the chemical industries for production of alkyl phenols, cresols, aniline and resins. It is also common in the coal oil and gas industries (Bruce *et al*., 1987). Phenol is utilised as a raw material in the textile, explosives and dyes (Anku *et al*., 2017). Water pollution by phenolic compounds can occur when the effluents from industrial activities containing phenol are discharged into the aquatic systems (Paasivirta *et al*., 1985). Other phenolic compounds can be released into the atmosphere

7

through vehicular activities and get transferred into water bodies as rainwater (Anku *et al*., 2017).

Agricultural waste

The use of insecticides, herbicides and pesticides in farming contributes vast amounts of water contamination by phenolic compounds (McBain *et al*., 1996). The degradation of these compounds has contributed to the availability and detection of phenols in the aquatic environment. Pesticides such as 2,4‑diclorophenoxyacetic acid, 4‑chloro‑2‑methyl‑phenoxyacetic acid, and 2,4,5‑tri‑chloro‑phenoxyacetic acid have been shown to form phenol as one of the degradation products (McBain *et al*., 1996). Agricultural run-offs lead to the deposition of herbicides and pesticides into the water bodies.

Domestic waste

Household chemicals which include disinfectants, ointments, antiseptics, mouthwashes, body lotions, soaps, perfumes, paints, varnish removers and oral sprays meant for anaesthetic purposes, contain phenols (Michałowicz & Duda, 2007). The household water that contains these products get drained through sinks and ends up contaminating water bodies.

Municipal waste

Municipal solid waste landfill sites do contribute to the presence of phenols in wastewater. Leachate of incineration residues are likely to contribute compounds, such as p‑cresols, 2,4,6‑trichlorophenol, 4‑tetra butyl phenol and BPA (Naguib & Badawy, 2020). The aquatic environment is contaminated with phenolic compounds when the leachates from landfill sites, residues of incineration and incombustible materials are released into water bodies.

2.1.3   Problems associated with phenol

Phenol is corrosive and causes chemical burns at the point of contact with its exposure by any route able to cause systemic poisoning (Michałowicz & Duda, 2007). Phenols can penetrate the skin through absorption and end-up in the gastrointestinal tract of human beings (Naguib & Badawy, 2020). Once in the system, they will then undergo metabolism and transform into various reactive intermediates that can form covalent bonds with proteins, thereby exerting toxic effects on human beings (Anku *et al*., 2017; Schweigert *et al*., 2001). BPA and alkylphenols have been pinpointed to exert endocrine disrupting effects in animals (Muñoz-de-Toro *et al*., 2005).

Drinking of phenol-contaminated water has been reported to cause protein degeneration, tissue erosion, paralysis of the central nervous system and damage to the kidneys, liver and pancreas in the human body (Geyikci & Coruh, 2013). The WHO recommends that the allowable concentration of phenols in potable water should be 1 mg L^{-1} (World Health Organization, 1996). The regulations by USEPA call for reduction of phenols in wastewaters to less than 1 mg L^{-1} (Anku *et al*., 2017).

2.1.4 Phenol remediation technologies

2.1.4.1 Biological processes

Microbial and enzymatic methods are the two subdivisions of biological techniques for treatment of phenolic compounds from wastewater. The microbial method entails the use of yeast, fungi and bacteria in the degradation of phenols to water (H_2O) and carbon dioxide (CO_2). The process is made possible by the dependency of certain microorganisms on aromatic compounds as their source of nutrient (Kanekar *et al*., 1998; Paller *et al*., 1995). According to Xiaojian *et al*. (1991), microbial degradation of phenols can occur through anaerobic or aerobic processes with the initial step being hydroxylation of the aromatic rings. Müller and Babel (1994) established that hydroxylation through aerobic degradation entails a two-step process where catechol is the end-product. The two steps are (i) reduction of one of the molecular oxygen to H_2O through the support of a hydrogen donor and demolishing of the oxygen atom, (ii) the second step is the formation of catechol in the presence of dioxygenase enzymes. Cleavage of the catechol aromatic rings are then converted to CO_2 and H_2O in the presence of enzymes (Anku *et al*., 2017).

Anaerobic degradation occurs in the presence of oxidising agents, such as nitrates, sulphates, light and CO_2 (Michałowicz & Duda, 2007). The aerobic process is suited for degradation of phenols with minimal halogen constituents, while the anaerobic process is best suited for reduction of halogenated phenols. The anaerobic process is known to produce methane (CH_4) gas in addition to CO_2 and H_2O (Fang *et al*., 2004). The anaerobic process presents major advantages over an aerobic process, which include minimal aeration costs, methane gas recovery and minimum biomass generation.

The enzymatic method uses enzymes (biological catalysts) for degradation of phenolic compounds. Enzymes can provide catalytic effects for effective removal of pollutants from

9

wastewater at moderate temperatures, pH and ionic strength (Demarche *et al.*, 2012). Enzymatic processes can occur under conditions that are deemed unfavourable for microbial degradation. Fang *et al.* (2004) stated that enzymatic processes are sustainable and effective over a wide range of pollutant concentrations, do not require acclimatisation of biomass nor generate any biomass and are not affected by shock loading.

2.1.4.2 Chemical processes

Chemical oxidation

Chemical oxidants can provide complete degradation of phenols in wastewater depending on the oxidant used. The chemical oxidation processes are characterised by low reagent and energy costs, operating under mild conditions (pH and temperature) and in a phenolic concentration range of parts per million and higher (Villegas *et al.*, 2016). Commonly used oxidants include chlorine dioxide, chlorine, chloramines, ozone, ferrate and permanganate. Ferrate and permanganate have been applied in many processes due to their high reduction potentials of 2.2 V and 1.68 V respectively. Villegas *et al.* (2016) reported that ferrate reduces to ferric hydroxide ($Fe(OH)_3$) which is a coagulant and thereby providing a better phenol removal efficiency. Permanganate is a relatively cheap material which does not form halogenated (brominated and chlorinated) by-products. Peings *et al.* (2015) reported that effective phenol degradation with ferrate, permanganate and hypochlorite was achievable with an excess oxidant. The degradation of 30 mg L^{-1} phenol under an oxidant to phenol molar ratio of 10 were found to be 57%, 70% and 61% using ferrate, permanganate and hypochlorite respectively. Hypochlorite was reported to have a shortfall in phenol removal from aqueous solutions due to the formation of chlorophenolic by-products (Peings *et al.*, 2015). Zhang *et al.* (2013) revealed that permanganate can remove over 99% of BPA through a reaction pathway which allows the benzene ring to be the reaction site at the early stages of the process.

Electrochemical oxidation

Electrochemical oxidation is another process that can be used for phenol degradation from wastewater. The process tends to incur less reagent costs but more on equipment and energy; it can be divided into direct and indirect oxidation (Tasic *et al.*, 2014). The former is also referred to as anodic treatment and occurs through the adsorption of contaminants onto the anode surface before degradation by the anodic electron transfer reaction (Ramírez *et al.*, 2017). The most used anode materials include platinum (Pt), lead dioxide (PbO_2), tin oxide

(SnO$_2$), iridium dioxide (IrO$_2$), and boron-based diamond (BDD) (Villegas *et al*., 2016). The efficiency of electrochemical oxidation is influenced by factors such as pH, anode materials, electrolytes and current density. The indirect electrochemical oxidation process utilises the intermediary redox reagents to cause electron transfer between the electrode and the contaminant, thereby preventing fouling of the electrode. The presence of chloride ions can enhance phenol degradation through the formation of chlorine gas (Cl$_2$) and hypochlorite in a process called electrochemical oxidation of active chlorine (Villegas *et al*., 2016). Rabaaoui *et al*. (2013) reported that 96% mineralisation of nitrophenol was achieved within 8 h at a current density of 60 mA cm^{-1} and pH of 3. The authors reported that a faster degradation rate occurred in the presence of sodium sulphate (Na$_2$SO$_4$) in comparison with sodium chloride (NaCl) and potassium chloride (KCl). Pillai and Gupta (2015) reported that ca. 94% of 2,4‑nitrophenol removal was achievable in both batch and continuous reactor configurations. The batch reactor was operated at pH 6.59, NaCl concentration of 1.12 g L^{-1} and current density of 1.44 mA cm^{-1} while the continuous reactor was operated at a flow rate of 500 mL h^{-1}, current density of 58 mA cm^{-1} and an electrolyte concentration of 0.5 g L^{-1}.

Advanced oxidation processes

Advanced oxidation processes (AOPs) are process technologies which are known for formation of hydroxyl radical (OH$^{\bullet}$) *in situ*; this radical has the capability to mineralise most organic materials (Andreozzi *et al*., 1999; Ramírez *et al*., 2017; Ribeiro *et al*., 2015). These process technologies include UV/H$_2$O$_2$, Fenton, ozonation and photocatalytic degradation. Microwave irradiation is an important addition to UV/H$_2$O$_2$ in wastewater treatment as it leads to reduced residence times, lessened activation energies, ease of operation, smaller equipment size and higher yield (Villegas *et al*., 2016). Karci *et al*. (2013) established that UV‑C/H$_2$O$_2$ process gave better degradation efficiencies in terms of total organic carbon (TOC) removal compared to UV‑C photolysis during the degradation of 2,4‑dichlorophenol. The Fenton reagent is one of the AOP capable of degrading aromatic contaminants (Lipczynska-Kochany, 1991; Perez- Moya *et al*., 2007). The Fenton process is mostly used as an initiation stage to reduce the quantity and toxicity of contaminants. Amor *et al*. (2015) was able to reduce olive mill wastewater which had up to 80 000 mg L^{-1} of phenolics by 83% within 8 h using the Fenton process. The effluent was further treated with anaerobic treatment as it was deemed to contain concentrations with low toxicity.

Ozonation involves the direct use of ozone (O_3) to react with contaminants or transformation of O_3 into reactive oxidants, such as ($OH^\bullet$), hydroperoxyl radical ($HO_2^\bullet$), $O_3^{\bullet-}$ or $HO_3^\bullet$ which then degrade target pollutants (Kuosa *et al*., 2015). Ozone is produced naturally as UV rays from the sun enter the earth's atmosphere or when lightning strikes during a thunderstorm (Babikov *et al*., 2003; Braslavsky & Rubin, 2011). Ozone is formed as oxygen molecules (O_2) split to produce a highly reactive radical ($O^\bullet$) that comes into contact with O_2 molecules. It can also be simulated using a UV-type ozone generator, before contacting the simulated UV radiation with clean dry air. The oxidizing potential for O_3 (- 2.74 V) is higher than that of commonly used oxidants such as hypochlorite (-1.49 V) and chlorine (-1.36 V) (Kamenev *et al*., 2003). According to Beltran *et al*. (1994), ozonation provides the following advantages:

(i)   No chemical addition or waste creation,

(ii)   High efficiency in eliminating micro-organisms,

(iii)   It is a self-sustaining process with the main source being atmospheric oxygen, and

(iv)   It can remove multi contaminants, such as organics, inorganics, microorganisms, and can enhance the taste and odor of the water.

Photocatalytic degradation involves the use of catalysts (usually metal oxides) in the reduction of contaminants; the catalyst gets activated through absorption of photons of appropriate energy and is susceptible of enhancing the reaction without being consumed (Dursun *et al*., 2005; Ugurlu *et al*., 2005). Photocatalytic properties of metal oxides are caused by the excitation of electrons from the valence to the conduction band when the catalyst is being irradiated under a light source of appropriate wavelength (Rodgher, 2012). This results in holes (h^+) at the valence band and build-up of electrons (e^-) at the conduction band of the catalyst. The holes in the valence band attack and oxidise H_2O molecules to form hydroxyl radicals ($OH^\bullet$) while the electrons in the conduction band reduce O_2 molecules to form superoxide radicals ($O_2^\bullet$). These highly reactive radicals can transform contaminants into less toxic products, such as CO_2 and H_2O (Dursun *et al*., 2005). The schematic diagram for the photocatalytic process is shown in Figure 2-1. Photocatalytic degradation is regarded as an effective process for the removal of contaminants from wastewater as it can degrade them completely rather than transforming them to other products (Anku *et al*., 2017). Laoufi *et al*. (2008) reported that the extent of photocatalytic degradation is dependent on the catalyst type and dose, reaction time, solution pH, and light source and intensity.
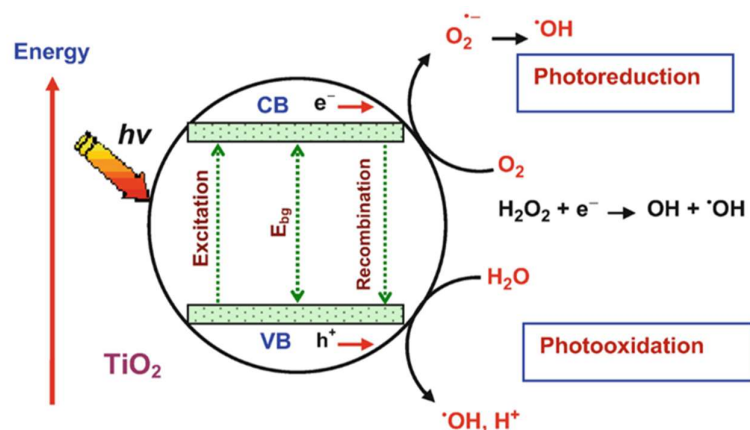
Figure 2-1: Schematic diagram of the photocatalytic process (Meenakshisundaram, 2017).

2.1.4.3 Physical processes

Adsorption

Adsorption can be defined as the phenomenon of the building-up of any species resulting in an elevated concentration of that species on the surface of another substance. The collection of gas or liquid molecules on the surface of a solid material with a porous surface structure is due to gas-solid or liquid-solid intermolecular forces of attraction (Rashed, 2013). Chiou (2003) stated that the adsorption phenomenon takes place when the attractive forces are greater than the cohesive forces keeping molecules in the bulk. The material upon which surface adsorption occurs is referred to as adsorbent, whereas the species which build-up on the adsorbent's surface is called adsorbate. Rashed (2013) described a good adsorbent as one with thermal stability, higher abrasion resistance and small pore diameters, which leads to a higher surface area and eventually a higher adsorption capacity.

The adsorption process can be operated through a batch, column flow or fixed-bed configurations. In batch systems, an adsorbent is continuously mixed with a solution containing the adsorbate of interest; mixing is maintained until the adsorbate content in the bulk solution is reduced to the targeted level or an equilibrium is reached. Spent adsorbent can either be disposed-off or be regenerated for reuse. For column operations, an adsorbent is continuously in contact with a fresh solution (Villegas *et al.*, 2016) and this causes it to have distinct advantages over batch operation as rates of adsorption are dependent on the concentration of the adsorbate in solution.

Activated carbon has been the most commonly used adsorbent for the treatment of contaminated water (Babel & Kurniawan, 2003; Derbyshire *et al.*, 2001). Commercial activated carbon (CAC), in particular, has been used for remediation of various phenols from wastewater. The structural characteristics and porous texture of CAC enable it to possess a large surface area (Ahmaruzzaman & Sharma, 2005). The disadvantages of using CAC for pollutant remediation are related to the regeneration of spent carbon as the process is uneconomical, complex and often leads to depletion of the adsorbent (Babel & Kurniawan, 2003). The use of costly materials for pollution control is also unjustified (Streat *et al.*, 1995). This has pushed researchers into exploring economically viable adsorbents, which include those derived from natural materials (clays), bio-adsorbents (activated sludge) and by-products from industrial and agricultural processes.

Natural clay materials are known to mankind from the earliest days of civilization due to their affordability and availability in most parts of the world (Ahmaruzzaman & Sharma, 2005; Crini, 2006). Clay materials contain layered structures and exist in several classes that include smectites (montmorillonite), mica, kaolinites, vermiculites and hydrotalcites. Their adsorption capabilities differ according to their physical and chemical properties. Montmorillonites have a higher cation exchange (He *et al.*, 2010) while hydrotalcites have higher anion exchange capacity (Cavani *et al.*, 1991). Banat *et al.* (2000) revealed that phenol adsorption by bentonite was influenced by the solvent type; aqueous media gave lower phenol adsorption than when phenol was dissolved in an organic solvent. Table 2-2 shows a variety of low-cost materials that have been reported for phenol adsorption from wastewater. Clay materials are susceptible to modification; hence their adsorption capacities can be enhanced by modifying them through various processes, such as thermal treatment, basic or acidic activation and through making of composites (Cardona *et al.*, 2020).

The collection of contaminants from solutions using biological materials is called bio-adsorption (Ahmaruzzaman & Sharma, 2005). Sewage sludge and activated sludge are some of the bio-adsorbents that have been explored for phenol removal (Otero *et al.*, 2003). The waste materials or by-products emanating from industrial and agricultural processes can be assumed to be economical as they are readily available and require minimal processing. Some of the industrial by-products which have been evaluated for phenol adsorption include lignite (Polat, *et al.*, 2006) and fly ash (Akgerman & Zardkoohi, 1996) as displayed in

Table 2-2. Garg *et al.* (2004) reported on the use of saw dust, rice husk and chicken feathers, which are wastes from agricultural processes and forest industries as adsorbents for phenols from wastewater. Banat *et al*. (2000) investigated the use of chicken feathers for adsorption of phenol from polluted water; the work was conducted at ambient temperature and pH 8 resulting in an adsorption capacity of ca. 20 mg g^{-1}.

Table 2-2: Previously utilised low-cost adsorbents for phenol remediation from wastewater

Adsorbent	Surface area ($m^2\,g^{-1}$)	Phenol initial concentration ($mg\,L^{-1}$)	Temperature (°C)	pH	Adsorption model	Adsorption capacity ($mg\,g^{-1}$)	References
Fly ash	1.8	-	20	-	Freundlich	67.4	(Akgerman & Zardkoohi, 1996)
Residual coal	167.2	1000	-	9	Langmuir	45.5	(Ahmaruzzaman & Sharma, 2005)
Lignite	7.7	100	25	-	Freundlich	10.3	(Polat *et al.*, 2006)
Rice husk	-	1000	25	-	Langmuir	4.5	(Ahmaruzzaman & Sharma, 2005)
Rice husk char	230.1	1000	25	-	Langmuir	7.9	
Chicken feathers	-	50	20	8	Langmuir	19.5	(Banat *et al.*, 2000)
Commercial activated carbon	-	1000	25	5	Langmuir	323.4	(Ahmaruzzaman & Sharma, 2005)
Powder activated carbon	-	1000	25	5	Langmuir	200.3	(Banat *et al.*, 2000)
Granular activated carbon	-	1000	25	5	Langmuir	21	(Banat *et al.*, 2000)

Table 2-2: Previously utilised low-cost adsorbents for phenol remediation from wastewater (continues)

Adsorbent	Surface area $(m^2\,g^{-1})$	Phenol initial concentration $(mg\,L^{-1})$	Temperature (°C)	pH	Adsorption model	Adsorption capacity $(mg\,g^{-1})$	References
Porous clay	250.3	100	25	-	Freundlich	14.5	(Arellano-Cárdenas *et al.*, 2005)
Natural clay	-	5	25	5	Langmuir	15.2	(Djebbar *et al.*, 2012)
Bentonite	-	500	25	5	Langmuir	1.7	(Banat & Al-Asheh, 1999)
Thermal bentonite	-	60	25	12	Freundlich	8.2	(Al-Asheh *et al.*, 2003)
Modified montmorillonite	-	47	25	6	Langmuir	0.5	(Luo *et al.*, 2015)
Neutralised red mud	-	60	25	2-8	Langmuir	4.1	(Tor *et al.*, 2006)
Sewage sludge	44.2	100	25	6	Freundlich	94.2	(Thawornchaisit & Pakulanon, 2007)
Activated sludge	390.1	100	25	-	Freundlich	29.5	(Otero *et al.*, 2003)
Pyrolysed sewage sludge	80	100	25	-	Freundlich	10.1	(Otero *et al.*, 2003)

17

Membrane filtration

Ion exchange

An ion exchange process occurs when there is interchange of ions between two phases. The solid phase is mostly the ion exchange resin while the pollutant under consideration is present in the aqueous medium. Typical ion exchange resins are made of a cross-linked polymer network with its surface covered with a uniform distribution of ions (Anku *et al*., 2017). The efficiency of the process is influenced by the concentration of ions in an aqueous medium and their affinity for the ion exchange resins. It is a unique process that is reversible, recyclable and environmentally benign (Alexandratos, 2009). According to Anku *et al*. (2017), polymer based anionic resins can remove phenolic compounds from polluted water.

Liquid-liquid extraction

Extraction using polar organic solvents is another technique that is available for phenol remediation from polluted water. It involves separation of compounds based on their solubilities in two immiscible liquids (Anku *et al*., 2017; Hu *et al*., 2019). Water and an organic solvent are usually used as immiscible liquids. Phenol removal efficiencies of between 75-96% were achieved by Rao *et al*. (2009) when they used solvents, such as Aliquat-336, 1‑hexanol, 1‑octanol, 1‑heptanol and castor oil organic solvents. The work was done with a solvent to wastewater ratio of 5:250 (v/v). The drawbacks for liquid liquid extraction (LLE) are longer residence times, and usage of large quantities of organic solvents of which some may be toxic (Dubey *et al*., 2006; Ma & Cantwell, 1998).

2.2 Layered double hydroxide clays

2.2.1 Background

LDHs are anionic clays that are usually called hydrotalcites-like materials. They do occur in nature and synthetic materials can also be prepared through mixtures of metal salts and a suitable base (Braterman *et al*., 2004; Forano *et al*., 2013). Their preparation is comprised of the partial substitution of divalent cations in brucite-like materials ($Mg(OH)_2$) by trivalent metals. This substitution results in a negative charge deficit that gets neutralised by anions positioned in the interlamellar space. The interlamellar space is easily accessible and provides a great prospect for capturing and exchanging of anions. The general formula for LDH is as follows:

$$(M^{II}_{1-x} M^{III}_{x} (OH)_2)^{x+} (A^{m-}_{x/m} \cdot H_2O)^{x-}$$
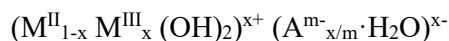
Where M^{II} and M^{III} represent divalent metal (Mg^{2+}, Cu^{2+}, Zn^{2+}) and trivalent (Al^{3+}, Fe^{3+}) respectively, A represents the balancing anion (CO_3^{2-}, NO_3^-), x is the fraction of the trivalent metal while m represents the charge of the balancing anion. In nature, the fraction of the trivalent metal cations, x=0.25 which corresponds to an M^{II}/M^{III} ratio of 3:1 (Cavani *et al*., 1991; Forano *et al*., 2013). Figure 2-2 shows the schematic diagram on an LDH clay.
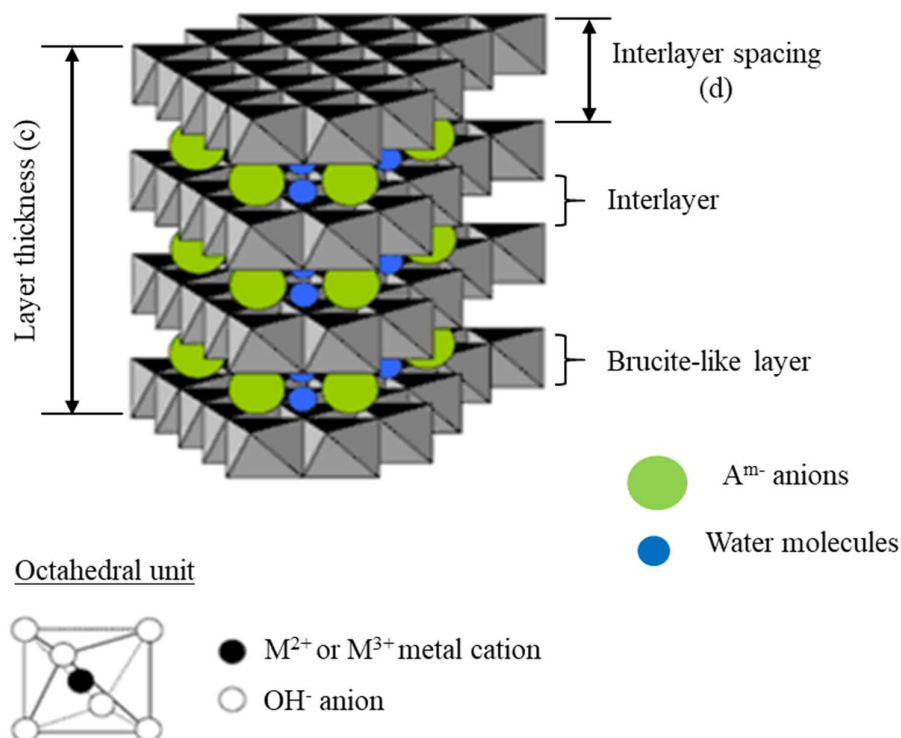
Figure 2-2: Schematic diagram of an LDH clay (Sokol et al., 2018)

2.2.2   Layered double hydroxide clays synthesis methods

The synthesis methods for LDH vary according to the specifications of the final product that includes high crystallinity, less energy and material consumption, residence time and purity. The most widely used methods of preparation for LDHs are co‑precipitation, hydrothermal synthesis and sol‑gel method. They can also be modified through thermal treatment, acid activation, and anion exchange to produce secondary products.

2.2.2.1 Co‑precipitation

This is the most widely used method for preparation of LDHs and it involves the dissolution of metallic salts in a basic solution at a constant or varying pH. Morphology and particle size

19

can be controlled through this method depending on the level of solution supersaturation. The structure of the precipitate produced through this process can be improved by controlling the M^{II}/M^{III} molar ratio, the type of interlayer anion, reaction time, operating pH and temperature of the solution (Cormenzana *et al.*, 2001; Sharma *et al.*, 2007). This process can be conducted at low or high supersaturation conditions depending on the required crystallisation state; the initial concentration of the reactants must be kept above saturation and pH be controlled in any case (Chaillot *et al.*, 2020). This is because low pH values will result in incomplete precipitation while higher pH values can result in leaching of metallic ions.

Low supersaturation co‑precipitation can be conducted by the addition of solutions containing the metal ions in predetermined molar ratios followed by the addition of an aqueous solution containing the interlayer anion of choice (Sharma *et al.*, 2007). An alkaline solution can then be added to control pH and promote co‑precipitation of the metals. This method allows for control of charge density by operating under low supersaturation with constant pH. The high supersaturation is achieved by adding dissolved metal salts to a solution containing little excess of alkali carbonates. Its resultant precipitate is less crystalline compared to the precipitate formed under low supersaturation.

This process can be an effective method for production of crystalline precipitates. However, particles formed through this method have been found to have a lower specific surface area (50-100 m^2 g^{-1}) compared to the sol‑gel method (150 -200 m^2 g^{-1}) (Zhao *et al.*, 2002). Gevers *et al.* (2019) reported on the possibility of partial substituting of Mg with transition metals to modify the crystal lattice parameters and thermal stability of hydrotalcite through this method. Precipitates produced through this method can undergo post-synthesis processes that include hydrothermal treatment, sonication or microwave irradiation in order to improve the crystallinity of the clay (Pérez-Barrado, 2015).

2.2.2.2 Sol‑gel method

This process is acknowledged for its efficiency in energy, costs, and time plus the possibility of producing pure materials containing several compositions (Paredes *et al.*, 2011; Sharma *et al.*, 2007). The structural properties of materials prepared through this method can be fine-tuned by altering the chemical nature of the reactants and residence time. The process of preparing LDHs through this method involves: dissolving the desired metal sources in water at ambient temperature, followed by the addition of a base to the metallic solution during

hydrolysis for condensation. The solution mixture gets aged for several hours before recovering the product. The precipitates from this method are known for high reproducibility, homogeneity, purity, nanoscale particles and a high surface area (Prince *et al.*, 2009). Its drawback is production of less crystalline precipitates. Crystallinity can be improved by post-synthesis treatment processes that include sonication (Hu *et al.*, 2007), microwave irradiation (Benito *et al.*, 2006) or hydrothermal treatment (Gu *et al.*, 2014; Kovanda *et al.,* 2005).

2.2.2.3 Hydrothermal treatment

Hydrothermal treatment is mostly used as an optimisation or post-precipitate treatment after other LDH synthesis methods. This is done to improve the crystallinity and crystallite sizes (Sharma *et al.*, 2007). Hydrothermal treatment is usually conducted at moderate conditions (200 °C), endogenous pressure and may last from a few hours to days. This process involves the dissolution of metallic salts in water, transferring the metal salts solution into a stainless-steel reactor and heating under hydrothermal conditions (Chaillot *et al.*, 2020). Hydrothermal conditions refer to a temperature between 30 and 300 °C with steam pressure (Jang *et al.*, 2014; Zhu *et al.*, 2006). Metal sources include metal hydroxides and oxides (Jang *et al.*, 2014; Labuschagne *et al.*, 2018), nitrates (Roelofs *et al.*, 2001) or natural minerals, such as brucite and gibbsite (Ogawa & Asai, 2000). The major drawback for this synthesis method is energy consumption that makes it less likely to be implemented at industrial level (Chaillot *et al.*, 2020).

2.2.3 Utilisation of layered double hydroxide clays

2.2.3.1 Applications in material science

One of the subjects of interest in material science is the preparation of high-performance polymer composites. High-performance polymers can be achieved through the addition of low-dimensional and nanoscale materials, such as nanofillers to improve the mechanical, thermal and electrical properties of polymers (Cao *et al.*, 2016). LDH clays are commonly used as nanofillers to improve the flammability of polymers due to their excellent fire-retardant effect (Pereira *et al.*, 2009; Zhao *et al.*, 2008). LDH embedded in polymers can absorb heat and release water and carbon dioxide; this lowers the temperature of the substrate and enhances the foam char structure. Porous thermal-decomposed products of LDH can give smoke suppression effects by absorbing smoke and gases produced during combustion (Wang *et al.*, 2005). According to Manzi‑Nshuti *et al.* (2009), LDHs containing transition

metals can be well dispersed in polymers and enhance thermal stability while reducing flammability of polymers.

2.2.3.2 Catalysis

The metal cations in LDH are evenly dispersed in the brucite-like layers (Varadwaj et al., 2017). The catalytic activity of LDHs can be well regulated by assimilating varying cations in fluctuating cationic ratios. According to Auerbach *et al.* (2004), catalytically active components of LDH include both metal ions and the hydroxide groups. Thermal treatment of LDHs at moderate temperatures gives rise to mixed metal oxides (MMOs) of a higher specific surface area and catalytic active (Zhao *et al.*, 2010). LDHs are broadly applied as catalysts for oxidation reactions (Zhu *et al.*, 1997), base catalysed reactions (Constantino & Pinnavaia, 1995; Velu & Swamy, 1997), halide substitution (Suzum *et al.*, 1990), acid catalysed reactions (Braterman *et al.*, 2004), alkylation (Kerchiche *et al.*, 2017; Shimada & Ogoshi, 2005), photocatalysis (Mohapatra & Parida, 2016; Yang *et al.*, 2007; Zhao *et al.*, 2016), alkane dehydrogenation (Mitran *et al.*, 2012; Sattler *et al.*, 2014), aldol condensation (Bharali *et al.*, 2015; Sahoo *et al.*, 2011) and as catalyst supports (Choudary *et al.*, 2002; Feng *et al.*, 2015; Takehira, 2017).

2.2.3.3 Layered double hydroxides as adsorbents in water remediation

Layered double hydroxide clays offer appealing physical and chemical properties that include high specific area, and adjustable compositions and structures (Gao *et al.*, 2018; Yang *et al.*, 2016; Zubair *et al.*, 2017). LDHs have been found to possess qualities that put them as contenders for efficient water treatment; those qualities include low synthesis cost, high catalytic performance, extensive adsorption capacities, non-toxicity, stability and ability to be regenerated with ease (Laipan *et al.*, 2018; Liang *et al.*, 2013; Yang *et al.*, 2016). Lei *et al.* (2014) reported that applications of LDHs in water remediation can be split into four categories:

(i) Usage as adsorbents through anion exchange and surface adsorption,

(ii) Utilisation of CLDHs and their regenerative capabilities,

(iii) Exploration of LDHs intercalated with organic molecules to take up organic pollutants through adsolubilisation (organic quests can enhance pollutant uptake efficiency), and

(iv) Usage as photocatalysts in the conversion of pollutants to less toxic materials.

Anion exchange and surface adsorption

Anion exchange is a chemical process whereby anions are exchanged or displaced for one or more varying anions (Lei *et al.*, 2014). LDH clays are suitable for this process due to their substantial interlamellar spaces and their ability to contain many exchangeable anions. According Braterman *et al.* (2004), LDHs containing nitrate as an interlayer anion offers higher exchange capacities in the presence of a suitable replacement anion, while carbonate is less likely to be replaced as it has a higher affinity for LDH. The difficulty in substituting interlayer anions can be labelled in the following sequence: $CO_3^{2-} > SO_4^{2-} > OH^- > F^- > HPO_4^-$ $> Cl^- > Br^- > NO_3^- > I^-$ (Auerbach *et al.*, 2004; Braterman *et al.*, 2004; Forano *et al.*, 2013). This process is influenced by physiochemical factors that include pH of the solution, adsorbent dosage, reaction or mixing time, and initial concentrations of the contaminants (Daud *et al.*, 2019; Zubair *et al.*, 2017).

The layers of the LDH clays bear positive charges, therefore, they can adsorb anions through electrostatic interactions (Chen *et al.*, 2009; Yang *et al.*, 2016) Table 2-3 shows selected organic pollutants that have been revealed to be removable through surface adsorption with LDH.

Table 2-3: Selected organics that can be removed through surface adsorption by LDH clays

LDH	Pollutant	Adsorption isotherm	References
MgAl–CO_3^{2-}	Acid blue 29	Langmuir	(Orthman *et al*., 2003)
MgAl–NO_3^-	Congo red	-	(Chen *et al*., 2011)
MgAl–NO_3^-	2,4–dichloro–phenoxyacetate	-	(Chao *et al*., 2009)
MgAl–CO_3^{2-}	Dodecyl benzene sulfonate	Langmuir	(You *et al*., 2002)
MgAl–NO_3^-	Eosin B	-	(Chen *et al*., 2011)
MgAl–Cl^-	Fulvic acid	Langmuir	(Vreysen & Maes, 2008)
NiAl–NO_3^-	Glufosinate	Langmuir	(Khenifi *et al*., 2010)
NiAl–NO_3^-	Glyphosate	Langmuir	(Khenifi *et al*., 2010)
MgFe–CO_3^{2-}	Humic acid	Langmuir	(Gasser *et al*., 2008)
MgAl–NO_3^-	Methyl orange	-	(Chen *et al*., 2011)
MgAl–NO_3^-	Orange II	-	(Chen *et al*., 2011)

Memory effect

Neat or as-prepared LDHs have specific surface areas of 15 -120 m^2 g^{-1} (Lei *et al*., 2014). Materials with elevated surface areas can be attained through thermal treatment of LDHs at moderate temperatures. This results in the formation of mixed metals oxide (MMO) with amplified anion uptake capacity. The operating temperature should be sufficient to enable an LDH clay to lose its layer structure and be converted into MMO with high thermal stability against sintering, large surface area and small crystallite size (Lei *et al*., 2014). The key feature of calcined LDHs (CLDHs) is the memory effect that arises when they are subjected to an aqueous solution; upon absorption of anions and water, CLDHs can be reconstructed into a layered structure (Braterman *et al*., 2004; Cavani *et al*., 1991; Forano *et al*., 2013). This is shown schematically in Figure 2-3. The interlayer anion in the reconstructed LDH depends on the concentration of the anion in solution and the affinity of LDH towards the anion (Chen *et al*., 2014; Crini & Lichtfouse, 2018). Hu *et al*. (2018a), Milanovic (2016), and Santos *et al*. (2017) revealed that the property of memory effect is possible if calcination was conducted

below 500°C. This is due to the formation of stable spinel ($M^{II}M_2^{III}O_4$) phase at temperatures above 600°C.

The high anion uptake capacity and ability to reconstruct make CLDHS to be potential adsorbents of anions in water. Lei *et al*. (2014) reported that the removal of anions by CLDHs can be defined in a four-step process that includes the movement of the anions in bulk solution, sub-surface diffusion, intraparticle diffusion and attachment of anions onto basal sites. A summary of organic contaminants that have been removed from water using CLDHs is detailed in Table 2-4.
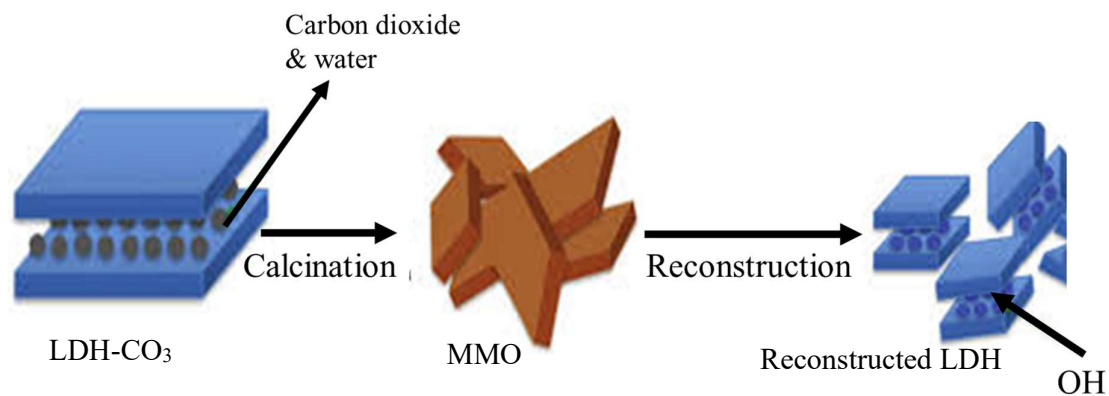
Figure 2-3: Memory effect of LDH clays (Hernández et al., 2017)

Table 2-4: Selected organic contaminants which have been removed from aqueous solutions using CLDHs

LDH	Pollutant	Calcination temperature (°C)	Adsorption isotherm	References
MgFe‑CO_3^{2-}	Acid brown 14	500	Langmuir	(Abdelkader *et al*., 2011)
MgFe‑CO_3^{2-}	Acid orange 10	500	Langmuir	(Abdelkader *et al*., 2011)
MgAl‑CO_3^{2-}	Aspartic aminoacid	500	-	(Silvério *et al*., 2013)
MgAl‑CO_3^{2-}	Benzopurpurine 4B	500	Freundlich	(Setti *et al*., 2010)
MgAl‑CO_3^{2-}	Glutamic aminoacid	500	-	(Silvério *et al*., 2013)
MgAl‑CO_3^{2-}	Humic acid	500	Langmuir	(Hussein *et al*., 2001)
ZnAl‑CO_3^{2-}	Methyl orange	500	Langmuir	(Ni *et al*., 2007)
CuZnAl‑CO_3^{2-}	Phenylalanine	500	Langmuir	(Jiao *et al*., 2012)

Adsolubilisation

Layered double hydroxide clays are inorganic and, hence, present hydrophilic properties. Therefore, they have a low affinity towards nonionic hydrophobic organic compounds. Their hydrophilicity can be altered through intercalation of hydrophobic anions, such as surfactants (Evans & Duan, 2006) to form organo-LDHs. Intercalation of organic anions result in the formation of interlayer regions followed by an increase in interlayer space. The organo-LDH clays are contenders for the uptake of organic molecules from water. The process involves dissolution of the organic contaminant into the hydrophobic interlayer space instead of adsorption onto the external surface (Ruan *et al*., 2013). This is referred to as adsolubilisation. A summary of selected organic contaminants reported to have been removed from an aqueous solution by adsolubilisation into LDH clays is shown in Table 2-5.

Lei *et al*. (2014) stated that the elevated adsorption capacities during adsolubilisation are caused by hydrophobic-hydrophobic interactions between the alkyl chains and benzene rings of intercalated anions and contaminants. Ruan *et al*. (2013) proposed a mechanism for uptake by dodecyl sulphate intercalated LDHs as shown in Figure 2-4. A partitioning mechanism

was found to be dominant for adsorption of compounds, such as naphthalene, nitrobenzene and acetophenone.

Table 2-5: Selected organic contaminants removed by adsolubilisation into LDH clays

LDH	Pollutant	Interlayer anion	References
MgAl	Pentachlorophenol	dodecyl benzenesulfonate	(Gao *et al*., 2011)
MgAl	2-Chlorophenol	Dodecyl sulfate	(Chuang *et al*., 2008)
MgAl	2,4,5-trichlorophenol	dodecyl benzenesulfonate	(Zaghouane-Boudiaf *et al*., 2011)
MgAl	p-nitrophenol	dodecyl benzenesulfonate	(Lei *et al*., 2014)
MgAl	p-cresol	Dodecyl sulfate	(Li *et al*., 2013)
ZnAl	Phenol	Carboxymethyl-β-cyclodextrin	(Hussein *et al*., 2001)
MgAl	1,3-dinitrophenol	1,3,6-naphlenetrisulfonate	(Kameda *et al*., 2010)
MgAl	Nitrobenzene	1,3,6-naphlenetrisulfonate	(Kameda *et al*., 2010)
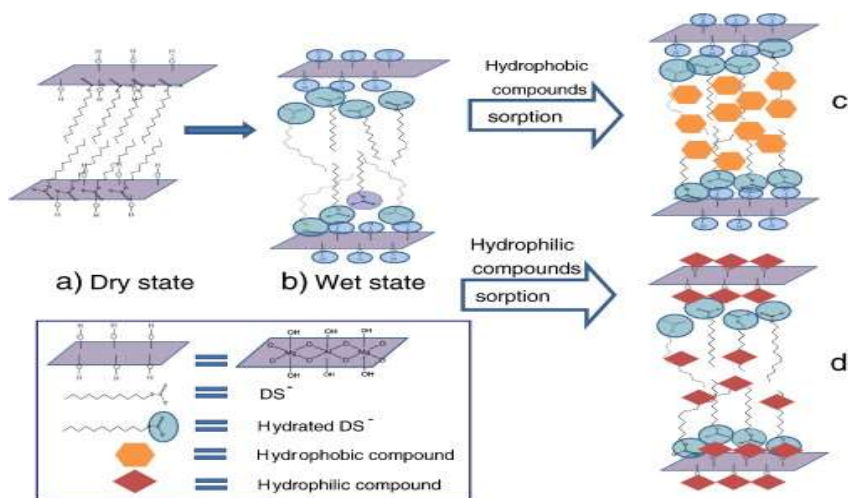
Figure 2-4: Adsolubilisation of organic pollutants in surfactant intercalated LDH (Ruan et al., 2013)

2.3   Modelling of adsorption process

Adsorption mechanism can be classified into two types depending on the attractions between adsorbate and adsorbent. Forces of attraction can be due to weak van der Waals forces or strong chemical bonds (Rashed, 2013; Samiey, 2015). The former is associated with physical adsorption (physisorption) while the latter is related to chemisorption. Physisorption results in the formation of a multilayer of adsorbate on the adsorbent. It is characterised by low enthalpy of adsorption (ΔH° =20 - 40 kJ·mol^{-1}) (Lavrich *et al*., 1998). It readily occurs at lower temperatures and decreases as temperature is elevated through Le Chatelier's principle. For gas adsorption onto solids, an increase in pressure causes an increase in extent of adsorption as volume decrease with respect to Le Chatelier's principle. The process is less selective towards adsorbates due to van der Waals forces being universal. The extent of adsorption is enhanced by an increase in surface area.

Chemisorption takes place because of strong chemical forces of attraction. It results in the formation of unilayer of adsorbate on adsorbent. It is accustomed to high enthalpy of adsorption (ΔH° =80 - 240 kJ·mol^{-1}) with an increase in temperature leading to an increase in chemisorption until a peak is reached (Chiou, 2003; Lavrich *et al*., 1998). This phenomenon is highly specific and occurs when there are possibilities of chemical bonding between adsorbent and adsorbate. Other factors that influence the extent of chemisorption include surface area, nature of adsorbent and pH of the solution. An increase in surface area leads to an increase in chemisorption as more sites become available for adsorption. A greater solubility of adsorbate in solution results in reduced chemisorption as the solute-solvent bond is perceived to be stronger.

2.3.1   Adsorption isotherms

An adsorption isotherm is the demonstration of the quantity of adsorbate per unit weight of adsorbent with respect to the equilibrium concentration in the bulk solution at constant temperature (Chiou, 2003; Rashed, 2013). Adsorption isotherms are able to reveal if adsorption is best operated at higher or lower concentrations of adsorbate. Moreover, the highest quantity of an adsorbate that can be removed through an adsorption cycle can be determined through isotherms (Naseer, 2018). For determination of any adsorption isotherm, the adsorbent and adsorbate should be kept in contact until equilibrium is reached. Generally, there are five classes of isotherms in which the adsorption process can follow (Khalfaoui *et al*., 2003). The first class, type I is denoted by Langmuir type adsorption as shown in Figure

2-5. It indicates a monotonic approach to a limiting value that correlates theoretically to the completion of surface monolayer (Chiou, 2003). Type II is mostly portrayed by the physical adsorption on relatively open surfaces whereby adsorption progresses from sub-monolayer to multilayer. This class displays a distinct concave-downward curvature at low concentration or pressure and sharply rise at higher concentration or pressure. Type III class depicts relatively weak adsorbate-adsorbent interactions. An example of this is the adsorption of water and alkanes on nonporous low polarity solids, such as Teflon (Kinloch, 2012). Type IV and Type V are attributes of vapor adsorption by capillary condensation into small adsorbent pores whereby adsorption attains an asymptotic value as saturation pressure is approached (Chiou, 2003). An example of Type IV is adsorption of organic vapours onto activated carbon whereas Type V can be exemplified by water vapor on activated carbon (Kinloch, 2012). Various isotherms have been studied in literature; they start from the simplest one parameter isotherm, such as Henry isotherm to more complex five parameter isotherm, such as Fritz and Schlunder isotherm. In the current work, the two mostly used isotherms i.e., Langmuir and Freundlich plus the Temkin isotherms were considered.
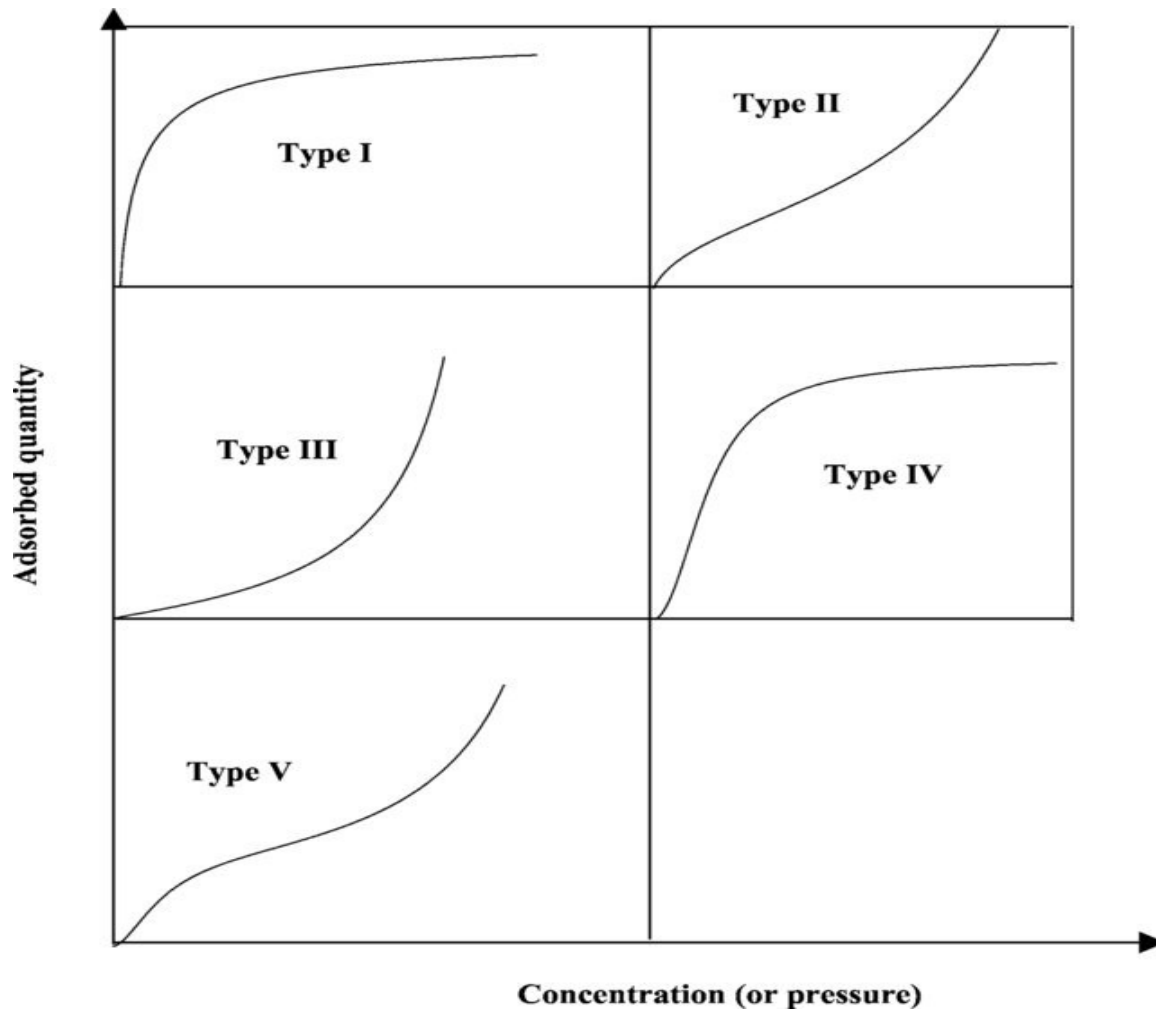
Figure 2-5: Types of adsorption isotherms (Khalfaoui et al., 2003)

2.3.1.1 Langmuir isotherm

Langmuir isotherm was initially designated to illustrate gas-solid phase adsorption (Ayawei *et al*., 2017). The isotherm accounts for surface coverage by counteracting the rate of adsorption with that of desorption. Adsorption is proportional to the portion of the uncovered surface of the adsorbent while desorption is proportional to the covered surface of the adsorbent (Günay *et al*., 2007). The Langmuir model can be represented, as shown in Equation 2-1, while its linearised form is presented in Equation 2-2. The vital parameters of the Langmuir isotherm can be demonstrated by a dimensionless constant called separation factor, R_L as in Equation 2-3. Adsorption is set to be unfavourable if $R_L > 1$, conducive if $0 < R_L < 1$, linear if $R_L = 1$ and irreversible if $R_L = 0$.

$$q_e = \frac{q_m K_L C_e}{1 + K_L C_e} \tag{2-1}$$

$$\frac{C_e}{q_m} = \frac{1}{K_L q_m} + \frac{C_e}{q_m} \tag{2-2}$$

$$R_L = \frac{1}{1 + K_L C_e} \tag{2-3}$$

Where:

C_e = equilibrium concentration of adsorbate (mg L^{-1})

q_e = equilibrium adsorption capacity (mg g^{-1})

q_m = maximum adsorption capacity (mg g^{-1})

K_L = Langmuir equilibrium constant (L mg^{-1})

2.3.1.2 Freundlich isotherm

Freundlich isotherm is appropriate for non-monolayer, reversible and heterogeneous adsorption (Ayawei *et al.*, 2015). The model can be described as in Equation 2-4 with its linearised form represented by Equation 2-5. The inverse of the adsorption intensity ($1/n$), which is a slope of the linearised Freundlich equation serves to describe the linearity of adsorption or the degree of curvature of the isotherm across the concentration tested (Ayawei *et al.*, 2017). When $1/n$=1, it shows that the relative adsorption of the pollutant was the same across the whole range tested. For $1/n$ values ranging between 0.7 to 1, they indicate that when the pollutant concentration increases, the relative adsorption decreases signifying saturation of adsorption sites. When $1/n$ is less than 0.7, it indicates a highly curved isotherm.

$$q_e = K_F C_e^{1/n} \tag{2-4}$$

$$\ln q_e = \ln K_F + \frac{1}{n} \ln C_e \tag{2-5}$$

Where:

K_F = Freundlich equilibrium constant (L g^{-1})

n = adsorption intensity

2.3.1.3 Temkin isotherm

This model considers the effect of indirect interactions between the adsorbate and adsorbent (Ayawei *et al.*, 2017). The heat of adsorption for all molecules in the layer is assumed to be decreasing linearly as the surface area increases (Ringot *et al.*, 2007). The model is relevant at intermediate range of concentrations (Shahbeig *et al.*, 2013). It is mostly applied for

chemisorption processes. The empirical equation for the Temkin isotherm is displayed in Equation 2-6 with its linear form expressed in Equation 2-7.

$$q_{\mathrm{e}} = \frac{RT}{b_{\mathrm{T}}} \ln(A_{\mathrm{T}} C_{\mathrm{e}}) \tag{2-6}$$

$$q_{\mathrm{e}} = \frac{RT}{b_{\mathrm{T}}} \ln A_{\mathrm{T}} + \frac{RT}{b_{\mathrm{T}}} \ln C_{\mathrm{e}} \tag{2-7}$$

Where:

A_{T} = equilibrium binding constant corresponding to the maximum binding energy (L g^{-1})

b_{T} = Temkin constant related to heat of sorption (dimensionless)

R= universal gas constant (8.314 J mol^{-1}K^{-1})

2.3.2   Adsorption kinetics

The estimation of the rate at which contaminants adsorption occurs in a set solid/solution system is an important factor for effective sorption system design. There has been limited progress in this field as description of sorption kinetics appear to be more complex than sorption equilibria (Plazinski *et al*., 2009). The sorption process can be simulated by the following steps:

      (i)   Transport of adsorbate in the bulk solution,

      (ii)   diffusion of adsorbate over the liquid film surrounding the adsorbent particles,

      (iii)   intraparticle diffusion and

      (iv)   adsorption/desorption of adsorbate on/from the adsorbent surface.

The overall adsorption rate can be controlled by any or a combination of the steps. Transport of adsorbate in the bulk solution is usually not considered as a rate limiting step as rigorous mixing is maintained in most systems. Most studies have assumed step (iv) as the one that makes a significant contribution in the kinetics of a system (Doğan *et al*., 2009; Nethaji *et al*., 2013). The step is often referred to as the surface reaction that arises not only due to chemical bonds but also through physical contact as with van der Waals forces (Ho *et al*., 2000; McCoy & Liapis, 1991; Plazinski *et al*., 2009).

An appropriate model can be developed through the acceptance of a fundamental approach to interfacial kinetics. The Langmuir model has led to derivatisation of other expressions related

to the postulation of a chemical reaction occurring on the surface (Plazinski *et al*., 2009). The derived models include Langmuir kinetics (Shooto *et al*., 2016), first order (El-Khaiary, 2008) and second order (Fost & Aly, 1981) reversible, and first order (Mohan *et al*., 2002) and second order (Chu & Hashim, 2003) irreversible reaction. Other simplified and compact models such as Lagergren (pseudo-first order), pseudo-second order and Elovich equations have also been applied to correlate kinetic data measured in numerous systems. These formulae are modelled based on surface reaction being a rate limiting step. They are frequently used because of their simplicity and require no advanced computational procedures.

The current study focused on the pseudo-first order, pseudo-second order and Elovich equations. These models are enormously popular and commonly used to correlate kinetics data. Modelling of data using these models enables one to compare the material properties of this study with those in literature.

2.3.2.1 The pseudo-first order equation
This empirical equation was developed by Lagergren for adsorption of oxalic and malonic acids onto charcoal (Plazinski *et al*., 2009). Hence it is also referred to as the Lagergren equation. The differential and linearised forms of the equation are as displayed by Equation 2-8 and Equation 2-9.

$$\frac{dq}{dt} = K_1(q_e - q_t) \qquad (2\text{-}8)$$

$$\ln(q_e - q_t) = \ln q_e - K_1 t \qquad (2\text{-}9)$$

Where:

K_1 = Lagergren rate constant (min^{-1})

t = time (min)

The Lagergren rate constant (K_1) represents a time scaling factor of which the value determines how fast equilibrium can be reached. The dependence of K_1 parameter on the initial concentration of adsorbate varies from one system to another. Allen *et al*. (2005) and Mckay and Ho (1999) revealed that K_1 had an inverse proportionality relationship with the initial concentration of adsorbate increases.

2.3.2.2 Pseudo second order

This model is for systems whereby the overall rate of sorption kinetics is controlled by a direct adsorption/desorption process (Plazinski *et al*., 2009). The mathematical formula corresponding to this model was derived by Blanchard *et al*. (1984) when describing kinetics of heavy metal adsorption by natural zeolites. An accepted assumption for this model was that the rate of ion exchange reaction taking place on the surface is responsible for the adsorption. The differential formulation of the most used form of pseudo-second order is presented by Equation 2-10 with its linearised form shown by Equation 2-11. Plazinski *et al*. (2009) reported that the rate constant K_2 had an inverse proportionality relationship with the initial concentration of adsorbate. The effects of pH and temperature on K_2 are yet to be studied extensively due to the complexity of the problem and other factors.

$$\frac{dq}{dt} = K_2(q_e - q_t)^2 \tag{2-10}$$

$$\frac{1}{q_t} = \frac{1}{K_2 q_e^2}\left(\frac{1}{t}\right) + \frac{1}{q_e} \tag{2-11}$$

Where:

K_2 = pseudo-second order rate constant (g mg^{-1}min^{-1})

2.3.2.3 The Elovich kinetic model

This model was first proposed by Roginsky and Zeldovich in 1934 to explain the kinetics of adsorption of carbon monoxide on manganese dioxide (Plazinski *et al*., 2009). It is mostly applied to chemisorption kinetics (Largitte & Pasquier, 2016). The model has been adequately applied to some chemisorption data and was established to cover a wide range of slow adsorption (Juang & Chen, 1997). Cheung *et al*. (2000) describe the Elovich equation as a kinetic model that is valid for systems in which the adsorbing surface is heterogeneous. Equation 2-12 and Equation 2-13 show the differential and integral form of the model, respectively.

$$\frac{dq}{dt} = \alpha e^{(-\beta_E \cdot t)} \tag{2-12}$$

$$q_t = \frac{1}{\beta_E}\ln(\alpha \cdot \beta_E) + \frac{1}{\beta_E}\ln t \tag{2-13}$$

Where:

α = initial sorption rate constant (mg g^{-1}min^{-1})

β_E = extent of surface coverage and activation energy for chemisorption (g mg^{-1})

2.3.3 Thermodynamics studies

Adsorption processes involve heterogeneous equilibrium whereby the adsorbate (gas or aqueous) is adsorbed onto a solid material. Changes in energy and spontaneity of the sorption process can be properly understood by estimation of the thermodynamics properties. Change in enthalpy ($\Delta H°$), entropy ($\Delta S°$) and Gibbs free energy ($\Delta G°$) can be determined through the changes in adsorbate concentration using appropriate thermodynamic relations, as shown by Equation 2-14 (Vant' Hoff equation) and Equation 2-15 (Ibrahim & Jimoh, 2012). K_a is the dimensionless equilibrium constant which is determined by converting the units of K_I (the best isotherm model fitted, such as K_L, the Langmuir equilibrium constant or K_F, Freundlich equilibrium constant), that are given initially in L mg^{-1} into L mol^{-1} (Leechart et al., 2009; Liu, 2009; Liu & Xu, 2007) as shown in Equation 2-16.

$$\ln K_a = \frac{\Delta S°}{R} - \frac{\Delta H°}{RT} \tag{2-14}$$

$$\Delta G° = -RT \ln K_a \tag{2-15}$$

$$K_a = \frac{1000 \times K_I \times MM_{ads} \times C°_{ads}}{\gamma} \tag{2-16}$$

Where:

$C°_{ads}$ = standard adsorbate concentration (1 mol L^{-1})

K_a = thermodynamic equilibrium constant (dimensionless)

K_I = equilibrium constant depending on the best isotherm model fitted (L mg^{-1})

MM_{ads} = molar mass of adsorbate (g mol^{-1})

$\Delta G°$ = change in Gibbs free energy (kJ mol^{-1})

$\Delta H°$ = change in enthalpy (kJ mol^{-1})

$\Delta S°$ = change in entropy (kJ mol^{-1}K^{-1})

γ = activity coefficient (dimensionless)

3 MATERIALS AND METHODS

This work involved the use of commercial clays and in-house synthesised clays as adsorbents in the remediation of phenol from contaminated water. Commercial clays were sourced from various manufacturers while in-house synthesised clays were prepared in the laboratory. The compositions of the in-house synthesised clays were based on the composition of the commercial clays, which gave rise to higher phenol adsorption efficiencies.

3.1 Commercial clays

3.1.1 Materials

Six commercial LDH clays were used in the first part of this work. Clay GF‑450 was supplied by Greenfield Additives (South Africa), DHT‑4A, and Alcamizer 1 were supplied by Kisuma Chemicals (Netherlands) while Sorbacid 944, Sorbacid 911, and Hycite 713 were supplied by Clariant (Germany). Analytical grade acetonitrile and acetic acid that were used as the mobile phase in High Performance Liquid Chromatography (HPLC) were procured from Sigma Aldrich (South Africa). Phenol used to prepare the synthetic phenolic wastewater was obtained from Merck (South Africa). Sodium hydroxide used for pH adjustment was also procured from Sigma Aldrich. Ultrapure water from an Elga Purelab Flex 3 was used for all the experiments.

3.1.2 Calcination

Calcination was conducted in an Aluminium Electric Muffle furnace. The furnace was pre-heated to the desired temperature before charging the sample. The samples weighing *ca*. 20 g were placed in porcelain crucibles before charging into the furnace at a pre-set temperature for 4 h. The operating temperatures were 250 °C, 500 °C and 1100 °C. Upon completion of the 4 h residence time, the crucibles were discharged from the furnace and covered with a lid to avoid sorption of any gases or moisture. The residues were collected for further analyses and phenol adsorption tests upon cooling.

3.1.3 Characterisation of clays and solution analysis

3.1.3.1 X-ray diffraction (XRD)

The composition and phases of the clays were determined using a PANalytical X'Pert Pro powder diffractometer in θ–θ configuration with an X'Celerator detector and variable divergence, and fixed receiving slits with Fe filtered Co-Kα radiation (λ=1.789 Å). Samples were prepared according to the standardised Panalytical backloading system that provides for

near-random distribution of the particles. Data was collected in the angular range from 5° to 90° 2θ with a step size of 0.008° 2θ and 13 s scan step time. The mineralogy was determined by selecting the best–fitting pattern from the Inorganic Crystal Structure Database (ICSD) to the measured diffraction pattern, using X'Pert Highscore plus software.The crystal lattice parameters can be estimated using the Equations (3-1) - (3-4)

$$d_{003} = \frac{N\lambda}{2\mathrm{Sin}\theta} \tag{3-1}$$

$$c = \frac{1}{3}(3d_{003} + 6d_{006} + 9d_{009}) \tag{3-2}$$

$$a = 2d_{110} \tag{3-3}$$

$$L_{003} = \frac{K\lambda}{\beta\mathrm{Cos}\theta} \tag{3-4}$$

Where:

d_{003} = layer distance at plane (003) (Å)

c= layer thickness (Å)

a = density of metal-ion stacking (Å)

L_{003} = crystallite size in the direction parallel to plane (003) (Å)

λ = wavelength (Å)

θ = angle of incidence (°)

N=order of the spectrum (dimensionless)

β = line broadening at half maximum (FWHM) of the diffraction peak (°)

3.1.3.2 X-ray fluorescence (XRF)

The Thermo Fisher ARL Perform'X Sequential XRF instrument with Uniquant software was used for elemental analysis. The software is capable of analysing all elements in the periodic table between sodium (Na) and uranium (U), however, only elements found above the detection limits were reported. One (1) g of the sample was mixed with 6 g Lithiumteraborate flux and fused at 1050 °C to make a stable fused glass bead. The samples were roasted in alumina refractory crucibles at 1000 °C to determine loss on ignition (LOI).

3.1.3.3 Thermal stability analysis

The thermal phase transitions of the clay samples were tracked by weighing ca. 10 mg of samples into alumina crucibles before running the samples on a TA instrument, Q5000 thermogravimetric analyzer (TGA). All the samples were subjected to a temperature scan

from 25 °C to 950 °C at a heating rate of 10 °C min^{-1} under a nitrogen flow rate of 50 ml min^{-1}.

3.1.3.4 Fourier transform infrared (FTIR) spectroscopy

Identification of the main functional groups and anions in the clay was done on a Perkin Elmer 100 Spectrophotometer. The instrument was equipped with a MIRacle attenuated total reflection (ATR) attachment which had a zinc-selenide (ZnSe) crystal plate. Background data of the sample holder was collected prior to sample runs. A powdered sample weighing ca. 20 mg was placed onto the crystal plate and pressed by lowering down the pressure arm until the force gauge was ca. 80 before data could be collected. The spectra were recorded between 550 cm^{-1} to 4000 cm^{-1} at a resolution of 2 cm^{-1} with data collected over 32 scans. The crystal plate was cleaned with acetone after acquisition of each spectrum.

3.1.3.5 Brunauer-Emmet-Teller (BET)

The specific surface areas were determined by the nitrogen (N_2) adsorption-desorption method using a Micrometrics Tristar 3000 BET analyzer at -196 °C (77 K), nitrogen's boiling point. All samples were degassed for 24 h at 100 °C to remove any moisture or dissolved gases prior to analysis. Degassing was done under a 10^{-5} Torr vacuum.

3.1.3.6 Scanning electron microscopy (SEM)

The average particle size and morphology of the clays were analysed using scanning electron microscopy (SEM). The images were obtained using a Zeiss Ultra Plus scanning electron microscope. SEM samples were prepared by distributing the clay samples on a carbon tape stuck to a microscopy stub, the samples were then sputter-coated with carbon under argon gas. The micrographs were taken at 3 kV.

3.1.3.7 High-performance liquid chromatography (HPLC)

The feed and residual phenol concentrations in solutions were analysed by a Waters HPLC (Waters 2695 separation module) with a photo diode array (PDA), Waters 2998 PDA detector. Separation was done in a Waters PAH C18 (4.6 ×250 mm, 5 μm) column while Empower software was used for data analysis. The two solvents that made up the mobile phase were, solvent A consisting of 1% acetic acid in water, and solvent B consisting of 1% acetic acid in acetonitrile. Phenol elution was done through a mixture containing 30% solvent A and 70% solvent B with operating conditions, as listed in Table 3-1. Phenol concentration was determined from calibration curves of prepared standards (the calibration curve is

attached in Appendix A). The separation column was conditioned for 5 min, purged for 13 min, and equilibrated for 5 min before sample sets were analysed; this was done to remove any contaminants from the column.

Table 3-1: HPLC operating conditions

Parameter	Value
Flowrate	1.2 mL min^{-1}
Injection volume	5 μL
Column temperature	30 °C
Wavelength	280 nm

3.1.4 Adsorption studies

3.1.4.1 Assessment of commercial clays for phenol adsorption

The first set of phenol adsorption experiments involved the screening of the six commercial clays. The clays were used as received (neat) by contacting 1 g of each clay material with 100 mL of 40 mg L^{-1} synthetic phenol solution in a 250 mL glass reactor with a lid; this resulted in a clay loading of 10 g L^{-1}. The suspensions were stirred continuously for 108 h to allow for maximum adsorption with samples taken after every 24 h. The suspensions were then centrifuged at 9000 rpm for 10 min; the centrate was further polished by filtering through a 0.45 μm Millipore filter. The resulting filtrate was taken for phenol analysis using the HPLC. Phenol adsorption efficiencies were determined as shown in Equation 3-5. The spent solids (after adsorption) were left to dry at ambient temperature, after which they were pulverised and submitted for further analyses. Based on the initial clays assessment results, the three best performing clays were identified, modified through calcination and evaluated for phenol adsorption.

$$R_{\mathrm{P}} = \left(1 - \frac{C_{\mathrm{t}}}{C_0}\right) \times 100 \qquad (3\text{-}5)$$

Where:

R_{P} = phenol removal efficiency (%)

C_0 = feed concentration of phenol (mg L$^{-1)}$)

C_{t} = phenol concentration at time t (mg L^{-1})

3.1.4.2 Evaluation of calcination temperature

Based on the results from screening experiments, as detailed in Section 3.1.4.1, the three best performing clays were calcined at 500 °C and evaluated for phenol adsorption. The clay with the highest phenol removal from the three was further calcined at 250 °C and 1100 °C (as detailed in Section 3.1.2) to establish the optimum calcination temperature. Further adsorption tests were conducted using the best performing clay calcined at optimum temperature.

3.1.4.3 Determination of optimum clay loading

Having established the best performing clay and optimum calcination temperature (as detailed in Section 3.1.4.2), the optimum clay loading was determined by evaluating loadings of 5 g L^{-1}, 10 g L^{-1}, 15 g L^{-1} and 20 g L^{-1} This was done by contacting 0.5 g, 1 g, 1.5 g and 2 g of calcined clay with 100 mL of 40 mg L^{-1} synthetic phenol solution in a 250 mL glass reactor over 24 h. The purpose of varying the adsorbent loading was to increase the adsorption sites.

3.1.4.4 The effect of initial pH of solution on phenol adsorption rate

The effect of solution pH was investigated by adjusting the synthetic wastewater to a pH of 9 and 12 from a pH of 6.75 ±0.05 using a 1 M NaOH solution prior to running of adsorption tests. No pH adjustments were done when conducting adsorption tests with an initial pH of 7. There were no experiments conducted in the acidic pH range since it is known to damage the structure of the LDH clay (Gong *et al.,* 2013; Grover *et al*., 2019; Zhang *et al.,* 2017). The adsorption tests were conducted with clay calcined at optimum temperature and optimum clay loading.

3.1.4.5 Establishment of phenol adsorption mechanism

One of the special features of LDH clays is their ability to reconstruct after calcination and upon contact with an aqueous solution (Forano *et al*., 2013). CLDH clays have been shown to have a high anion uptake during the reconstruction process (Lupa *et al*., 2018). In order to establish the phenol adsorption mechanism, tests were conducted with optimum conditions, as indicated in Sections 3.1.4.1 to 3.1.4.4. Both solution and solid samples were taken every 2 h for 24 h. The solution samples were analysed for phenol using HPLC to establish the adsorption kinetics, while the solid samples were analysed for crystallinity and phase identification through XRD. The interlayer spacing (d) was calculated using Bragg's law

(Equation 3-1) for each time interval to establish the degree of intercalation in the reformed clay.

3.1.4.6 Determination of phenol adsorption isotherm

The effect of pollutant concentration was determined by varying the initial phenol concentrations as follows: 20 mg L^{-1}, 40 mg L^{-1}, 80 mg L^{-1}, 120 mg L^{-1} and 200 mg L^{-1} while maintaining an adsorbent loading of 10 g L^{-1}. The experiments were conducted at 25°C, 35°C, 45°C and 65°C over 24 h. Phenol adsorption capacities were calculated using Equation 3-6 and fitted to the Langmuir, Freundlich and Temkin isothermal models.

$$q_e = \frac{V}{m}(C_0 - C_e) \hspace{2cm} (3\text{-}6)$$

Where:

C_e = phenol equilibrium concentration (mg L^{-1})

m = mass of adsorbent (g)

V = volume of solution (L)

3.1.4.7 Modelling of phenol adsorption kinetics

Once the optimum conditions were determined, adsorption tests were carried out under these conditions, and samples were taken on an hourly basis for the first two hours, and every 2 h thereafter for 24 h to investigate the kinetics. The adsorption kinetics were evaluated at 25°C, 35°C, 45°C and 65°C.

3.1.4.8 Evaluation of thermodynamic studies

Thermodynamic analysis can provide the quantitative relationship between the amount of pollutant adsorbed and the heat of adsorption. Myers and Monson (2014) reported that the driving forces of mass transfer, such as molecular interactions between adsorbents and adsorbates, selectivity, heats of adsorption and the difference between the actual and equilibrium chemical potentials can be explained through this analysis. Using the data obtained from Section 3.1.4.6, thermodynamic equilibrium constants (K_a) were determined, as shown in Equation 2-16 while the change in Gibbs free energy ($\Delta G°$) was calculated as indicated by Equation 2-17 for all the evaluated temperatures. The change in enthalpy ($\Delta H°$) and change in entropy ($\Delta S°$) were determined from the slope and intercept of a linear plot of ln (K_a) against $1/T$ respectively.

3.1.4.9 Clay's regeneration and reusability studies

Recycling and reusability of an adsorbent is an important aspect for the viability of the adsorption process. Adsorption experiments on the best performing clay at optimum conditions were conducted with a higher volume to obtain a substantial amount of residues for proceeding tests. In order to make a clay loading of $10\ g\ L^{-1}$, 15 g of calcined clay was contacted with 1.5 L synthetic wastewater; the suspensions were mixed for 24 h. The suspensions were then centrifuged as indicated in Section 3.1.4.1, a portion of the centrate was refined by filtration with a 0.45 μm Millipore filter prior to phenol analysis with HPLC. The solid residues were dried in air at an ambient temperature; a portion of the residues was re-calcined at 500 °C under the same procedure as stated in Section 3.1.2 for use in the second cycle of regeneration and reusability studies. The other portion of the residues was submitted for characterisation, as detailed in Section 3.1.3. The cycles were repeated until phenol adsorption efficiency showed a significant decrease.

3.2   In-house synthesised clays

3.2.1   Materials

Magnesium chloride hexahydrate ($MgCl_2 \cdot 6H_2O$), aluminium chloride hexahydrate ($AlCl_3 \cdot 6H_2O$), and zinc chloride ($ZnCl_2$), which were used for preparations of salts solutions to synthesise LDH clays, were procured from Glassworld (South Africa). Anhydrous sodium carbonate (Na_2CO_3) which was used as a source of interlayer carbonate during LDH synthesis was also purchased from Glassworld, while the sodium hydroxide (NaOH) used for pH adjustment was procured from Merck (South Africa). Ultrapure water from an Elga Purelab Flex 3 was used for all the experiments.

3.2.2   Clay synthesis

A range of LDH clays were synthesised using the co‑precipitation method at a constant pH of 10 to suppress the formation of metal hydroxides (Rives, 2001; Tian *et al*., 2016). The required amounts of metal salts were dissolved in ultrapure water to form a 1 M solution based on cations; this was prepared to a total volume of 250 mL. The salt solutions were prepared in such a way that the divalent to the trivalent metal ratio (M^{2+}/M^{3+}) lies between 2 to 4 while varying the amount of Mg^{2+} and Zn^{2+} as shown in Table 3-2. Synthesised clays were named as $Mg_xZn_yAl_z$ with x, y and z indicating the molar ratio of Mg, Zn and Al respectively. The salt solutions were added slowly into a 1 L glass reactor containing 250 mL of 1 M Na_2CO_3 solution, which had been pre-heated to 60 °C. The pH of the slurry was kept

42

at 10 ± 0.5 by adding 2 M NaOH solution. The resulting slurry was vigorously stirred at 500 rpm with the temperature kept at 60 °C over a period of 24 h. A Daihan Scientific magnetic stirrer (MSH-20D) with a hot plate and temperature controller was used for mixing and controlling temperature of the reactor contents. The schematic diagram of the reactor setup for LDH clay synthesis is shown in Figure 3-1. Upon completion of the reaction, the suspensions were allowed to cool to an ambient temperature before centrifuging at 9000 rpm for 10 mins at 20 °C. The precipitates were then washed three times with excess ultrapure water before drying in an oven at 50 °C for 12 h. The dried precipitates were pulverised before application in phenol adsorption from wastewater.

Table 3-2: Metallic compositions for LDH synthesis

Clay	Target mol (%)			M^{2+}/M^{3+}
short name	Mg	Zn	Al	
$Mg_{0.8}Al_{0.2}$	80	0	20	4
$Mg_{0.6}Zn_{0.2}Al_{0.2}$	60	20	20	4
$Mg_{0.4}Zn_{0.4}Al_{0.2}$	40	40	20	4
$Mg_{0.75}Al_{0.25}$	75	0	25	3
$Mg_{0.5}Zn_{0.25}Al_{0.25}$	50	25	25	3
$Mg_{0.25}Zn_{0.5}Al_{0.25}$	25	50	25	3
$Zn_{0.75}Al_{0.25}$	0	75	25	3
$Mg_{0.67}Al_{0.33}$	67	0	33	2
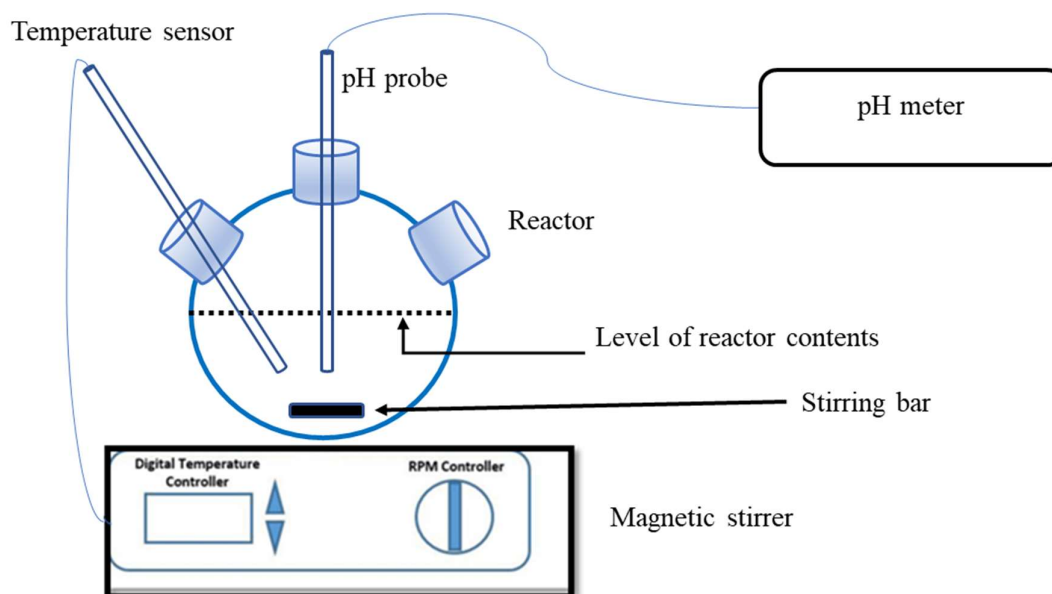
Figure 3-1: Schematic diagram of a reactor setup for LDH clay synthesis

3.2.3 Calcination

The furnace was pre-heated to the desired temperature before charging the sample. The samples weighing ca. 20 g were placed in porcelain crucibles before charging into the furnace at a pre-set temperature for 4 h. Calcination on in-house synthesised clays was done at 250 °C, 300 °C, 350 °C, 400 °C, 450 °C, 500 °C and 1100 °C. Upon completion of the 4 h residence time, the porcelain crucibles were discharged from the furnace and closed with a lid to avoid sorption of any gases or moisture. The residues were collected for further tests and analyses upon cooling.

3.2.4 Characterisation of clays and solution analysis

Characterisation of the clays and analysis of solution samples were conducted as indicated in Section 3.1.3.

3.2.5 Adsorption studies on in-house synthesised clays

3.2.5.1 Assessment of clays compositions for phenol adsorption

The effect of the clays' metallic composition on phenol adsorption was evaluated by testing the clays as synthesised and after calcination at 500 °C. The tests were conducted at a clay loading of 10 g L^{-1} over 24 h. The suspensions were further processed as detailed in Section 3.1.4.1. Phenol adsorption efficiencies were determined, as shown in Equation 3-5. The best

performing clay was further assessed for optimum calcination temperature, equilibrium isotherms, adsorption kinetics and thermodynamics studies.

3.2.5.2 Evaluation of calcination temperature

Having established the best performing clay, it was further calcined as detailed in Section 3.2.3; the residues were tested using the same method as in Section 3.2.5.1. Further experiments were conducted with clays calcined at the optimum temperature.

3.2.5.3 Determination of phenol adsorption isotherm

Isothermal equilibrium studies were conducted, as detailed in Section 3.1.4.6, using the synthesised clay calcined at optimum temperature.

3.2.5.4 Modelling of phenol adsorption kinetics

Kinetics studies were conducted, as indicated in Section 3.1.4.7; however, only two temperatures were evaluated namely, 25°C and 65°C. This was to compare the highest and lowest operational temperatures for phenol adsorption using commercial and in-house synthesised clays.

3.2.5.5 Evaluation of thermodynamic studies

Thermodynamic analysis was conducted, as indicated in Section 3.1.4.8, using data from Section 3.2.5.3.

4   CHARACTERISATION AND APPLICATION OF COMMERCIAL CLAYS

4.1   Crystallinity and phase identification of commercial clays

4.1.1   The effect of impurities on hydrotalcite crystallinity

Qualitative and quantitative X-ray diffraction (XRD) analyses were conducted, as indicated in Section 3.1.3.1. The XRD patterns for DHT‑4A, GF‑450 and Sorbacid 944 are shown in Figure 4-1. The 2θ values for the basal planes (110), (009), (006) and (003), crystallite sizes and parameters are presented in Table 4-1 (the figures showing the positions of the basal planes are displayed in Appendix B). The crystal lattice parameters were estimated using Equations (3-1) - (3-4). Sorbacid 944 displayed narrow reflections and was quantified to contain a pure hydrotalcite. The presence of symmetric, intense and sharp diffractograms at low 2θ values corresponding with less intense and asymmetric diffractograms at higher 2θ values indicated higher orderliness and crystallinity of the clay (Gevers *et al*., 2019). DHT‑4A also displayed narrow reflections; however, it was quantified to contain ca. 94% hydrotalcite and 6% boehmite (AlO(OH)) The layer distances for Sorbacid 944 and DHT‑4A were estimated to be 7.58 Å and 7.61 Å respectively. The slight difference in interlayer distances between the two clays can be due to the presence of a significant amount of water in DHT‑4A than in Sorbacid 944. The crystal lattice parameters, c and a were determined to be 22.92 Å and 3.05 Å for both clays. These values correspond with those reported in the literature with crystallite parameter (a) ranging between 3.04 Å and 3.12 Å (Cavani *et al*., 1991; Forano *et al*., 2006). The average crystallite size in the direction parallel to plane (003) for Sorbacid 944 was estimated to be 281.5 Å which is equal to the value reported by Hibino (2018) for MgAl-CO$_3$ LDH. DHT‑4A had crystallite size in the direction parallel to plane (003) of 211 Å indicating lower crystallinity when compared to Sorbacid 944. This is due to the presence of a significant amount of boehmite that led to a decrease in crystallinity of the clay (Theiss, 2012). Clay GF‑450 was quantified to contain hydrotalcite (65%), calcite (25%), quartz (4%), gibbsite (3%) and nordstrandite (3%). The layer distance was estimated to be 7.58 Å similar to that of Sorbacid 944. The other crystal lattice parameters were not determined as the hydrotalcite peaks were overlapped by those of the impurities.
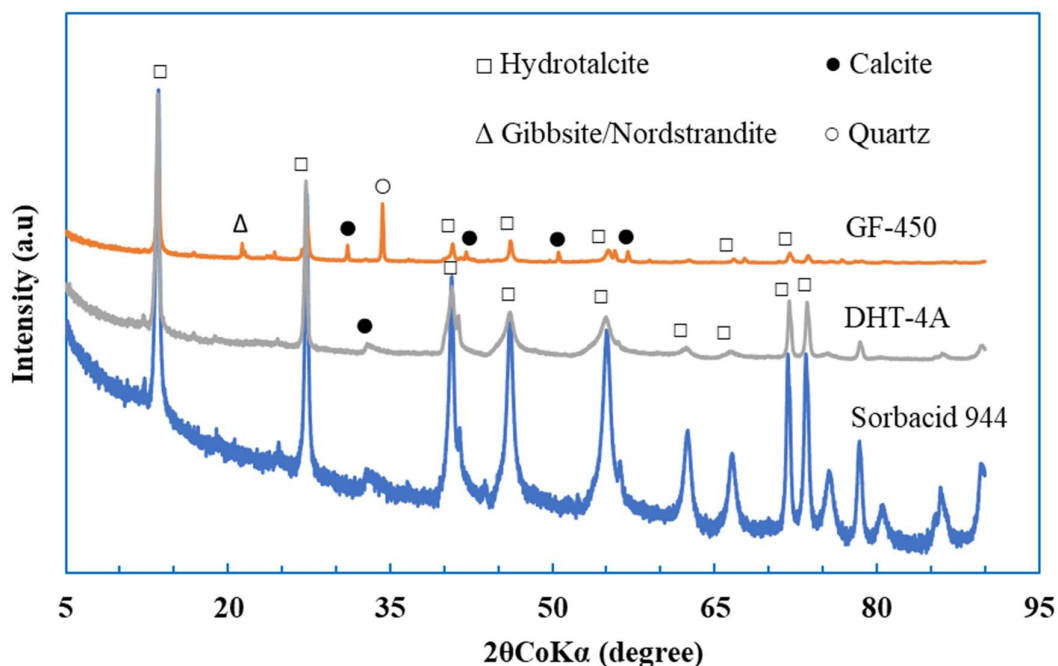
Figure 4-1: X-ray diffraction peaks for DHT- 4A, GF‑450 and Sorbacid 944

Table 4-1: Crystallite parameters for commercial clays

Sample name	Alcamizer	DHT‑4A	GF‑450	Hycite 713	Sorbacid 911	Sorbacid 944
$2\theta(003)(°)$	13.61	13.50	13.55	13.50	13.50	13.55
$2\theta(006)(°)$	27.40	27.20	-	27.30	27.25	27.30
$2\theta(009)(°)$	40.78	40.73	-	40.75	40.75	40.50
$2\theta(110)(°)$	72.00	71.90	72.00	71.90	71.90	71.80
d(003)(Å)	7.55	7.61	7.58	7.61	7.61	7.58
c (Å)	22.80	22.93	-	22.90	22.91	22.92
a (Å)	3.04	3.05	3.04	3.05	3.05	3.05
L(003)(Å)	238.22	221.18	221.19	232.24	221.18	281.52

4.1.2   Comparison between hydrotalcite and quintinite

The XRD patterns for Alcamizer, Hycite 713 and Sorbacid 911 are displayed in Figure 4-2. The 2θ values for the basal planes (110), (009), (006) and (003), crystallite sizes and parameters are presented in Table 4-1 (the figures showing the positions of the basal planes are displayed in Appendix B). Sorbacid 911 was quantified to contain 98.8 % hydrotalcite,

47

0.7 % calcite and 0.5% quartz. Hycite 713 was quantified to contain 99.4% hydrotalcite and 0.6% calcite, while Alcamizer was established to be a pure quintinite. The crystal lattice parameters for Sorbacid 911 and Hycite 713 were similar with c and a values of 22.9 Å and 3.05 Å. The layer distance in both clays was estimated to be 7.61 Å, which is higher than that of Sorbacid 944. Sorbacid 911 had a lower average crystallite size of 221 Å compared to 232 Å for Hycite 713 due to higher impurity contents in Sorbacid 911. The layer distance for Alcamizer was established to be 7.55 Å, which was lower compared 7.61 Å for the other two clays. This can be attributed to reduced water content in quintinite ($Mg_4Al_2(OH)_{12}CO_3 . 3H_2O$) compared to hydrotalcite ($Mg_6Al_2(OH)_{16}CO_3 . 4H_2O$). The crystallite size in the direction parallel to (003) plane for Alcamizer was estimated to be 238 Å, which was higher than that of Sorbacid 911 (221 Å) and Hycite 713 (232 Å). This meant that Alcamizer was highly crystalline compared to the other two clays.
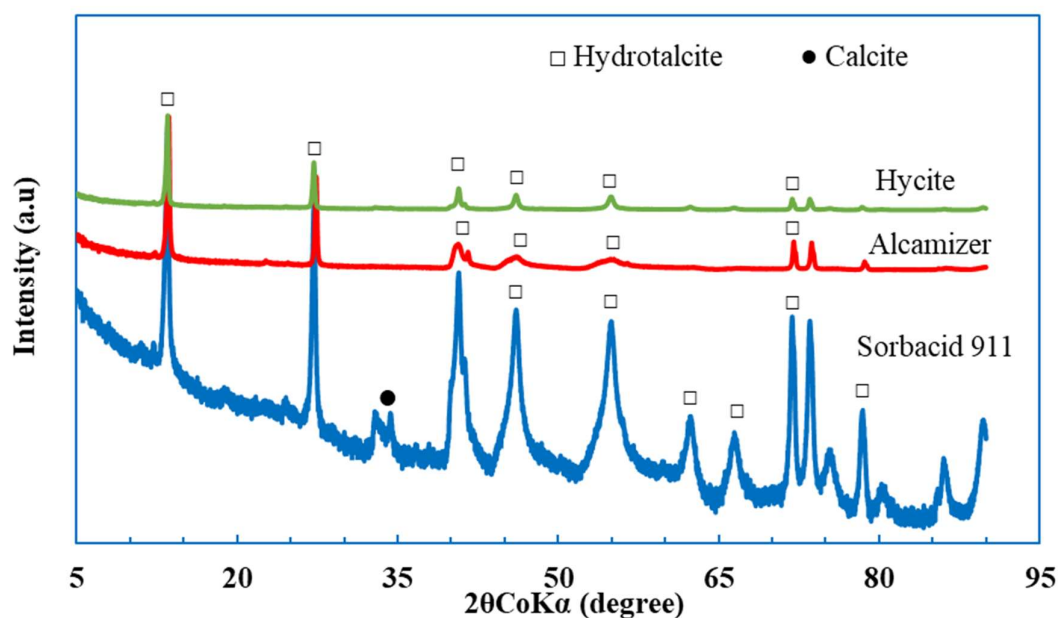
Figure 4-2: X-ray diffraction peaks for Alcamizer, Hycite 713 and Sorbacid 911

4.1.3   Phase identification on calcined Sorbacid 944

Figure 4-3 shows the XRD spectra for Sorbacid 944 treated at various calcination temperatures. The XRD spectra of the residues after 250 °C were aligned with those of the neat clay even though they were withered and displayed signs of reduced crystallinity. A significant change was apparent in the (003) plane; this was due to the partial loss of

interlayer and surface water, and interlayer molecules indicating the beginning of transformation to MMO (Milanovic, 2016).

The periclase (MgO) and spinel (MgAl$_2$O$_4$) phases were established to be the dominant phases for the clays calcined at 500°C and 1100°C. The residues after calcination at 500 °C were more amorphous and had the periclase and spinel distribution of 59% and 41%, respectively. Periclase content of the highly crystalline residues obtained after calcination at 1100 °C was lower by 20-39% in comparison to the residues after calcination at 500 °C; the spinel content had increased by the same magnitude to 61%. This is in line with the studies conducted by Milanovic (2016) who reported that calcination of LDH clays at temperatures above 850 °C leads to a significant increase in the spinel content and highly crystalline residues. The XRD spectra for calcined DHT‑4A and GF‑450 are displayed in Appendix B.
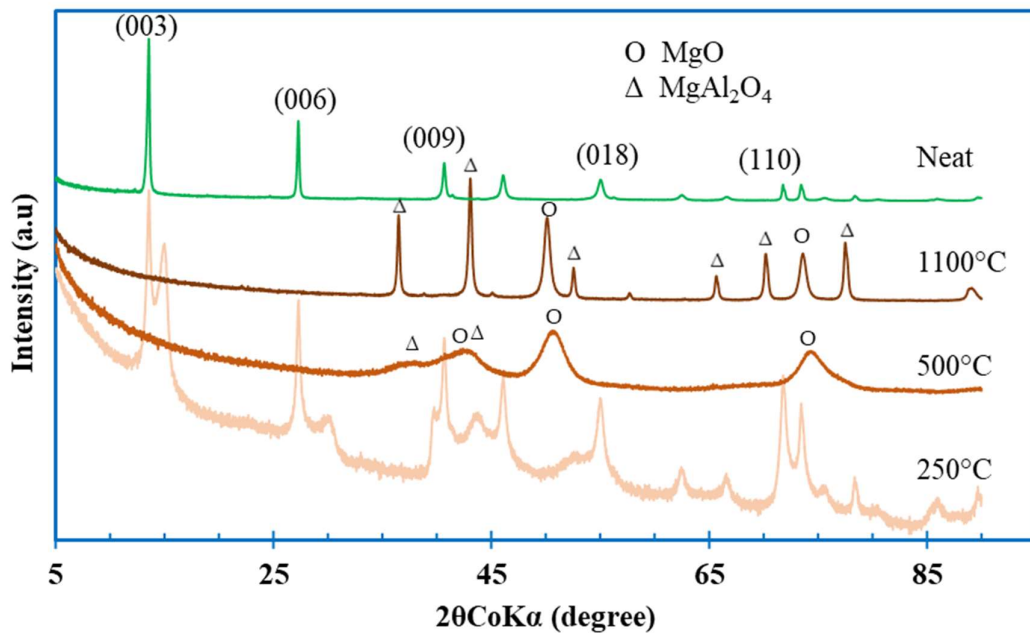
Figure 4-3: X-ray diffraction peaks for calcined Sorbacid 944

4.2 Elemental analysis

Table 4-2 shows the elemental compositions (wt/wt) of the neat clays. Alcamizer, DHT‑4A, Hycite and Sorbacid 911 had an Mg content of ca. 37 %, while GF‑450 and Sorbacid 944 had Mg contents of 24% and 23% respectively. The Al contents for all the clays ranged between 16% and 20% with Sorbacid 944 containing the least. Sorbacid 944 and GF‑450 had triple metallic contents of Mg-Zn-Al and Mg-Ca-Al respectively. GF‑450 had a significant amount of Si (7%) compared to other clays which had less than 0.7% Si. The loss on ignition (LOI) for all the clays ranged between 38% and 45%, which is within the range of mostly reported values (39-46%) in literature (Harizi *et al*., 2019). The divalent to trivalent molar ratios ($M^{2+}/M^{3+)}$) for Alcamizer, DHT‑4A, Hycite, Sorbacid 911 and Sorbacid 944 were between 2 and 2.3, which falls within the limits (2 to 4) for LDH clays (Zhao *et al*., 2002). GF‑450 had a molar ratio of less than 2 at 1.8; furthermore, it shows the presence of other phases other than hydrotalcite, such as calcite ($CaCO_3$) and gibbsite ($Al(OH)_3$).

Based on the XRD and XRF analyses, the chemical formulae of the neat clays were postulated as shown in Table 4-3. The hypothesised formulae correlated with the limits for each clay as set out by the respective manufacturers. GF‑450 contained a substantial amount of impurities, therefore, no chemical formula was proposed for it.

Table 4-2: Elemental compositions of the commercial LDH clays

Element	Mass (%)					
	Alcamizer	DHT‑4A	GF‑450	Hycite 713	Sorbacid 911	Sorbacid 944
Mg	35.56	36.48	24.31	36.36	36.88	22.99
Zn	0.01	0.01	0.01	0.02	0.01	19.07
Al	19.58	18.24	19.50	17.58	18.25	15.62
Na	0.01	0.01	0.01	0.20	0.01	0.01
Si	0.07	0.01	6.93	0.06	0.07	0.01
Ca	0.03	0.02	10.72	0.27	0.33	0.01
S	0.05	0.01	0.01	0.04	0.05	0.01
Cr	0.02	0.02	0.02	0.01	0.02	0.01
K	0.01	0.01	0.01	0.01	0.01	0.01
Nb	0.01	0.01	0.01	0.01	0.01	0.01
Fe	0.01	0.01	0.01	0.02	0.01	0.01
LOI	44.60	45.10	38.41	45.37	44.30	42.10
Total	**99.97**	**99.93**	**99.95**	**99.94**	**99.95**	**99.86**
Molar ratio (M^{2+}/M^{3+})	**2.00**	**2.20**	**1.80**	**2.30**	**2.20**	**2.10**

Table 4-3: Postulated formulae for commercial neat clays

| Clay name | Molar ratio (M^{2+}/M^{3+}) | | Chemical formula |
	XRF	manufacturer	
Alcamizer 1	2.0	1.8 - 2.3	$Mg_4Al_2(OH)_{12.1}CO_3.nH_2O$
DHT‑4A	2.2	1.5 - 2.3	$Mg_{4.4}Al_2(OH)_{12.9}CO_3.nH_2O$
Hycite 713	2.3	1.5 - 2.6	$Mg_{4.6}Al_2(OH)_{13.2}CO_3.nH_2O$
Sorbacid 911	2.2	2.0 - 3.0	$Mg_{4.4}Al_2(OH)_{12.8}CO_3.nH_2O$
Sorbacid 944	2.1	2.0 - 4.0	$Mg_{3.27}ZnAl_2(OH)_{12.8}CO_3.nH_2O$

4.3 Thermal stability

4.3.1 The effect of impurities on hydrotalcites thermal stability

Thermal analyses for Sorbacid 944, DHT‑4A and GF‑450 are shown in Figure 4-4 (a) - (d). LDH clays are expected to undergo a two-stage thermal decomposition; the initial stage occurs when interlayer and surface water are desorbed below 225 °C followed by decomposition of interlayer anions (OH^- and CO_3^{2-}) and dehydroxylation of metal hydroxides at temperatures between 225 °C and 500 °C (Costa *et al*., 2008; Milanovic, 2016). The decomposition at higher temperatures can occur in two distinct steps when the M^{2+}/M^{3+} ratio is equal or higher than two (Zhao *et al*., 2002); the initial step is the partial loss of OH^- from hydroxide layers followed by the complete loss of OH^- and CO_3^{2-} (Cavani *et al*., 1991).

Sorbacid 944 showed a three-stage thermal decomposition, which correlates with the findings by Costa *et al*. (2008) and Milanovic (2016), for LDH clays with an M^{2+}/M^{3+} ratio of two. This is displayed in Figure 4-4(a) and (b). The maximum loss of surface and interlayer water occurred at 190 °C (13%) followed by the partial loss of OH^- from hydroxide layers at 250 °C (6%) until the complete dehydroxylation and decomposition of carbonate occurred at 410 °C. The complete removal of interlayer anions stage showed a wide peak indicating a slow process and had mass loss of ca. 21%. This made a cumulative mass loss for Sorbacid 944 to be 40%.

Figures 4-4 (a) and (c) display the TGA and derivative thermogravimetric (DTG) for DHT‑4A. The clay showed a three-stage thermal decomposition as expected for LDH clays (Costa *et al.*, 2008; Milanovic, 2016). Physiosorbed and interlayer water were removed up to 240 °C with mass losses of 14% (8% higher than that of Sorbacid 944); additional water content can be attributed to the presence of boehmite in DHT‑4A. The second decomposition stage occurred at 320 °C with a mass loss of 8%; this occurred at 70 °C higher than that of Sorbacid 944 due to the presence of boehmite and its conversion gamma-aluminium oxide (γ-Al_2O_3). Complete decomposition of interlayer anions and formation of γ-Al_2O_3 occurred at 420 °C with a mass loss of 21% resulting in a. cumulative mass loss of 43%.

Thermal analysis on GF‑450 showed five decomposition steps as indicated in Figures 4-4 (a) and (d). An 8% mass loss of physiosorbed and interlayer water occurred at 220 °C. The small endothermic peak at 250 °C with a mass loss of 3% can be attributed to partial dehydroxylation of gibbsite and formation of boehmite (, Hu *et al.*, 2018b; Redaoui *et al.*, 2017). This was followed by another endothermic peak at 312 °C (with a mass loss of 4%), which was caused by two processes, (i) conversion of gibbsite to χ-Al_2O_3 and (ii) continuous transformation of gibbsite to boehmite (Redaoui *et al.*, 2017). The 11% mass loss at 430 °C can be associated with dehydroxylation and carbonate decomposition within the hydrotalcite structure. The last peak at 690 °C can be attributed to the decomposition of calcite to CaO (Chang & Huang, 1997) and the complete conversion of boehmite to ɣ-Al_2O_3. The TGA and DTG profiles for Sorbacid 911, Alcamizer 1 and Hycite 713 were similar to those of DHT‑4A and are shown in Appendix C.
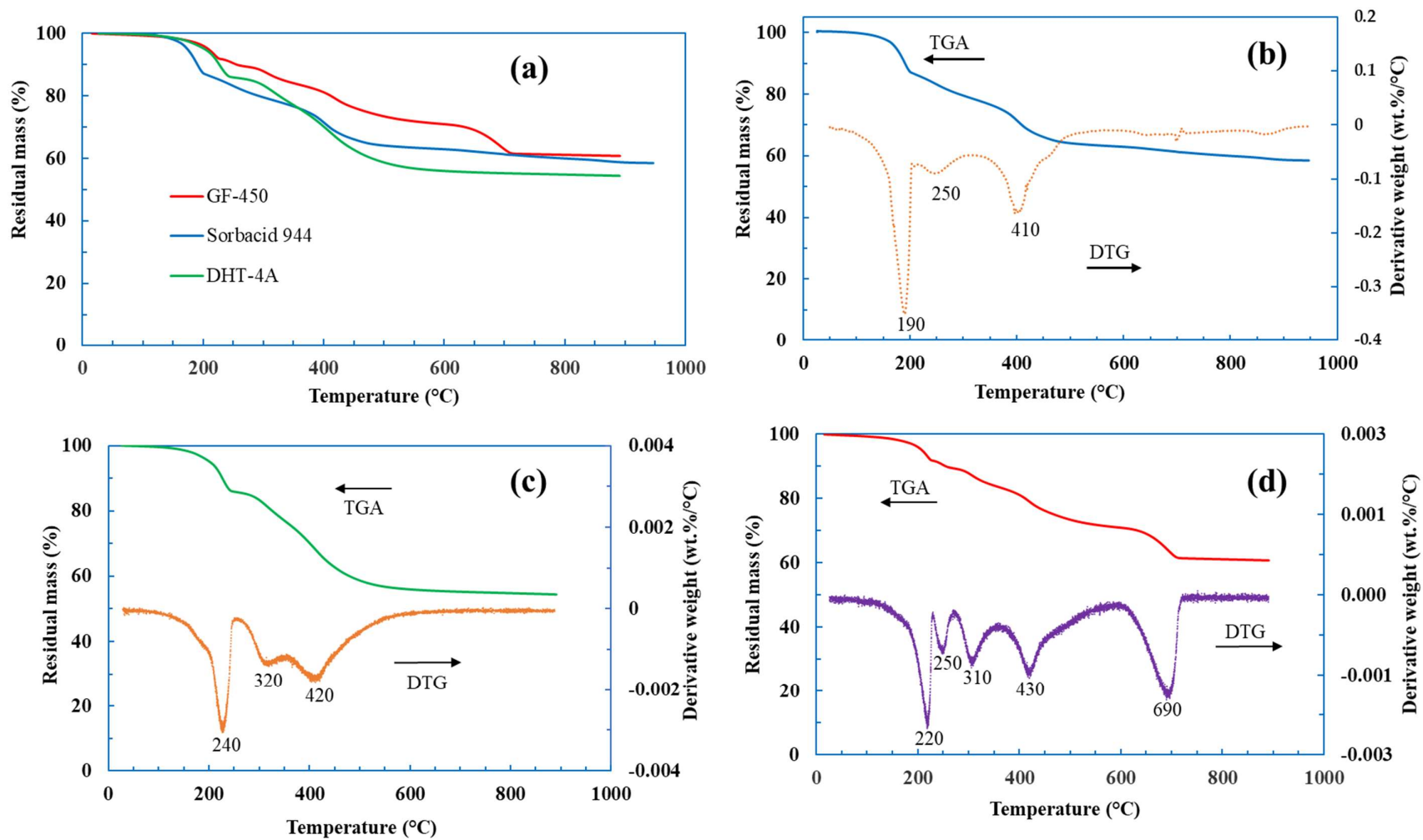
Figure 4-4: Thermogravimetric and derivative thermogravimetric curves for Sorbacid 944 (a) and (b), DHT‑4A (a) and (c) and GF‑450 (a) and (d)

4.3.2 Thermal stability of Sorbacid 944

Figures 4-5 (a) - (d) display the TGA and DTG for neat, calcined and spent Sorbacid 944. Decomposition of neat Sorbacid 944 occurred as detailed in Section 4.3.1. The loss of interlayer water in the spent clay occurred at 100 °C with an amount of 9% while dehydroxylation, decomposition of carbonate and any adsorbed phenol occurred at 345 °C (16%), as shown in Figures 4-5 (a) and (d). The shift in decomposition stages of spent clay to lower temperatures can be attributed to the reduced strength of hydrogen bonding, which is known to keep water molecules in close interaction with interlayer carbonate anions and hydroxide layers (Costa *et al*., 2008). The maximum weight loss for spent clay was low at 25% compared to 40% of neat clay; this was attributed to the spent clay containing an appreciable amount of the stable spinel ($MgAl_2O_4$) phase. The cumulative mass loss of ca.10% by the clay calcined at 500 °C can be attributed to physiosorbed water and other labile substances, since its structure had already been converted to metal oxides as displayed in Figures 4-5 (a) and (c). Any further increases in temperature were likely to alter the crystal phases of the metal oxides. Milanovic (2016) reported that the residues of a complete dehydroxylation and decomposition of interlayer carbonate anions were mainly periclase (MgO) and spinel ($MgAl_2O_4$) phases.
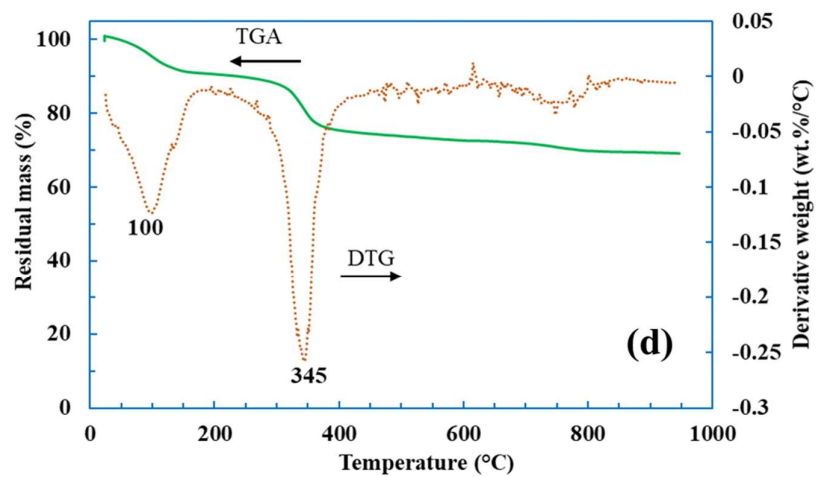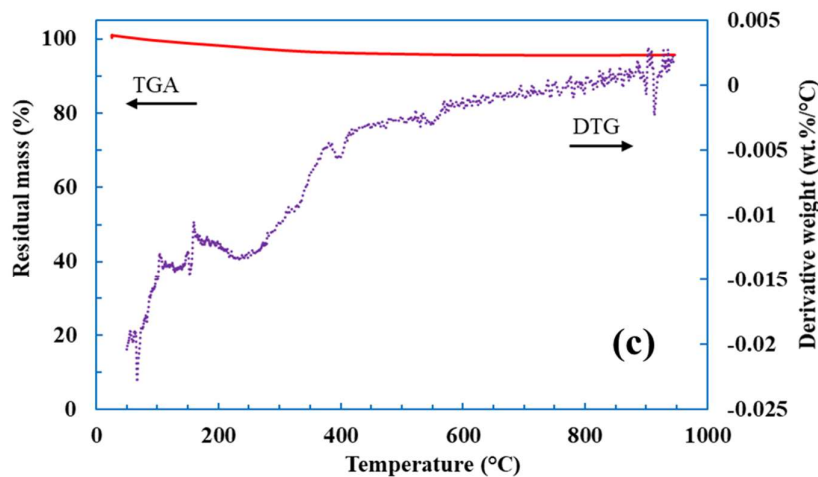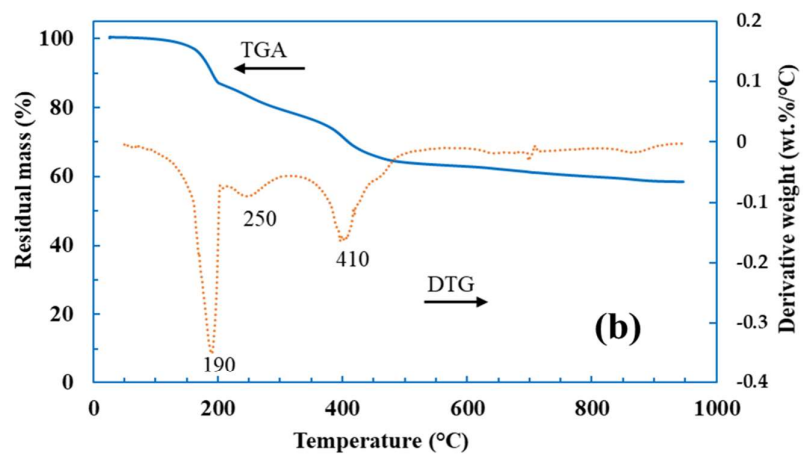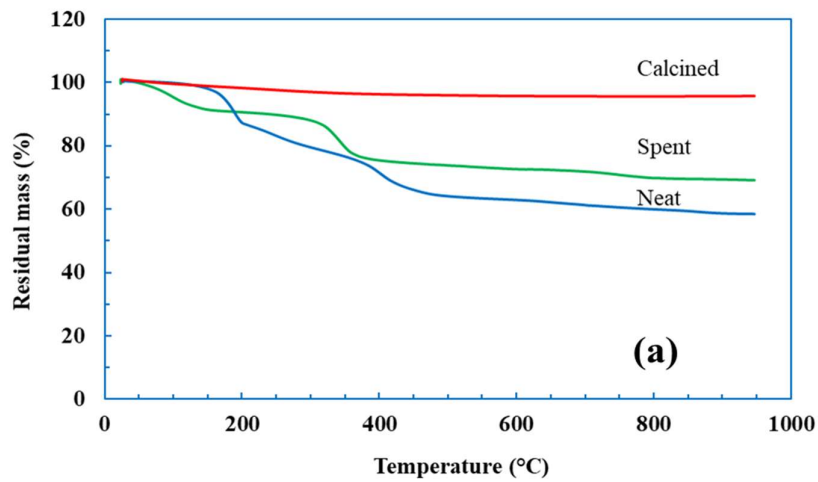
Figure 4-5: Thermal analyses for Sorbacid 944; neat (a) and (b), calcined (a) and (c) and spent (a) and (d)

56

4.4 Chemical bonds identification through infrared spectra

The infrared spectra for Sorbacid 944, DHT‑4A and GF‑450 are shown in Figures 4-6 (a) - (c). The peaks are displayed over a wavenumber range of 4000 cm^{-1} to 550 cm^{-1}. The clays showed a strong and broad peak at 3420 cm^{-1} which is correlated with the vibration of water molecules in the interlayer space (Bernardo & Ribeiro, 2018; Elmoubarki *et al*., 2017). The band at 1640 cm^{-1} can be associated with water deformation while the asymmetric stretching of the carbonate (CO_3^{2-}) ion in the interlayer corresponds to the band at 1365 cm^{-1}. The bands at 770 cm^{-1} and 640 cm^{-1} can be interpreted as out-of-plane stretching vibrations and in-plane bending of CO_3^{2-} ions (Lin *et* al., 2005; Narayanan & Krishna, 1998). This is due to the hydroxyl groups in the interlayer and brucite-like layers being restrained under electrostatic interactions (Schouten *et al*., 2007). The band at 935 cm^{-1} can be assigned to metal-oxygen vibration in the brucite-like layers.The infrared spectra for Alcamizer 1, Hycite 713 and Sorbacid 911 are shown in Appendix D.
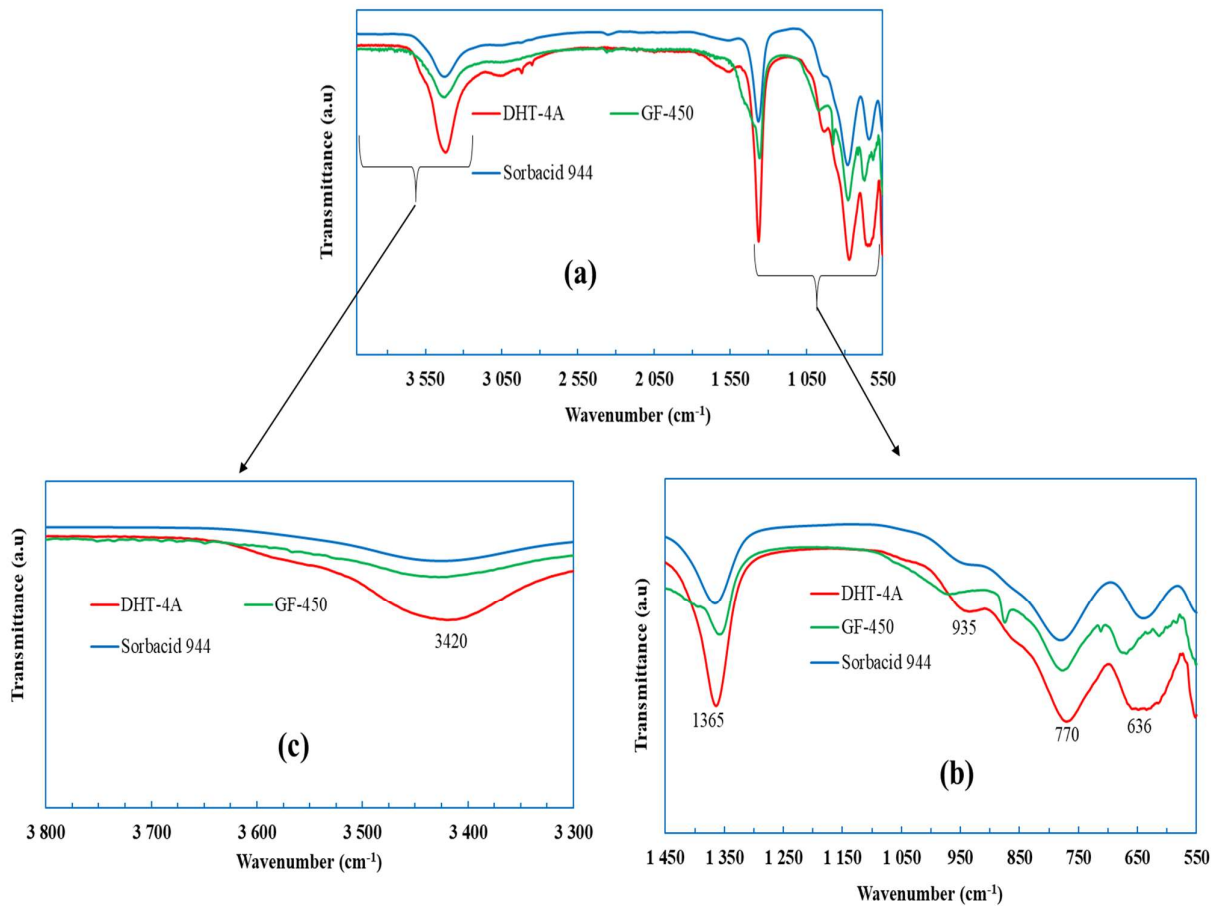
Figure 4-6: FTIR scans for DHT‑4A, GF‑450 and Sorbacid 944 at wavenumbers 4000-500 cm^{-1} (a), 1450-500 cm^{-1} (b) and 4000-3300 cm^{-1}(c)

4.5   Brunauer-Emmett-Teller specific surface area

The Brunauer-Emmett-Teller (BET) surface area results for the neat and calcined clays are shown in Table 4-4. Sorbacid 944, DHT‑4A and GF‑450 were the only clays to be calcined and evaluated further based on the phenol adsorption efficiencies of the neat clays. More than 200% increases in specific surface area for DHT‑4A and Sorbacid 944 were attained upon calcination of the clays while only 40% increase for GF‑450 was observed under the same conditions. The increase in BET surface area can be ascribed to the breakage of layered materials and the formation of MMO (Milanovic, 2016).

Table 4-4: BET surface areas for commercial clays

Clay	BET surface area ($m^2\,g^{-1}$)	
	Neat	**Calcined**
Alcamizer	12.0	-
DHT‑4A	4.3	15.1
GF‑ 450	17.5	24.4
Hycite 713	15.0	-
Sorbacid 911	15.0	-
Sorbacid 944	8.7	29.7

4.6   Clays morphologies and structures

Figures 4-7 (a) - (d) show the SEM micrographs for (a) GF‑450, (b) Alcamizer 1, (c) DHT‑4A and (d) Sorbacid 944. GF‑450's morphology was that of regular LDH clay in plate like structures. Alcamizer 1, and Sorbacid 944 displayed hexagonal-like shapes with microcrystals covering the entire DHT‑4A surface. Similar results were reported by Iqbal and Fedel (2018) who revealed that the presence of microcrystals was due to lower synthesis temperature and shorter aging time. The authors reported that pH 10, temperature of 60 °C and aging time of 24 h were optimum conditions to synthesise a well-developed MgAl LDH clay. Figure 4-8 (a)-(b) displayed the SEM micrographs for calcined and reconstructed Sorbacid 944 respectively. CLDH clay showed a non-uniform shape of particles that were poorly arranged. Reconstructed clay's SEM micrograph displayed both platelets structures and irregular agglomerated particles. The platelets structures are seemingly the reformed LDH particles, while irregular structures can be ascribed to agglomeration of unreactive spinel particles.
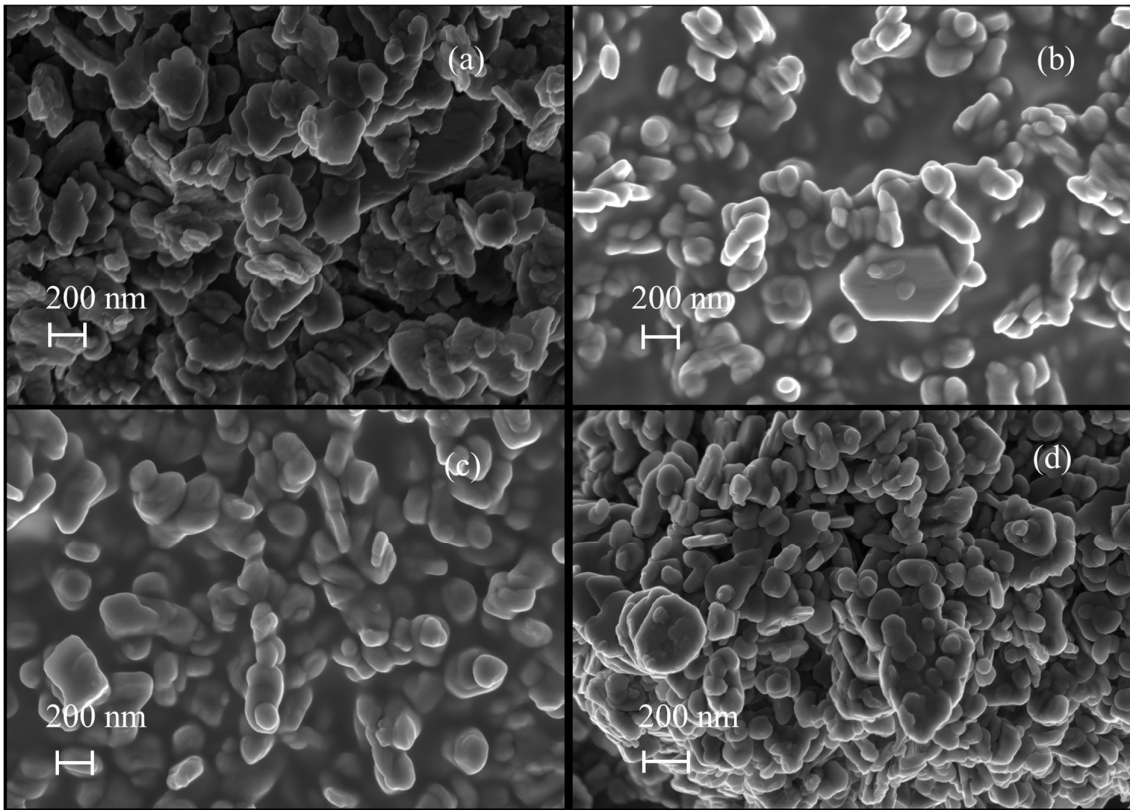
Figure 4-7: SEM micrographs for (a) GF‑450, (b) Alcamizer 1, (c) DHT‑4A and (d) Sorbacid 944
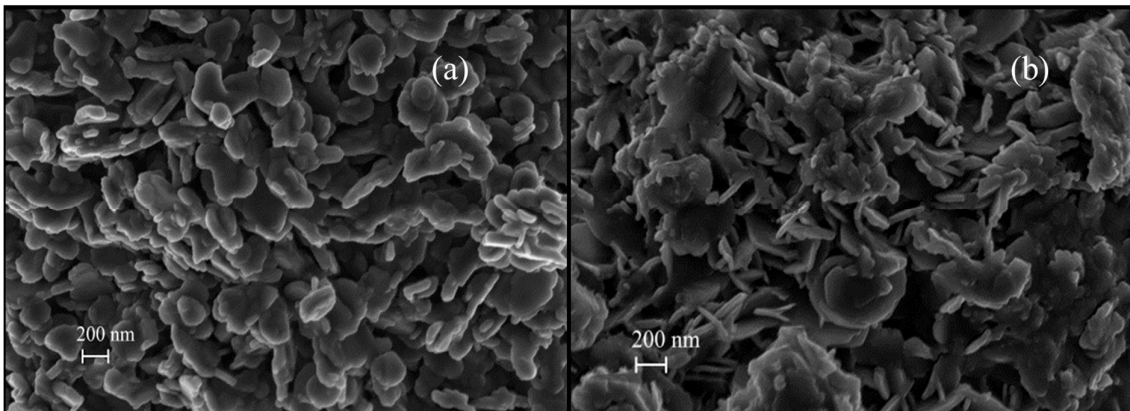
Figure 4-8: SEM micrographs for Sorbacid 944, (a) calcined and (b) reconstructed

4.7 Remediation of phenol contaminated water with commercial clays

4.7.1 Effect of clays compositions on phenol removal efficiencies

Figure 4-9 shows phenol adsorption efficiencies of the neat clays over 108 h residence time. GF‑450 and Sorbacid 944 showed better adsorption efficiencies of 9% and 6% respectively. DHT‑4A showed a phenol adsorption efficiency of ca. 3% while other clays were below 2%. Sorption of an organic solute from water is reliant on its affinity towards the solvent and/or sorbent (Delle Site, 2001). This is also related to the nature of the forces which exist between solute molecules and those of sorbent and solvent phases. Possible interactions between the adsorbate and adsorbent will depend on the nature of the adsorbent and physico-chemical features of the adsorbate (Pignatello, 1998). Weber *et al.* (1991) stated that interactions between adsorbate and adsorbent may include three categories: physical, chemical and electrostatic. The interactions between dipole moments of adsorbate molecules and adsorbent are imperative for the physical sorption process. The weak bonding forces related to physical sorption are often amplified in the case of hydrophobic molecules by substantial thermodynamic gradients for repulsion from solution in which they are dissolved (Weber *et al.*, 1991). Chemical interactions involve the covalent and hydrogen bonding, while electrostatic interactions involve ion-ion and ion-dipole forces (Stoytcheva, 2011). Electrostatic interactions between LDH clay and phenol are highly unlikely due to LDH's high affinity for carbonate (Braterman *et al*., 2004; Forano *et al*., 2013) and due to phenol being a weak acid that does not dissociate completely to phenoxide ion. In order to improve the interactions between the adsorbent (clay) and adsorbate (phenol), it is imperative to modify the clay accordingly. Thermal treatment of LDH clays is one of the processes that can modify the clay into an effective adsorbent. It gives rise to MMOs which have higher specific surface areas and are good adsorbents (Braterman *et al*., 2004; Forano *et al*., 2013; Lei *et al*., 2014). Hence DHT‑4A, GF‑450 and Sorbacid 944 were modified through calcination and evaluated for phenol adsorption.
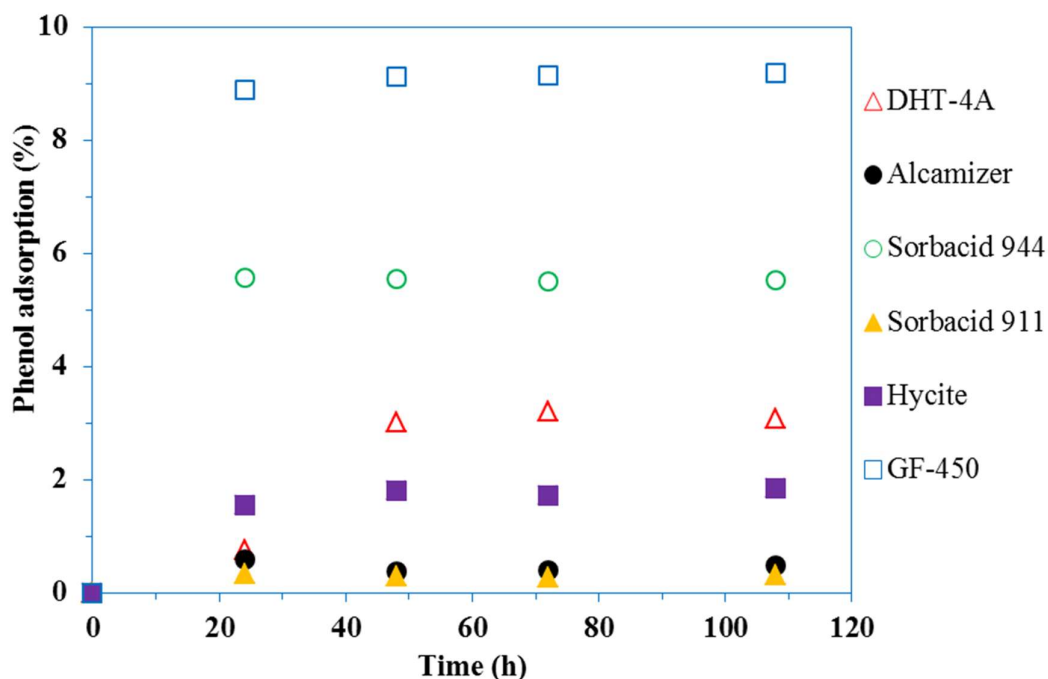
Figure 4-9: Phenol adsorption efficiencies of neat commercial clays

4.7.2   Effect of calcination temperature on phenol adsorption efficiencies

Figure 4-10 shows phenol adsorption efficiencies of the neat and calcined Sorbacid 944 clay at various temperatures. Both the neat and the clay calcined at 250°C attained phenol removals below 10%; this was expected since the structure and composition of the two clays were virtually similar despite the thermal treatment, as detailed in Section 3.1.2. Higher phenol adsorption efficiencies of 85% and 50% were observed for clay calcined at 500°C and 1100°C, respectively. These higher phenol removal amounts were ascribed to the presence of the amorphous periclase (MgO) phase. This accession is in line with results from other researchers who found excellent organic pollutant removal rates using amorphous nanosized metal oxides such as MgO, CaO, Al_2O_3 and MnO_2 as adsorbents (Cai *et al*., 2010; Chen *et al*., 2016; Hu *et al*., 2010). The decrease in adsorption efficiency of ca. 37% when calcination temperature was increased from 500°C to 1100°C can be postulated to be a result of an increase in the crystallinity and spinel content of the calcination products. It should also be noted that the higher adsorption observed for clays calcined at 500°C and above can also be due to phenol being incorporated into the interlayer galleries of the LDH during reconstruction. Since the LDH clay calcined at 500°C had the highest phenol removal, it was used as the primary adsorbent in all subsequent experiments. Calcined DHT‑4A and GF‑450

gave rise to phenol adsorption efficiencies of 56% and 6% respectively as shown in Appendix E. Hence only Sorbacid 944 was evaluated further.
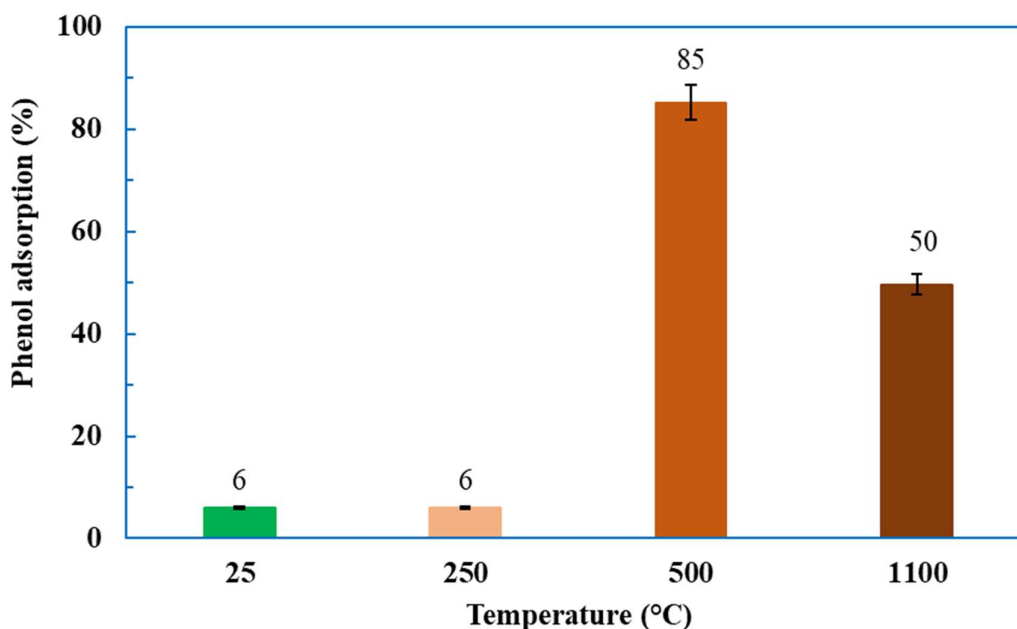
Figure 4-10: Adsorption efficiencies of calcined Sorbacid 944 (25 °C represents neat clay)

4.7.3 Effect of clay loading on phenol removal

Figure 4-11 shows the phenol adsorption efficiencies as a function of adsorbent loading. A 15% increase in phenol adsorption was observed when the clay loading increased from 5 g L^{-1} (68%) to 10 g L^{-1} (83%). Marginal increases in phenol adsorption efficiencies (3% and 5%) were observed when clay loadings were further increased to 15 g L^{-1} and 20 g L^{-1}. An increase in adsorbent loading is generally expected to increase the adsorption efficiency due to an increase in adsorption sites. According to Zubair *et al*. (2017), the dispersion of an adsorbent in an aqueous solution is uniform below a certain limit at which all the active sites are fully exposed and accessible by adsorbates. The surfaces of most solid adsorbents are heterogeneous and are characterised by varying adsorption energies (Chiou, 2003). During adsorption, the sites are taken up sequentially, starting from the highest-energy sites to the lowest-energy sites. An increase in adsorbent loading beyond the optimum limit can result in decreased dispersion efficiency leading to agglomerate formation and blocking of adsorption sites. It is hypothesised that a similar phenomenon might have taken place in the current study, leading to the marginal increase in phenol removal beyond 10 g L^{-1} loading. Based on

the adsorption efficiencies and the hypothesized phenomenon, a loading of 10 g L^{-1} was chosen as the optimum loading.
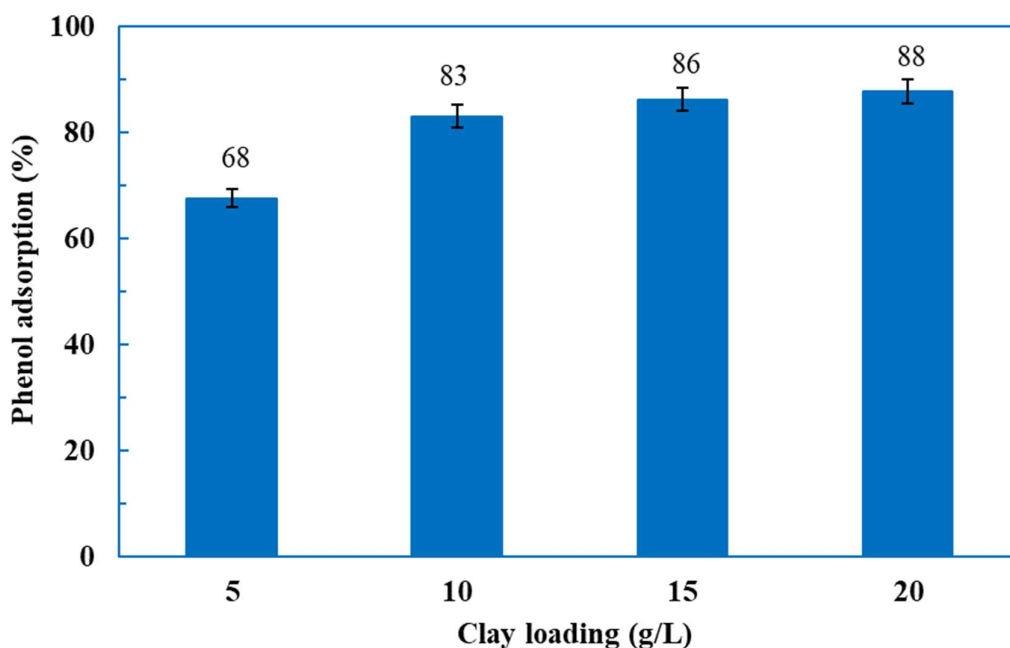
Figure 4-11: Phenol adsorption efficiencies at various clay loadings of CLDH

4.7.4 The effect of initial pH of solution on phenol adsorption efficiency

The initial pH of contaminated water is an important parameter for the efficient removal of pollutants using LDH clays. LDH clays can neutralise hydrogen ions in a solution with a low pH, while they get deprotonated in solutions with a high pH (Grover *et al*., 2019). In this study, the effect of the initial pH on the adsorption of phenol was evaluated over the 7-12 pH range, with pH 7 indicating simulated wastewater with no pH adjustment. The results shown in Figure 4-12 indicate a low adsorption rate at high pH. This can be attributed to an increase in hydroxyl ions at higher pH values, thereby increasing the LDH reconstruction rate. Since the hydroxyl ions have a high affinity for LDH compared to phenol, an increase in hydroxyl ions will lead to a decrease in intercalation of phenolate ions. These observations are like those presented by Zaghouane-Boudiaf *et al*. (2012) who reported that the removal of methyl orange in an aqueous solution by LDH decreased as OH$^-$ increased. Crini (2006), Dos Santos *et al*. (2017) and Gong *et al*. (2011) reported that the adsorption of dyes from acidic aqueous solutions using CLDH was less in comparison to the adsorption from neutral solutions due to the dissolution of LDH at a lower pH. Based on this background, acidic conditions were not

considered for this work. It should be noted that measurements of the equilibrium pH after 24 h contact time did not reveal a marked difference from the initial pH.

During reconstruction, phenol had to compete with dissolved CO_2 for intercalation into the galleries of the clay. Phenol is an acid that gives away a proton in an aqueous solution to form a phenoxide ion. The phenoxide ion has resonance structures that show that the most stable resonance structure is the one that has the negative charge attached to the oxygen atom, as shown in Figure E-4 (Appendix E). Since phenol is classified as a weak acid, complete dissociation is not expected, which means that it is more likely to remain as a phenol rather than a phenoxide ion. Therefore, its chances of being intercalated are minimal, as intercalation of anions occurs to balance charges since the layers of an LDH clay are made of divalent and trivalent metallic ions. According to carbonic acid speciation, the dominant species at pHs greater than 7 are bicarbonate and carbonate ions while CO_2 is dominant at pHs below 7, as shown in Figure E-5 (Appendix E). Since LDH clays are known to have a greater affinity for carbonate (Auerbach *et al.*, 2004; Braterman *et al.*, 2004; Forano *et al.*, 2013); carbonate intercalation was favored over phenoxide intercalation. It was concluded that neutral pH was optimum for removal of phenol from wastewater using CLDH clay and the proceeding adsorption equilibrium tests were conducted at this pH.
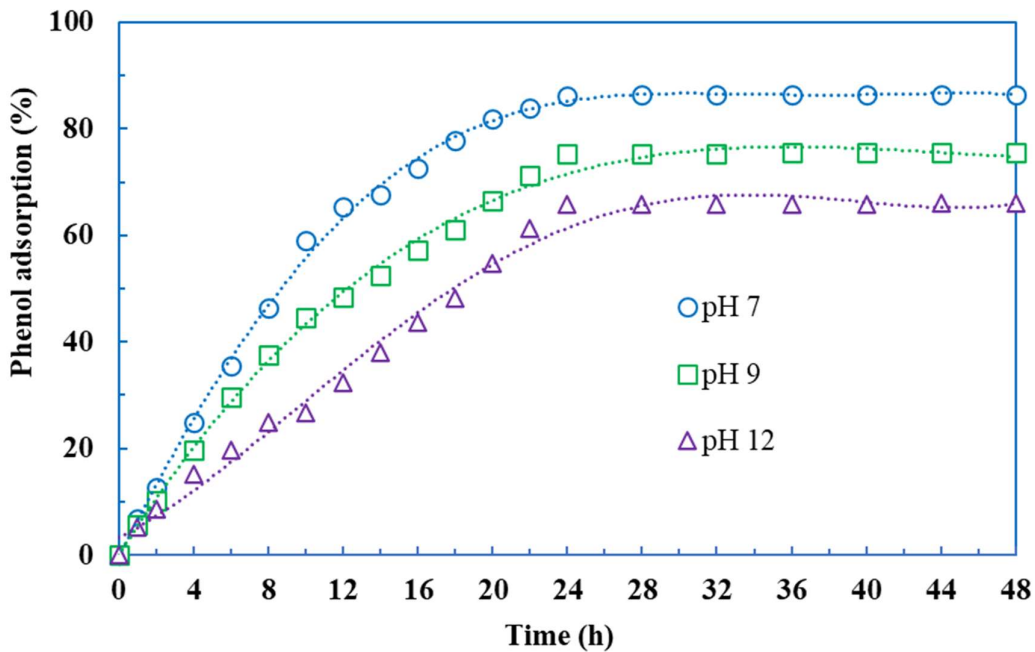
Figure 4-12: Effect of initial pH of solution on phenol adsorption

4.7.5 Phenol adsorption mechanism

Figure 4-13 shows the XRD spectra of the neat and the calcined clay before and after adsorption (at various residence times). The neat clay shows sharp diffraction peaks at low 2θ values with planes of (003) and (006) and small diffraction peaks at higher 2θ values, which can be expected from LDH clays (Cavani *et al.*, 1991; Forano *et al.*, 2013; Lupa *et al.*, 2018). The presence of mixed-metal oxides from the calcined clay was apparent through their respective diffraction peaks: MgO ($2\theta = 52°$ and $70°$) and $MgAl_2O_4$ ($2\theta = 37°$ and $43°$). The diffraction peaks after adsorption at the plane (003) shifted to the lower 2θ values; this was attributed to an increase in d-spacing due to adsorbed phenol. The d-spacing after adsorption, as determined by Bragg's law, was 8.25 Å having increased from a d-spacing of 7.57 Å (for neat clay). It was further observed that the clay fully reconstructed after 12 h, however, phenol adsorption efficiency at that time was ca. 65%, as displayed in Figure 4-12. There was no further increase in d-spacing after 12 h even though more phenol was removed from wastewater. This showed that no further intercalation occurred after 12 h. Therefore, it can be concluded that a dual process mechanism exists for phenol adsorption using calcined clay. Both intercalation and adsorption occur in the early stages until the clay is fully reconstructed; thereafter, surface adsorption becomes the dominant process. Chen *et al.* (2014) reported that the degree of phenolate adsorption by intercalation into a calcined MgAl‑CO_3 LDH was about 3.6%, with most of phenolate ions adsorbed on the surface. This showed that phenol removal from aqueous solutions with LDH clay is achieved through a two-stage process mechanism. They concluded that less phenolate was intercalated because the bulky hydrophobic phenyl ring in phenolate was unable to provide electrostatic interaction with the hydroxide layer, thereby showing weaker affinity for LDH clay. Figure 4-13 further shows the disappearance of the diffraction peaks associated with the periclase phase, while the spinel phase at $2\theta = 37°$ and $43°$ remained unchanged as the clay underwent a reconstruction process. Two more diffraction peaks associated with the spinel phase became clearer at $2\theta = 70°$ and $78°$. This confirmed the lack of adsorption activity by the spinel phase. The XRD spectra from the residues obtained after 24 h indicated the reduction in crystallinity as the peaks associated with hydrotalcite were not as sharp and prominent as the neat clay.
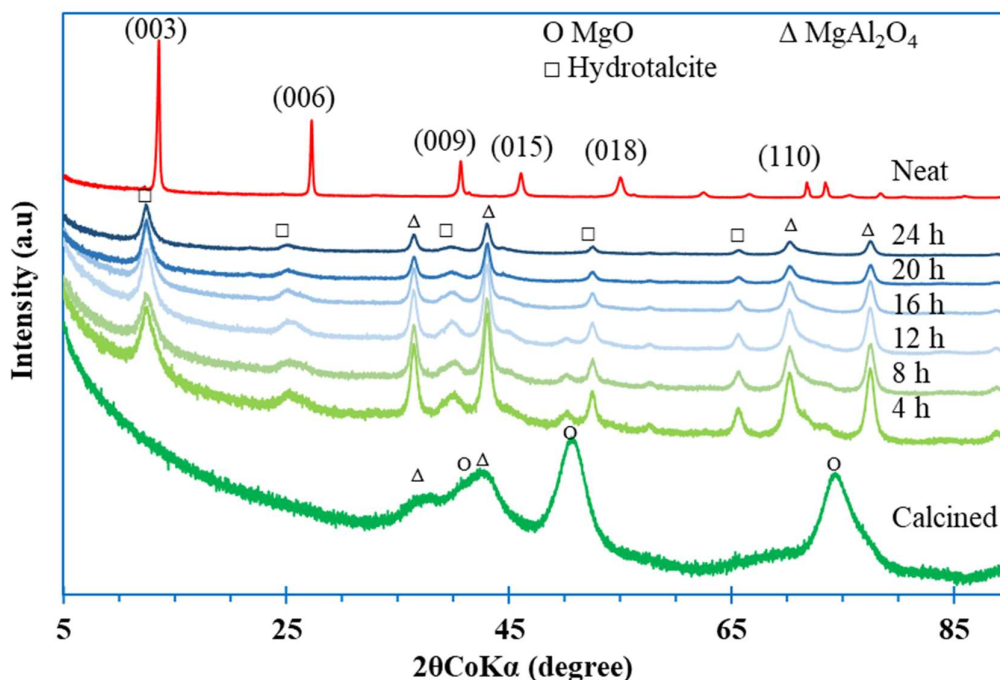
Figure 4-13: X-ray diffraction spectra of the neat, calcined and spent Sorbacid 944 at various residence times

4.7.6   Phenol adsorption isotherms

In order to gain some insight into the nature of interaction between the CLDH clay and the phenol solution, experimental adsorption data was fitted to the Langmuir, Freundlich and Temkin isothermal models. The Langmuir isotherm was developed with the assumption that homogeneous adsorption occurs on the adsorbent with all sites possessing uniform energy (Piccin *et al*., 2011). According to Dada *et al*. (2012), the Langmuir isotherm is valid for monolayer adsorption onto a surface containing a finite number of identical sites. The Freundlich isotherm is mostly applied to heterogeneous adsorption and chemisorption processes (Nethaji *et al*., 2013). Sepehr *et al*. (2017) described the Freundlich equilibrium isotherm as an empirical equation used for the description of multilayer adsorption with interaction between adsorbed molecules. Temkin isotherm considers the adsorbent and adsorbate interactions in intermediate regions as extremely large and low concentrations are ignored (Al-Ghouti & Da'ana, 2020). Figure 4-14 and Table 4-5 show the fitted adsorption data and the corresponding adsorption isotherms parameters. The adsorption isotherm parameters were calculated using Equations (2-1) - (2-7). The equilibrium data was found to be best fitted onto the Freundlich model over the evaluated temperature range. The heterogeneity factors were determined to be above unity and less than 10 (2.21-3.83), indicating strong physical interactions in the system. The maximum adsorption capacity

66

based on the Langmuir model was established to be ca. 17 mg g^{-1} at 65 °C; having increased from ca. 12 mg g^{-1} at 25 °C.

Numerous authors have investigated various waste products, natural materials and bio adsorbents for phenol removal from wastewater. Those adsorbents were deemed to have unique physical and chemical characteristics, which include porosity, surface area, physical strength and adsorption capacities. Table 2-2 shows some of the low‑cost adsorbents (including CAC) and their respective phenol adsorption capacities. The adsorption capacity of calcined Sorbacid 944 is comparable with those of natural clay (15 mg g^{-1}) and porous clay (14.5 mg g^{-1}); however, they are still low compared to CAC (322 mg g^{-1}). This is expected as CAC has a higher surface area compared to most adsorbents and it boosts the presence of micropores that are efficient in pollutant adsorption (Ahmaruzzaman, 2008; Banat *et al*., 2000; Sharma *et al*., 2007).

Table 4-5: Phenol adsorption isotherms parameters

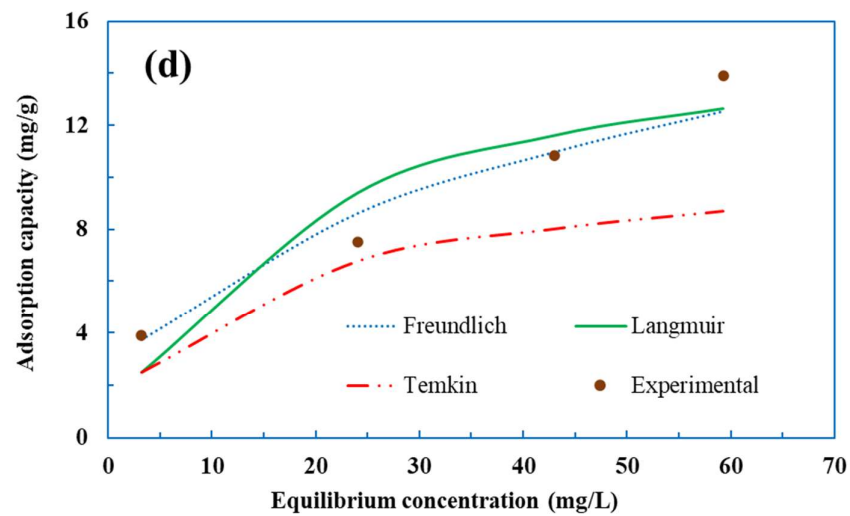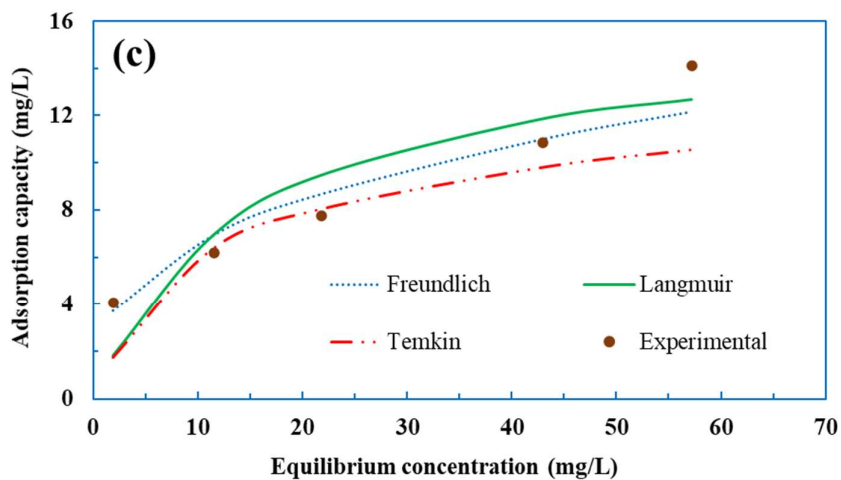| Temperature (°C)	Freundlich			Langmuir			Temkin		
	K_F (L g^{-1})	N	R^2	K_L (L mg^{-1})	q_m (mg g^{-1})	R^2	K_T (L mg^{-1})	b_T (J g^{-1}mol^{-2})	R^2
25	1.36	2.21	0.98	0.05	12.14	0.93	1.00	81.03	0.83
35	2.30	2.41	0.97	0.06	13.96	0.88	1.00	112.93	0.87
45	2.93	2.85	0.94	0.07	16.00	0.89	1.00	95.05	0.95
65	3.69	3.83	0.95	0.14	16.56	0.94	1.00	58.14	0.86
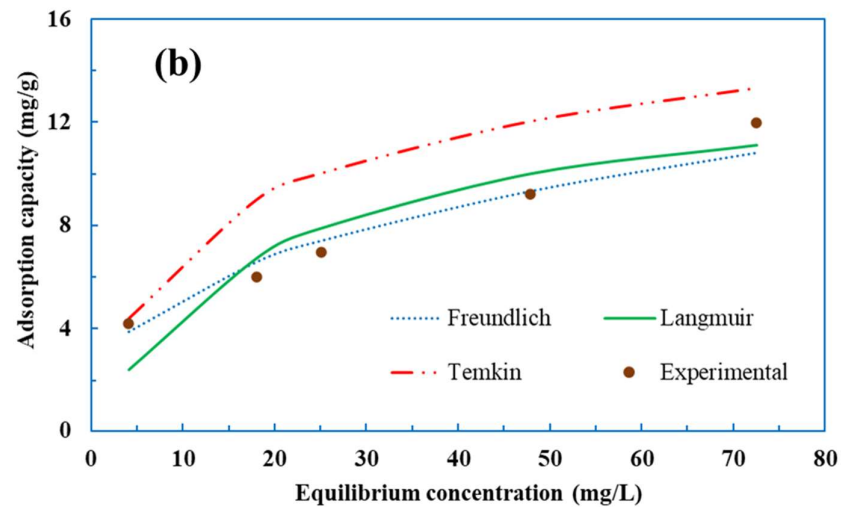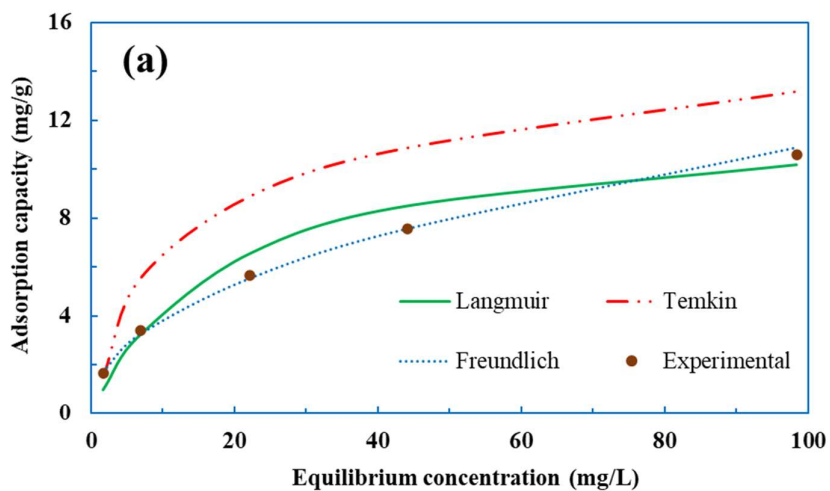
Figure 4-14: Phenol adsorption isotherms at various temperatures, (a)25 °C, (b) 35 °C, (c) 45 °C and (d) 65 °C

4.7.7   Phenol adsorption kinetics on Sorbacid 944

Modelling of the adsorption rate and the establishment of time dependence under various process conditions helps with practical applications of adsorption, such as process design and control. The kinetics of a process details how fast the rate of chemical reaction occurs and the factors affecting it. Chingombe *et al*. (2006) reported that sorption reactions can be represented by three mechanisms, namely: (1) film or surface diffusion where sorbate is transported from the bulk solution to the external surface of the sorbent; (2) intraparticle or diffusion, where sorbate molecules move into the interior of the sorbent particles; and (3) sorption on the interior sites of the sorbent. In the present study, surface or film diffusion can be ignored, since vigorous, turbulent mixing was maintained throughout the experiments. Therefore, a two-stage adsorption mechanism, as detailed in Section 4.7.5 was proposed. The three most used kinetics models were considered to investigate the kinetics of phenol onto CLDH. The evaluated kinetics models were the pseudo-first order, pseudo-second order and Elovich kinetics models. Phenol adsorption data was established to be better described by the pseudo-second order model, as shown in Figure 4-15, with the time interval divided into two periods: Period A between 0 h to 12 h (Figure 4-15(a)) and Period B between 14 h to 24 h (Figure 4-15(b)). The estimated kinetics parameters for the three models are shown in Table 4-6 (determined from Equations (2-8) - (2-13). The maximum phenol removal at 65 °C was achieved within 12 h. The pseudo second order adsorption rate constant at 65 °C was established to have increased by a factor of ca.20 compared to the adsorption rate constant at 25 °C (from 2×10^{-4} g mg^{-1}min^{-1} to 3.8×10^{-3} g mg^{-1}min^{-1}). This was attributed to a low reformation rate of CLDH, as solubility of carbon dioxide (CO_2) decreases with temperature (a plot of the solubility of CO_2 against temperature is shown in Appendix E) (Abas & Khan, 2014). A decrease in CO_2 results in a decrease in carbonate (CO_3^{2-}), which is an interlayer anion, hence a low reformation rate. Low reconstruction rates of CLDH can be deemed to enhance phenol removal from wastewater as higher reconstruction rates were established to reduce phenol adsorption efficiencies, as discussed in Section 4.7.5 (effect of initial pH). The kinetics data fitted onto the Pseudo-first order and Elovich model are displayed in Appendix E.
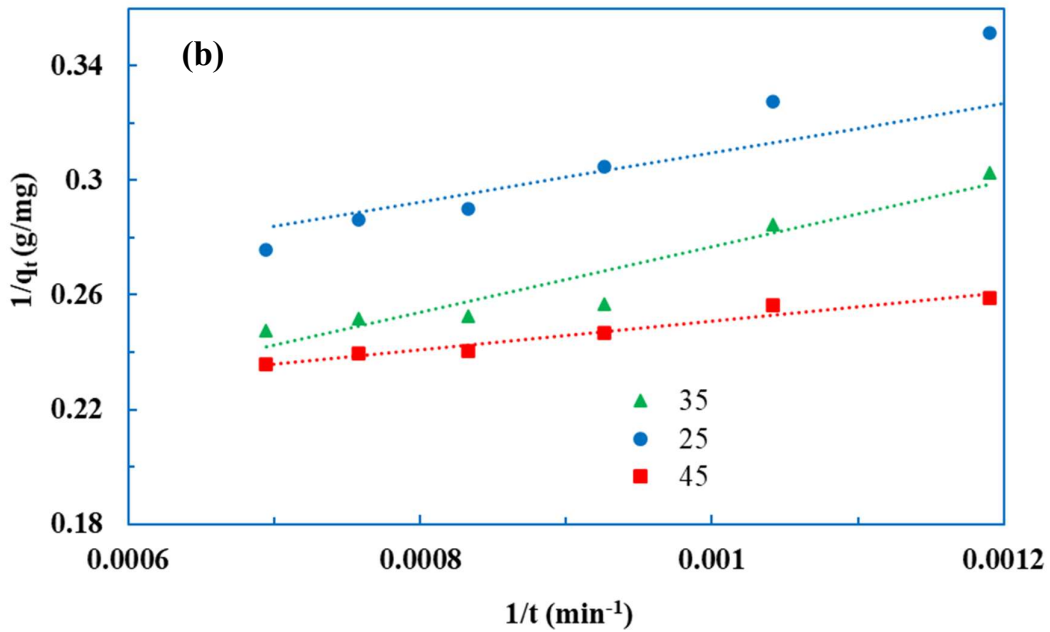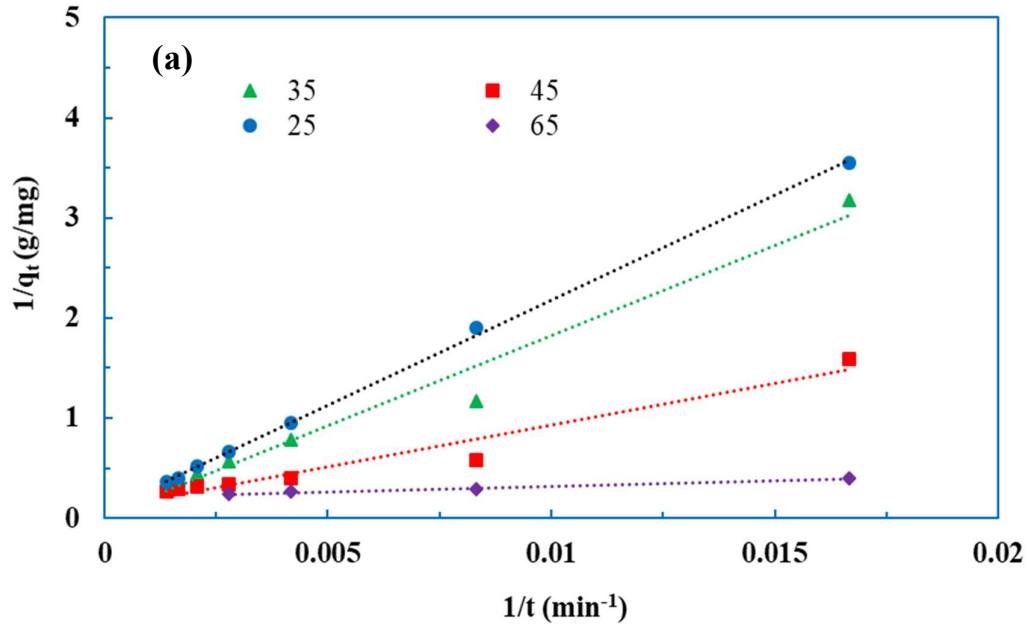
Figure 4-15: Pseudo-second order model plots at various temperatures, (a) Period A (0-12 h) and (b) Period B (12-24 h)

Table 4-6: Kinetic model parameters for Sorbacid 944

Temperature (°C)	Period	$q_{e\,(exp)}$ (mg g^{-1})	Pseudo-First Order			Pseudo-Second Order			Elovich		
			$q_{e\,(Cal)}$ (mg g^{-1})	K_1 x10^{-3} (min^{-1})	R^2	$q_{e\,(Cal)}$ (mg g^{-1})	K_2 x 10^{-4} (g mg^{-1}min^{-1})	R^2	β_E (g mg^{-1})	α (mg g^{-1}min^{-1})	R^2
25	A	3.63	4.06	2.00	0.98	12.3	0.31	1.00	1.02	0.02	0.92
	B		23.11	3.90	0.98	5.98	2.01	0.99	0.69	0.01	0.98
35	A	4.04	4.35	2.00	0.92	52.91	0.02	0.97	0.72	0.02	0.88
	B		80.73	5.66	0.94	6.17	2.0	0.91	0.92	0.02	0.94
45	A	4.24	3.68	2.70	0.98	10.12	1.00	0.95	0.84	0.04	0.99
	B		14.28	4.10	0.95	4.97	8.00	0.96	1.34	0.15	0.96
65	A	4.24	2.42	7.70	0.96	4.84	38.00	0.99	1.09	0.27	0.97

71

4.7.8 Thermodynamics studies of Sorbacid 944

The phenol adsorption equilibrium data onto Sorbacid 944 was best described by the Freundlich-model, as discussed in Section 4.7.6 (phenol adsorption isotherms). The Gibbs free energies at all the evaluated temperatures were determined to be less than zero as shown in Table 4-7. The thermodynamics parameters were estimated using Equations (2-14) - (2-16). This indicated that phenol adsorption on the clay was a spontaneous process. A linear correlation between ln K_a and inverse of temperature ($1/T$) was used to determine the change in enthalpy and change in entropy is depicted in Figure 4-16. The change in enthalpy ($\Delta H°$) was estimated to be 19.93 kJ mol^{-1} signifying an endothermic and physical process. This is in line with the study conducted by Peng *et al.* (2009) on the adsorption of p‑nitrophenol (PNP) on CLDH clay. The authors assumed that water molecules desorbed by the clay were being replaced by PNP with desorption of water being an endothermic process, while adsorption of PNP being an exothermic process. Since more water was desorbed per molecule of PNP adsorbed, the energy gained was higher than the energy released, thus resulting in an overall endothermic process. The change in entropy ($\Delta S°$) was estimated to be greater than zero at 108.4 J mol^{-1}K^{-1} indicating increased randomness at the solid-solution interface (Farah & Elgendy, 2013). The entropy gained due to desorption of water is higher than the entropy lost due to adsorption of phenol resulting in a positive change in entropy. The increased randomness at the solid-liquid interface can be expected as CLDH clay undergoes reformation upon contact with aqueous solution (Bhattacharyya & Sen Gupta, 2006).

Table 4-7: Thermodynamics parameters for phenol adsorption onto Sorbacid 944

Temperature (K)	K_a	$\Delta G°$ (kJ mol^{-1})	$\Delta H°$ (kJ mol^{-1})	$\Delta S°$ (J mol^{-1}K^{-1})
298	127.99	-12.02	19.93	108.40
308	216.56	-13.77		
318	276.07	-14.86		
338	347.60	-16.44		
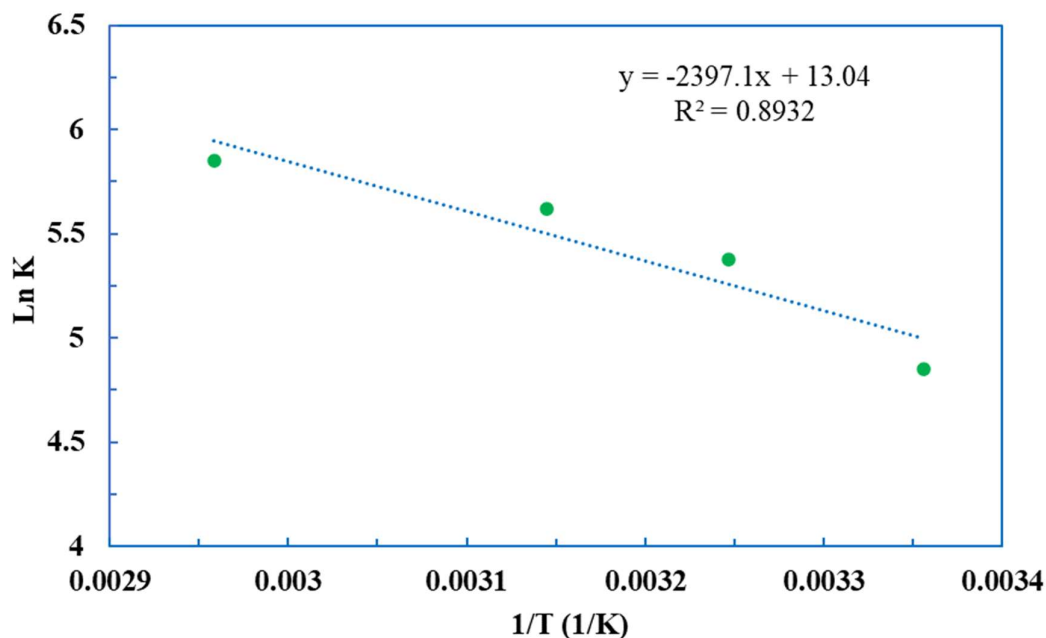
Figure 4-16: Temperature dependence of phenol adsorption onto calcined Sorbacid 944

4.7.9   Regeneration and reusability of Sorbacid 944

Recycling and reusability of an adsorbent is an important aspect for the viability of the adsorption process. CLDH clays are capable of being regenerated due to a "memory effect". Phenol adsorbed on the LDH clay can be completely decomposed upon re-calcination of the spent clay, hence the suspensions were recovered after completing equilibrium adsorption experiments and recalcined at 500°C for 4 h. The adsorption efficiencies of phenol using regenerated clay after thermal recycling are shown in Figure 4-17. The reduction in phenol adsorption over the first three cycles was relatively small at 2% (from 86% to 84%). There was a significant decrease in phenol adsorption efficiency of 25% on the fourth cycle. These results showed that thermal regeneration of clay for re-use is only feasible over three cycles after which the clay loses its sorption capacity. This was also observed by Zhang *et al*. (2009) when they investigated the removal of Naphthol Green B from an aqueous solution by CLDH clay. Zhu *et al*. (2005) reported that clay can lose its adsorption capacity upon repeated calcinations due to an increase in its crystallinity. Alcaraz *et al*. (1998) reported that the spinel content increased upon calcination of clay above 850 °C on repeated calcination steps, which leads to a decrease in the clay's adsorption capacity. Quantification of the XRD analysis showed that the periclase phase decreased from 59% in Cycle 1 to 35% in Cycle 4, as shown in Table 4-8. Figure 4-18 further proves that the diffraction peaks for Cycle 1 were dominated by the amorphous periclase

73

characterised by broad peaks, while the spinel content became more dominant after Cycle 2 with sharp peaks indicating increased crystallinity.
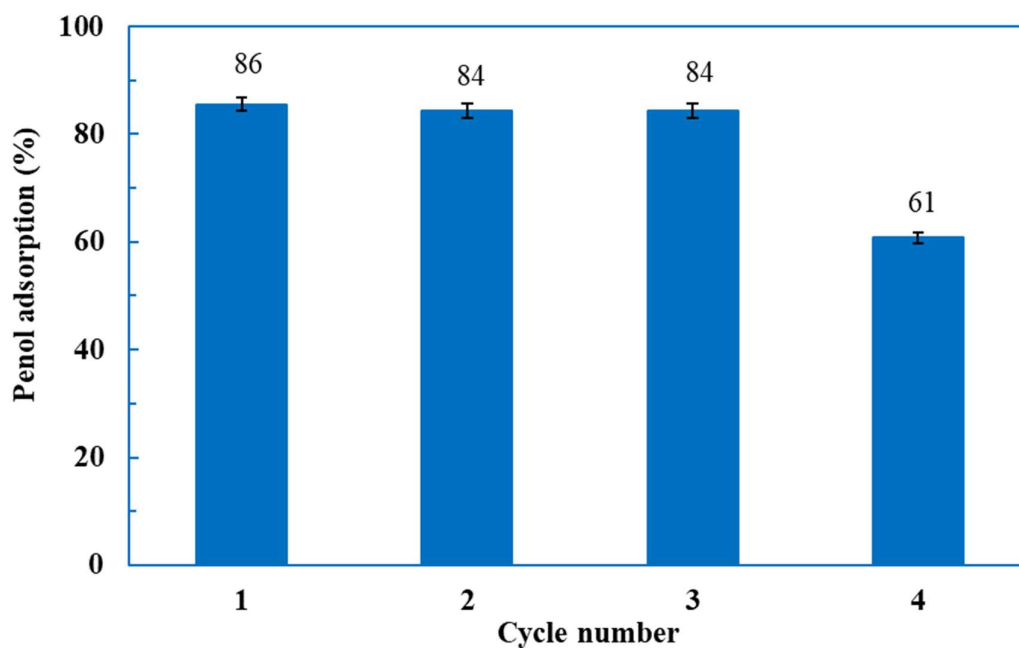
Figure 4-17: Clay's regeneration and reusability potential
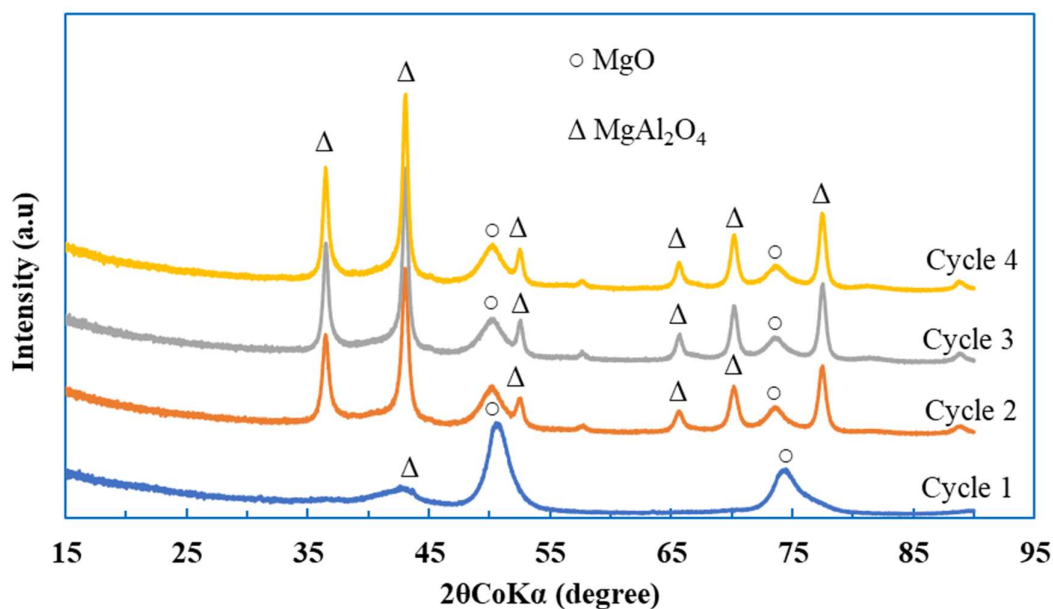
Figure 4-18: X-ray diffraction peaks of regenerated Sorbacid 944

74

Table 4-8: Phase quantification of regenerated Sorbacid 944

Cycle number	Periclase	Spinel
1	58.97	41.03
2	55.07	44.93
3	51.67	48.33
4	35.12	64.88

5   CHARACTERISATION AND APPLICATION OF SYNTHESISED CLAYS

5.1   Crystallinity and phase identification of in-house synthesised clays

5.1.1   Effect of aluminium composition

The XRD patterns for $Mg_{0.8}Al_{0.2}$, $Mg_{0.75}Al_{0.25}$ and $Mg_{0.67}Al_{0.33}$ clays are displayed in Figure 5-1. Clay $Mg_{0.8}Al_{0.2}$ was quantified to contain 58% nesquehonite ($MgCO_3.3H_2O$) and 42% hydrotalcite. Cavani *et al*. (1991) reported that low aluminium contents (x < 0.33) in LDH clays synthesis lead to a high density of divalent metals (Mg^{2+}) octahedral in the brucite-like sheet and the formation of metal hydroxides and carbonates. A similar trend was observed upon the synthesis of clay $Mg_{0.8}Al_{0.2}$. Crystal lattice parameters for this clay were not determined due to a substantial amount of nesquehonite that had its XRD peaks overlapping those of the hydrotalcite phase.

Clay $Mg_{0.75}Al_{0.25}$ was quantified to contain pure hydrotalcite characterised by highly intense peaks at lower 2θ values, and low intense and asymmetric peaks at higher 2θ values (Nundkumar, 2017). The clay's layer distance was slightly higher at 7.78 Å as compared to that of Sorbacid 944 (7.58 Å), as shown in Table 5-1 (the figures showing the positions of the basal planes are displayed in Appendix F). The crystal lattice parameters were estimated using Equations (3-1) - (3-4). It had a smaller crystallite size of below 150 Å, which can be expected from clays prepared by the co‑precipitation method without post-aging treatment (Cavani *et al*., 1991). Forano *et al*. (2013) stated that precipitates prepared through a co‑precipitation method are likely to have low crystallinity, due to non-homogeneity of mixing in a batch reactor setup and the possibility of competitive reactions.

Clay $Mg_{0.67}Al_{0.33}$ was quantified to contain pure hydrotalcite. The clay also had a higher layer distance of 7.70 Å and a lower crystallite size of 111 Å compared to Sorbacid 944. This showed that the clay's crystallinity was low, and it contained more interstitial water than Sorbacid 944. Its crystal lattice parameters were similar to those of clay $Mg_{0.75}Al_{0.25}$. It can be concluded that clays with low substitution of trivalent metal ions (Al^{3+}) are more susceptible to contain phases of metal hydroxide and carbonates. Furthermore, the co‑precipitation synthesis method should be followed by other post-treatment methods, such as sonication and hydrothermal treatment to improve the crystallinity of the clays.
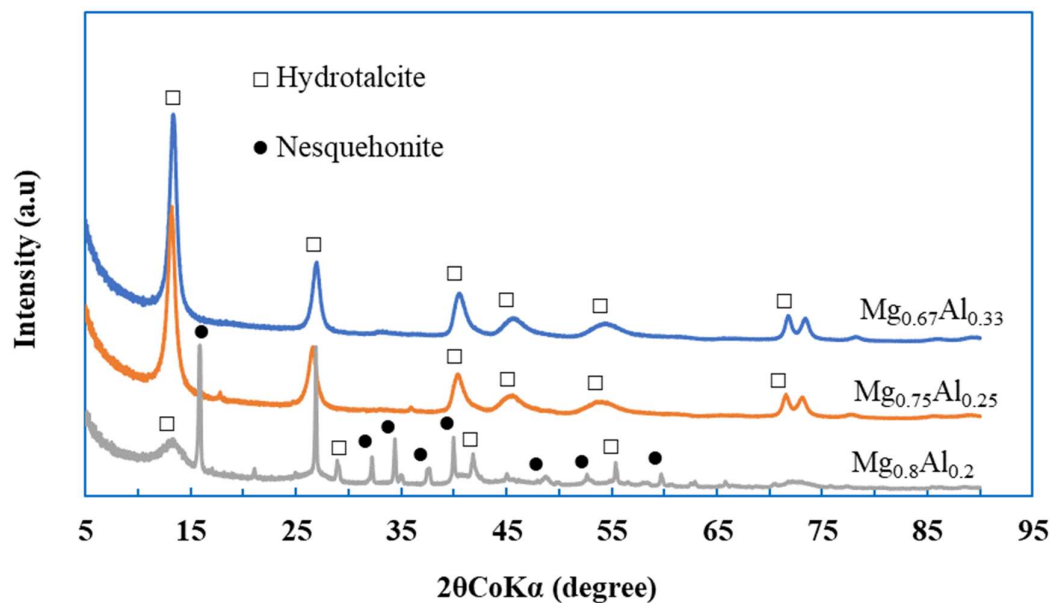
Figure 5-1: XRD patterns for Mg$_{0.8}$Al$_{0.2}$, Mg$_{0.75}$Al$_{0.25}$ and Mg$_{0.67}$Al$_{0.33}$

Table 5-1: Crystal lattice parameters for synthesized clays

Clay short name	2θ (003) (°)	2θ (006) (°)	2θ (009) (°)	2θ (110) (°)	d (003) (Å)	c (Å)	a (Å)	L(003) (Å)
Mg$_{0.6}$Zn$_{0.2}$Al$_{0.2}$	13.46	26.32	40.63	71.96	7.63	23.22	3.05	51.61
Mg$_{0.4}$Zn$_{0.4}$Al$_{0.2}$	13.25	26.60	40.37	71.40	7.75	23.31	3.07	103.19
Mg$_{0.75}$Al$_{0.25}$	13.20	26.61	40.42	71.56	7.78	23.32	3.06	123.82
Mg$_{0.5}$Zn$_{0.25}$Al$_{0.25}$	13.30	26.82	40.56	71.59	7.72	23.18	3.06	91.06
Mg$_{0.25}$Zn$_{0.5}$Al$_{0.25}$	13.40	26.82	40.56	71.58	7.67	23.12	3.06	86.01
Mg$_{0.67}$Al$_{0.33}$	13.34	26.97	40.62	71.78	7.70	23.10	3.05	111.90

5.1.2 Effect of zinc composition

The XRD patterns for Mg$_{0.8}$Al$_{0.2}$, Mg$_{0.6}$ Zn$_{0.2}$Al$_{0.2}$, Mg$_{0.4}$ Zn$_{0.4}$Al$_{0.2}$ and Zn$_{0.75}$Al$_{0.25}$ clays are displayed in Figure 5-2. Clay Mg$_{0.8}$Al$_{0.2}$ and Zn$_{0.75}$Al$_{0.2}$ were quantified to containing hydroxides and carbonate phases, as detailed in Section 5.1.1. Clays Mg$_{0.6}$ Zn$_{0.2}$Al$_{0.2}$ and Mg$_{0.4}$ Zn$_{0.4}$Al$_{0.2}$ were quantified to be quintinites with a chemical formula of Mg$_4$Al$_2$(OH)$_{12}$CO$_3$·3H$_2$O. Both clays displayed less intense and asymmetric peaks throughout the 2θ values indicating

77

amorphous clays. The results are in line with the studies conducted by Cavani *et al*. (1991) who reported that preparation of LDH clays under supersaturation gives rise to less crystalline materials. This was hypothesised to be caused by the high number of crystallisation nuclei under supersaturation conditions. The positions of the basal planes (110), (009), (006) and (003), interlayer spacing, crystallite sizes and parameters are presented in Table 5-1 (the figures showing the positions of the basal planes are displayed in Appendix F). The crystallite sizes were smaller at ca. 100 Å compared to that of Sorbacid 944 at ca.282 Å; this further proved the lack of crystallinity by the clays. The interlayer spacings were estimated to be 7.72 Å and 7.67 Å for $Mg_{0.8}Al_{0.2}$ and $Mg_{0.4}Zn_{0.4}Al_{0.2}$ respectively. The crystal lattice parameters, c and a were determined to be 23.18 Å and 3.06 Å for $Mg_{0.8}Al_{0.2}$ while those for $Mg_{0.4}Zn_{0.4}Al_{0.2}$ were estimated to be 23.12 Å and 3.06 Å. These parameters correlate to those reported by Cavani *et al*. (1991) for an LDH clay having an M^{2+}/M^{3+} ratio of 4; the reported parameters were 7.77 Å, 23.32 Å and 3.06 Å for interlayer spacing, crystal lattice parameters c and a respectively.
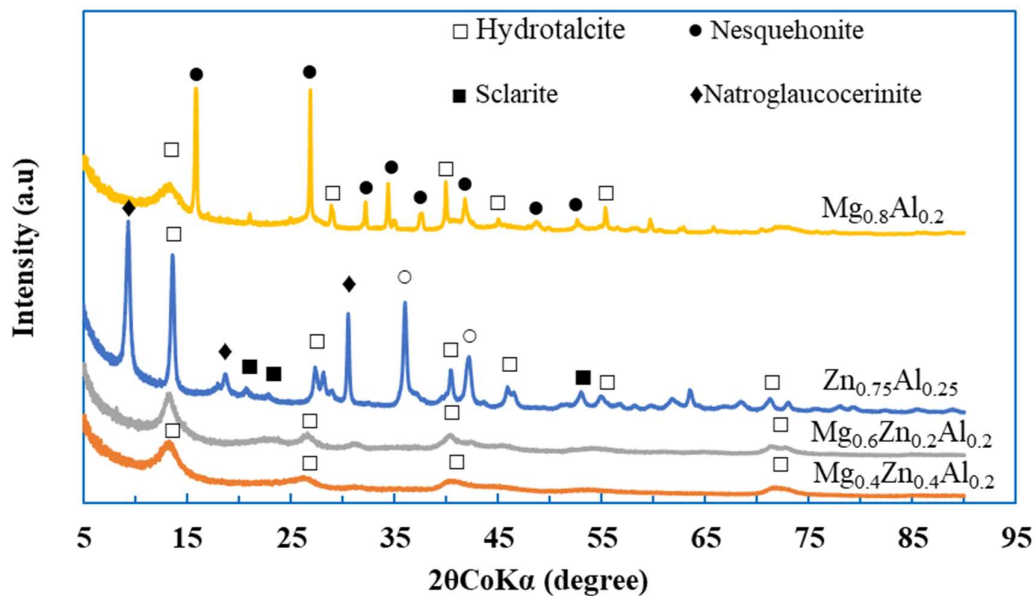
Figure 5-2: X-ray diffraction peaks for $Mg_{0.8}Al_{0.2}$, $Zn_{0.75}Al_{0.25}$, $Mg_{0.6}Zn_{0.2}Al_{0.2}$ and $Mg_{0.4}Zn_{0.4}Al_{0.2}$

5.1.3 Phase identification on calcined $Mg_{0.2}Zn_{0.6}Al_{0.2}$

Figure 5-3 shows the XRD spectra for clay $Mg_{0.6}Zn_{0.2}Al_{0.2}$ calcined at various temperatures. Similar profiles as in Section 4.1.3 were observed. The XRD spectra of the residues after 250 °C and 300 °C were aligned with those of the neat clay with an apparent reduction in crystallinity. The peak at 2θ ~ 15° (corresponding to (003) plane) was completely broken after treatment at 350 °C. This indicated the complete loss of interlayer water (Milanovic, 2016). The MMO

phases were detected from 400 °C but more apparent after 450 °C. The residues after 1100 °C displayed sharp and more intense peaks indicating increased crystallinity as the spinel phase became more dominant.
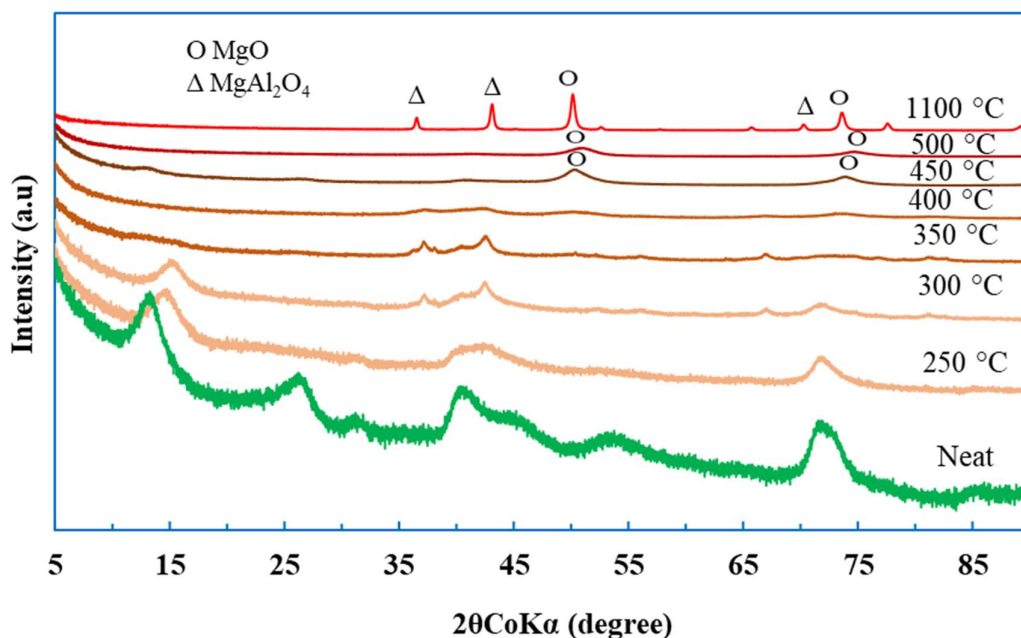
Figure 5-3: X-ray diffraction peaks for calcined Mg$_{0.6}$Zn$_{0.2}$Al$_{0.2}$

5.2   Elemental analysis

Clays containing various concentrations of Mg, Zn and Al were prepared through co‑precipitation at a constant pH of 10. The metallic compositions were based on the best performing commercial clay, Sorbacid 944, as discussed in Chapter 4. The determined molar compositions were close to the expected values, as shown in Table 5-2 and Table 5-3. The general formula for LDH is $(M^{II}_{(1-x)}M^{III}_x(OH)_2)^{x+}(A^{m-})_{x/m}).nH_2O$ which shows the possibility of synthesising clays with distinguished stoichiometries. Naturally occurring hydrotalcites have a fraction of trivalent metals, x equal to 0.25 (Cavani *et al*., 1991). Numerous authors have reported that pure LDHs can be obtained within x values range of 0.20 to 0.33 (Forano *et al*., 2013; Harizi *et al*., 2019; Klemkaite *et al*., 2011).

Based on the XRD and XRF results, the chemical formulae of the neat clays were postulated, as shown in Table 5-4. The hypothesised formulae correlated with the general limits for LDH clays

There were no formulae for $Mg_{0.8}Al_{0.2}$ and $Zn_{0.75}Al_{0.25}$ postulated as the clays contained substantial amounts of impurities.

Table 5-2: Elemental compositions of the in-house synthesised LDH clays.

Element	Mass (%)							
	$Mg_{0.8}Al_{0.2}$	$Mg_{0.6}Zn_{0.2}Al_{0.2}$	$Mg_{0.4}Zn_{0.4}Al_{0.2}$	$Mg_{0.75}Al_{0.25}$	$Mg_{0.5}Zn_{0.25}Al_{0.25}$	$Mg_{0.25}Zn_{0.5}Al_{0.25}$	$Zn_{0.75}Al_{0.25}$	$Mg_{0.67}Al_{0.33}$
Mg	42.78	23.24	16.19	40.43	23.10	10.10	0.25	38.08
Zn	0.18	21.56	40.42	0.65	26.06	44.84	44.72	0.37
Al	12.56	8.98	8.38	14.13	11.70	10.02	6.53	17.05
Na	0.58	0.01	0.01	0.01	0.01	0.01	8.57	0.01
Si	0.02	0.03	0.07	0.07	0.06	0.06	5.15	0.06
Ca	0.02	0.03	0.17	0.03	0.10	0.22	0.25	0.04
S	0.01	0.01	0.01	0.05	0.03	0.02	0.01	0.01
Cr	0.01	0.01	0.01	0.01	0.01	0.01	0.01	0.04
K	0.02	0.01	0.01	0.03	0.01	0.01	0.08	0.03
Nb	0.04	0.01	0.01	0.01	0.01	0.01	0.01	0.01
Fe	0.01	0.01	0.01	0.01	0.01	0.01	0.02	0.02
LOI	43.55	45.69	34.36	44.24	38.49	34.28	33.99	43.96
Total	**99.94**	**99.58**	**99.65**	**99.67**	**99.58**	**99.59**	**99.60**	**99.68**
Molar ratio (M^{2+}/M^{3+})	**3.80**	**3.90**	**4.10**	**3.20**	**3.10**	**3.00**	**2.90**	**2.50**

81

Table 5-3: Molar concentrations for in-house synthesised clays

Clay short name	Target mol (%)			M^{2+}/M^{3+}	Actual mol (%)			M^{2+}/M^{3+}	Offset (%)		
	Mg	Zn	Al		Mg	Zn	Al		Mg	Zn	Al
$Mg_{0.8}Al_{0.2}$	80	0	20	4.0	79	0	21	3.8	-1.3	0.0	5.0
$Mg_{0.6}Zn_{0.2}Al_{0.2}$	60	20	20	4.0	59	20	21	3.8	-1.7	0.0	5.0
$Mg_{0.4}Zn_{0.4}Al_{0.2}$	40	40	20	4.0	42	39	19	4.3	5.0	-3	-5.0
$Mg_{0.75}Al_{0.25}$	75	0	25	3.0	76	0	24	3.2	1.3	0.0	-4.0
$Mg_{0.5}Zn_{0.25}Al_{0.25}$	50	25	25	3.0	53	23	24	3.2	6.0	-8	-4.0
$Mg_{0.25}Zn_{0.5}Al_{0.25}$	25	50	25	3.0	28	47	25	3.0	12.0	-6	0.0
$Zn_{0.75}Al_{0.25}$	0	75	25	3.0	0	74	26	2.8	0.0	-1	-4
$Mg_{0.67}Al_{0.33}$	67	0	33	2.0	71	0	29	2.4	6.0	0.0	12.1

Table 5-4: Postulated formulae for in-house synthesised clays

Clay short name	Chemical formula
$Mg_{0.6}Zn_{0.2}Al_{0.2}$	$Mg_{5.6}Zn_{1.9}Al_2(OH)_{19}CO_3 \cdot nH_2O$
$Mg_{0.4}Zn_{0.4}Al_{0.2}$	$Mg_{4.4}Zn_{4.1}Al_2(OH)_{21}CO_3 \cdot nH_2O$
$Mg_{0.75}Al_{0.25}$	$Mg_{6.3}Al_2(OH)_{16.7}CO_3 \cdot nH_2O$
$Mg_{0.5}Zn_{0.25}Al_{0.25}$	$Mg_{4.4}Zn_{1.9}Al_2(OH)_{16.7}CO_3 \cdot nH_2O$
$Mg_{0.25}Zn_{0.5}Al_{0.25}$	$Mg_{2.24}Zn_{3.8}Al_2(OH)_{16}CO_3 \cdot nH_2O$
$Mg_{0.67}Al_{0.33}$	$Mg_{4.9}Al_2(OH)_{13.8}CO_3 \cdot nH_2O$

5.3   Chemical bonds identification through infrared spectra

Figure 5-4 (a) to (c) displays the infrared spectra for $Mg_{0.6}Zn_{0.2}Al_{0.2}$, $Mg_{0.75}Al_{0.25}$, $Zn_{0.75}Al_{0.25}$, $Mg_{0.4}Zn_{0.4}Al_{0.2}$ and Sorbacid 944 (as reference) between 4000 cm^{-1} and 500 cm^{-1}. Cavani *et al*. (1991) described infrared analysis as a non-diagnostic tool that has the ability to identify the presence of foreign ions in-between the layers. The weak band at 945 cm^{-1} can be associated with metal-O-metal vibrations in the brucite-like layers. The infrared spectra for clay displayed a band at 840 cm^{-1} that was due to $v1$ vibrational modes of CO_3^{2-} interacting with hydroxyl groups. The metal-O-metal linkages correspond to the band at 960 cm^{-1}. The *v*1 vibrational mode of CO_3^{2-} is further represented by the weaker band at 1100 cm^{-1} with asymmetric stretching of CO_3^{2-} in the interlayer being observed at 1390 cm^{-1}. The bands between 1515 cm^{-1} and 1455 cm^{-1} correlate to the vibration of OH^{-}. The broad peak at 3430 cm^{-1} correlates to the deformation of water (Kloprogge *et al*., 2002). Infrared analyses on $Mg_{0.6}Zn_{0.2}Al_{0.2}$ and $Mg_{0.75}Al_{0.25}$ showed broad and weak peaks as they were characterised to be more amorphous than a regular LDH clay.
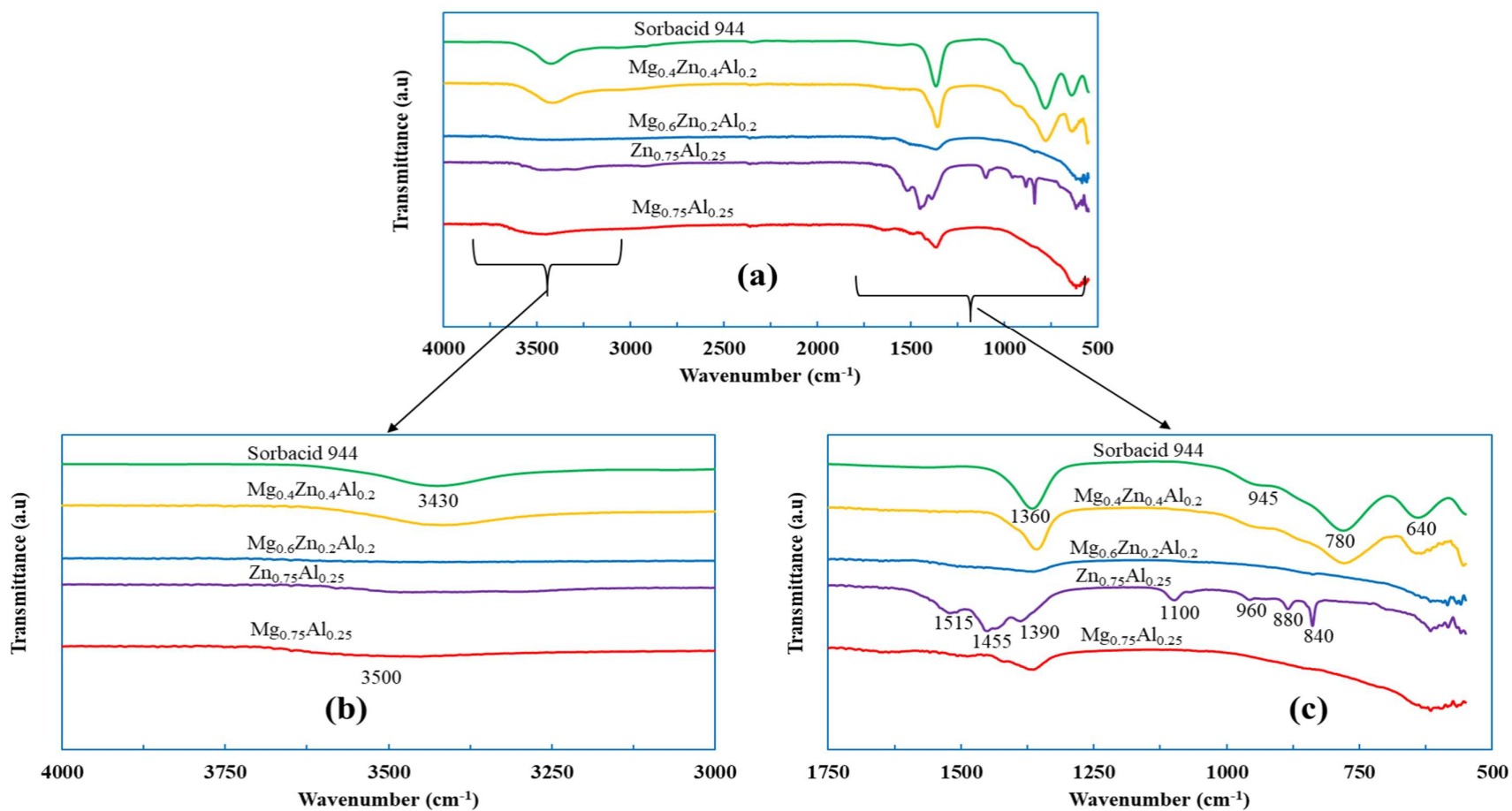
Figure 5-4: Infrared spectra for $Mg_{0.75}Al_{0.25}$, $Zn_{0.75}Al_{0.25}$, $Mg_{0.6}Zn_{0.2}Al_{0.2}$ and $Mg_{0.4}Zn_{0.4}Al_{0.2}$, (a) 4000-500 cm^{-1}, (b) 4000-3000 cm^{-1} and (c)1750-500 cm^{-1}

84

5.4 Thermal stability

Effect of impurities on thermal stability of clays

As discussed in Section 5.1.1, synthesis of clays with Al^{3+} molar fraction of less than 0.33 can lead to the formation of metal hydroxide and carbonates. Impurities in the clay can result in variations in thermal stability depending on the type and quantity. The TGA and DTG curves for $Mg_{0.8}Al_{0.2}$, $Mg_{0.75}Al_{0.25}$ and $Mg_{0.67}Al_{0.33}$ clays are shown in Figures 5-5 (a) to (d). Clay $Mg_{0.8}Al_{0.2}$ was quantified to contain a hydrotalcite and nesquehonite, as detailed in Section 5.1.1. Thermal analysis on the $Mg_{0.8}Al_{0.2}$ showed a three-stage process as shown in Figures 5-5 (a) and (b). The maximum loss of physiosorbed and interstitial water from LDH phase and water content attached to nesquehonite occurred at 230 °C with a mass loss of 14%. This was followed by the initiation of carbonate decomposition in both phases at 315 °C with a mass loss of 5%. The final decomposition step can be attributed to the decarbonation process (Bera *et al*., 2000; Lanas & Alvarez, 2004). It had a mass loss of 24% to make the cumulative mass loss of 43%. Thermal analyses for $Mg_{0.75}Al_{0.25}$ and $Mg_{0.67}Al_{0.33}$ are shown in Figures 5-5 (a) and (c) and Figures 5-5 (a) and (d) respectively. The thermal analysis on $Mg_{0.67}Al_{0.33}$ displayed two decomposition stages, which is expected for LDH clays with M^{2+}/M^{3+} of 2 (Zhao *et al*., 2002). The first decomposition stage occurred at 210 °C with a corresponding mass loss of 18%. This can be attributed to the loss of physiosorbed water and partial loss of OH^-. The second step was caused by the complete decomposition of interlayer ions resulting in a mass loss of 25% at 385 °C. Clay $Mg_{0.75}Al_{0.25}$ displayed a similar thermal decomposition profile as Clay $Mg_{0.67}Al_{0.33}$; however, its maximum losses occurred at 10 °C higher than those for $Mg_{0.67}Al_{0.33}$ (210 °C for water desorption and 400 °C for decarbonation). All three clays underwent a cumulative mass loss of ca. 43%. All three clays displayed a similar cumulative mass loss while the intermediates' decomposition and temperature profiles varied according to the compositions of the clays. Thermal analyses of the other clays' bearings are shown in Appendix G.
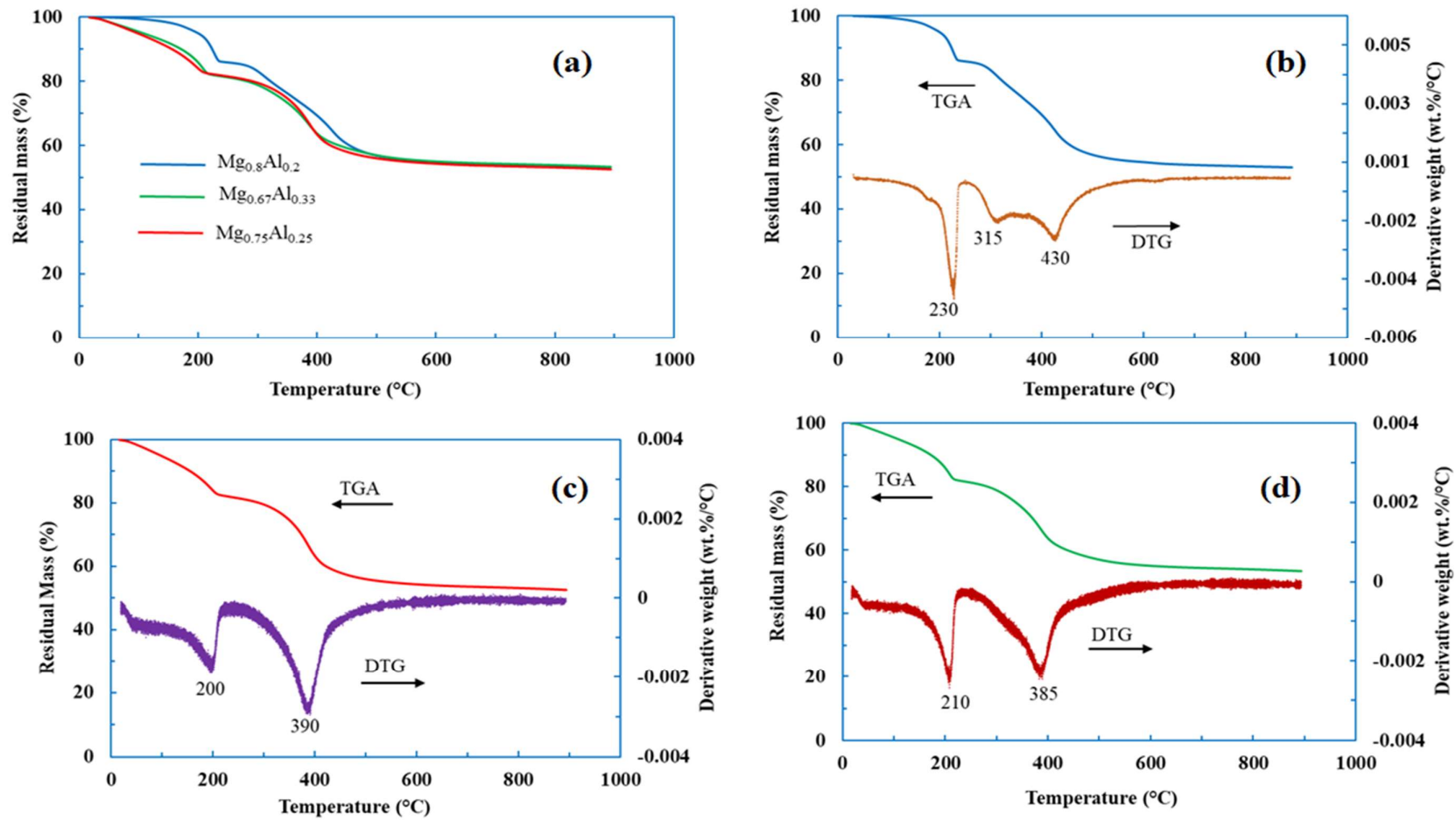
Figure 5-5: Thermal analyses for Mg0.8Al0.2 (a) and (b), Mg0.75Al0.25 (a) and (c) and Mg0.67Al0.33 (a) and (d)

5.5 Specific surface areas of in-housed synthesised clays

The specific surface areas for neat and calcined clays are displayed in Table 5-5. Calcined clays are the residues from thermal treatment of the clays at 500 °C over 4 h. The surface areas for the neat clays were determined to be higher than those of the commercial clays as they ranged between 35-83 $m^2\,g^{-1}$, while those of commercial clays ranged between 4-18 $m^2\,g^{-1}$. This can be attributed to lack of crystallinity by in-house synthesised clays (Raj & Viswanathan, 2009). The BET specific surface areas were established to have increased by 13-52% upon calcination of the clays; this can be attributed to the destruction of brucite layers and the formation of amorphous MMO phases.

Table 5-5: BET Surface area results for in-house synthesized clays

Clay short name	BET surface area ($m^2\,g^{-1}$)	
	Neat	**Calcined**
$Mg_{0.8}Al_{0.2}$	78.9	90.4
$Mg_{0.6}Zn_{0.2}Al_{0.2}$	62.8	84.6
$Mg_{0.4}Zn_{0.4}Al_{0.2}$	82.7	93.5
$Mg_{0.75}Al_{0.25}$	40.0	57.1
$Mg_{0.5}Zn_{0.25}Al_{0.25}$	38.5	51.6
$Mg_{0.25}Zn_{0.5}Al_{0.25}$	52.1	79.2
$Zn_{0.75}Al_{0.25}$	54.8	80.4
$Mg_{0.67}Al_{0.33}$	34.9	47.6

5.6 Morphologies and structures for in-house synthesised clays

The SEM micrographs for $Mg_{0.75}Al_{0.25}$, $Mg_{0.6}Zn_{0.2}Al_{0.2}$, $Mg_{0.4}Zn_{0.4}Al_{0.2}$ and $Zn_{0.75}Al_{0.25}$ are shown in Figures 5-6 (a)-(d). Similar morphologies were obtained for all LDHs. The resultant morphologies indicated that LDHs were synthesised as globular assemblies of nano-sized platelets which are synonymous to unaged co-precipitated LDHs (Gevers *et al*., 2019). Similar results were reported by Khitous *et al*. (2016) who described the morphologies as stone-like shapes.
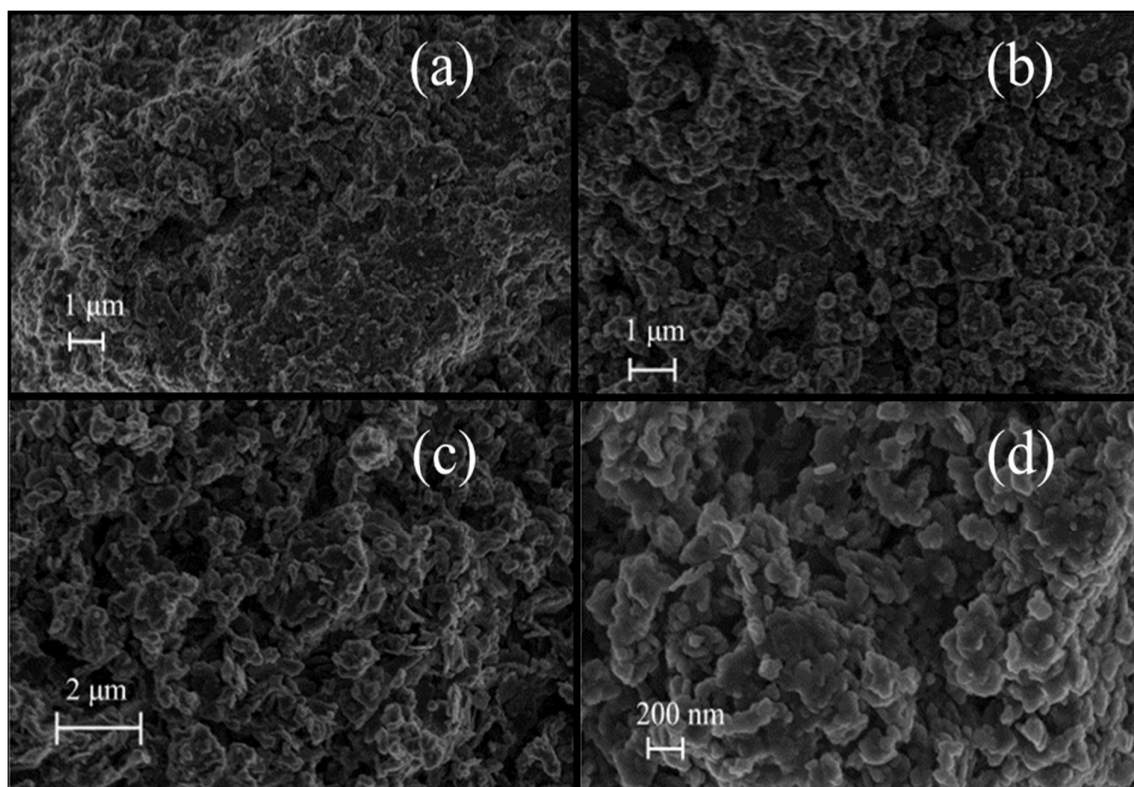
Figure 5-6: SEM micrographs for $Mg_{0.75}Al_{0.25}$ (a), $Mg_{0.6}Zn_{0.2}Al_{0.2}$ (b), $Mg_{0.4}Zn_{0.4}Al_{0.2}$ (c) and $Zn_{0.75}Al_{0.25}$ (d)

5.7 Remediation of phenol contaminated water with in-house synthesised clays

5.7.1 Effect of clay composition on phenol adsorption efficiency

Figure 5-7 shows the extent of phenol adsorption on synthesised LDH clays containing various compositions of Mg, Zn and Al. The neat clays describe LDH clays as synthesised, while calcined refers to clays that were calcined at 500 °C over 4 h. Phenol adsorption on the neat clays was restricted to about 11%, which was comparable with the results obtained using commercial clays. Neat carbonated LDH clays are expected to adsorb phenol on the surface because CO_3^{2-} ions have a higher affinity to LDH and cannot be exchanged with ease (Iyi & Sasaki, 2008). Furthermore, phenol is a weak acid and does not dissociate fully in water (Calace *et al.*, 2002). The phenoxide ion, which is formed when phenol is in contact with water, is not stable and will always revert back to phenol. Hence, phenol was less likely to be intercalated by neat LDH clays. This meant that adsorption of phenol was due to surface interaction with acid-base interactions between phenolic water and LDH clay being the central mechanism of adsorption.

88

There was a great improvement on phenol adsorption upon the utilisation of CLDH clays. The extent of phenol adsorption on calcined clays was in the range of 49-89 % compared to a maximum of ca. 11% for neat clays. The increase in adsorption efficiencies can be attributed to the transition from crystalline LDH clays to amorphous layered double oxides (LDO) upon calcination of neat clays. This accession is in line with the studies conducted by Cai *et al*. (2010) who reported on excellent organic removal rates using amorphous metal oxides. Clays that had a Zn/Mg ratio greater than 1, $Mg_{0.4}Zn_{0.4}Al_{0.2}$, $Mg_{0.25}Zn_{0.5}Al_{0.25}$ and $Zn_{0.75}Al_{0.25}$ showed lower phenol adsorption efficiencies of 63%, 65% and 50% respectively. This was due to the presence of Zn^{2+} causing an increase in the concentration of surface acidic sites compared to binary Mg-Al systems (Hernández *et al*., 2017). Clays with a Zn/Mg ratio less than 1, $Mg_{0.6}Zn_{0.2}Al_{0.2}$ and $Mg_{0.5}Zn_{0.25}Al_{0.25}$ showed an optimal ratio of acidic and basic sites hence higher phenol adsorption efficiencies of 89% and 80% respectively. A higher aluminium compositions in the clay increased the spinel ($MgAl_2O_4$) upon calcination resulting in a decrease in phenol adsorption. The clay which contained molar ratios of Mg (60%), Zn (20%) and Al (20%) ($Mg_{0.6}Zn_{0.2}Al_{0.2}$) was found to possess higher adsorption efficiency upon calcination at 500 °C over 4 h. Therefore, it was used in the proceeding sections.
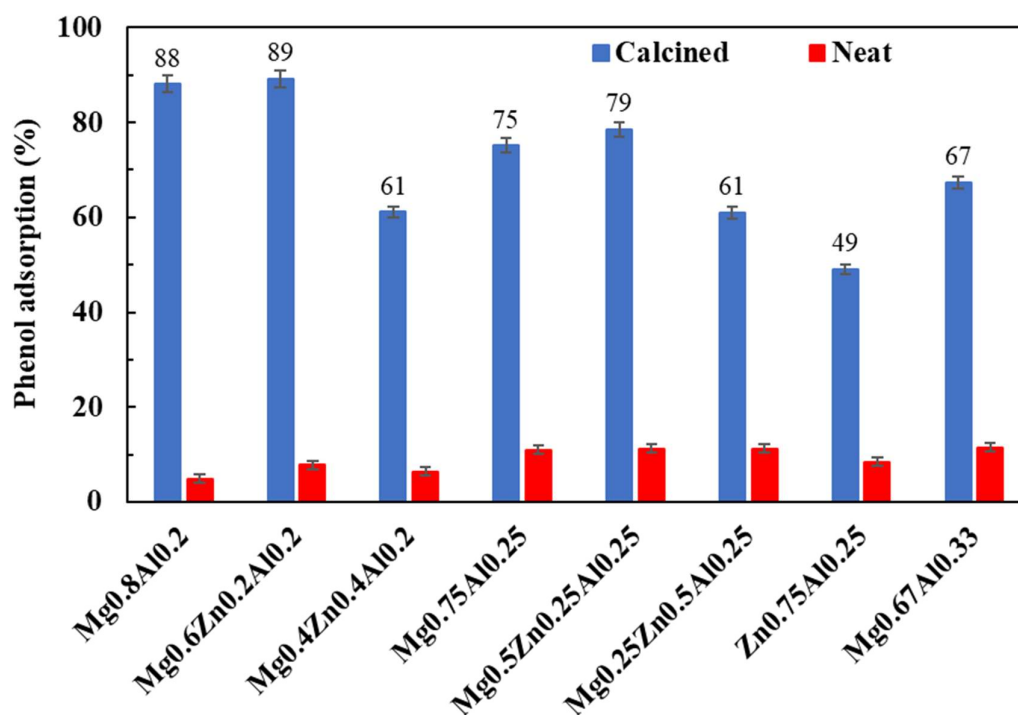
Figure 5-7: Phenol adsorption efficiecies for synthesised clays (neat and calcined)

89

5.7.2 Effect of calcination temperature on phenol removal

The extents of phenol adsorption on clays calcined at various temperatures (250 °C -1100 °C) are shown in Figure 5-8. As discussed in Section 4.1.3, calcination of LDH clays results in the formation of various phases depending on the calcination temperature. The clays calcined at 350 °C and below showed a low adsorption efficiency of ca.14%. This was expected as the clays had only undergone partial decomposition, which meant that less basal sites were available for phenol adsorption (Lv *et al.*, 2006). The extent of phenol adsorption improved by more than 50-66% for clay calcined at 400 °C, as the layered structure was completely destroyed and more basal sites were exposed. The highest phenol adsorption efficiency of ca. 90% was achieved with clay calcined at 450 °C and 500 °C (89%). At this stage, the clay had transformed into an amorphous phase dominated by periclase (MgO). This transformation led to an increase in the clay's basicity and basal site, hence a higher phenol adsorption efficiency. However, as the calcination temperature was increased to 1100 °C, phenol adsorption efficiency was reduced to 57%. This was expected as the clay became more crystalline with an increased amount of spinel phase. LDH clay was calcined at 450 °C over 4 h for proceeding test works.
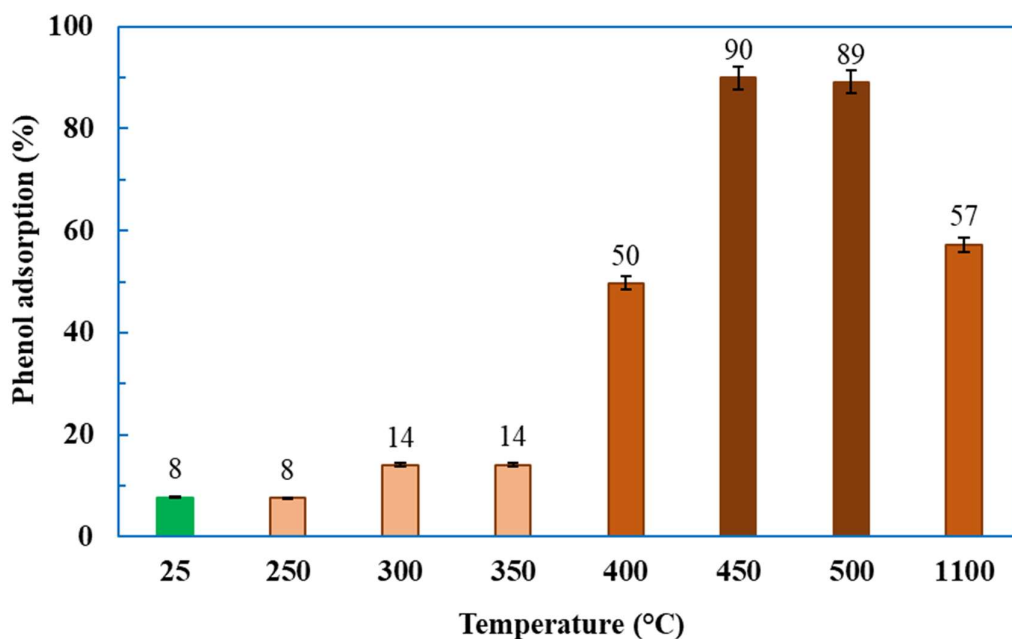
Figure 5-8: The effect of calcination temperature on phenol adsorption (25 °C represents neat clay)

5.7.3 Phenol adsorption isotherms for in-house synthesised clays

Phenol adsorption equilibrium data and the corresponding adsorption isotherm parameters are displayed in Figure 5-9 and Table 5-6 respectively. The Freundlich isotherm was established to be the best fit for the data as with Sorbacid 944. The maximum adsorption capacity based on the Langmuir isotherm was determined to be 14.7 mg g^{-1} at 65 °C; this is 13% less than the adsorption capacity for Sorbacid 944. The major discrepancies between the two values could be an experimental error rather than the actual performance.

Table 5-6: Phenol adsorption isotherms onto clay Mg$_{0.6}$Zn$_{0.2}$Al$_{0.2}$

Temperature (°C)	Freundlich			Langmuir			Temkin		
	K_F (L g^{-1})	N	R^2	K_L (L g^{-1})	q_m (mg g^{-1})	R^2	K_T (L mg^{-1})	b_T (J g^{-1}mol^{-2})	R^2
25	2.10	2.90	0.98	7.30	11.90	0.93	1.00	72.50	0.91
35	2.40	2.80	0.96	5.10	14.20	0.92	1.00	85.00	0.88
45	3.00	3.10	0.96	7.10	14.40	0.94	1.00	81.40	0.88
65	3.00	3.00	0.98	7.50	14.70	0.95	1.00	85.70	0.90
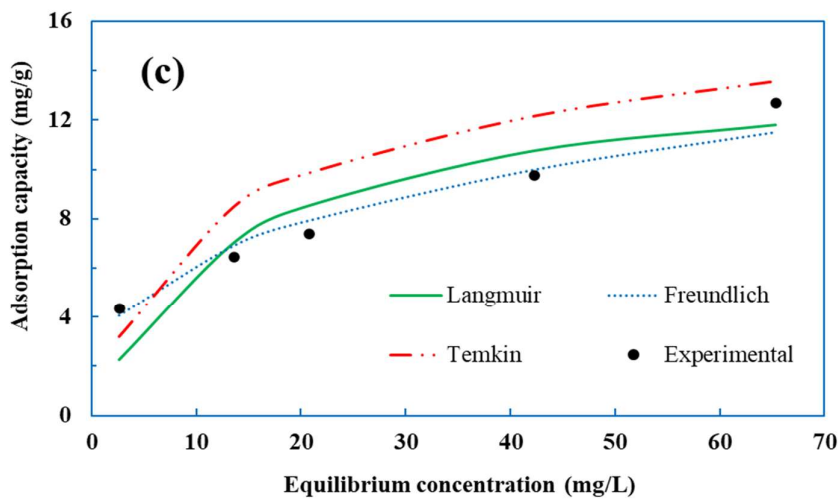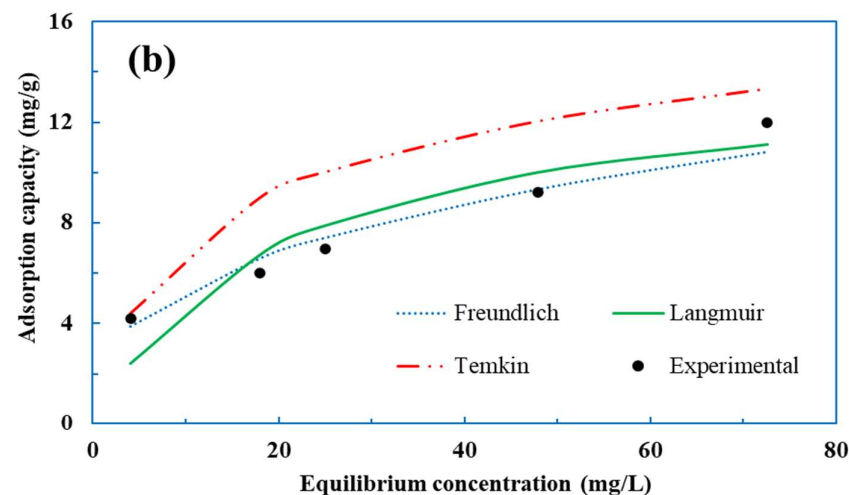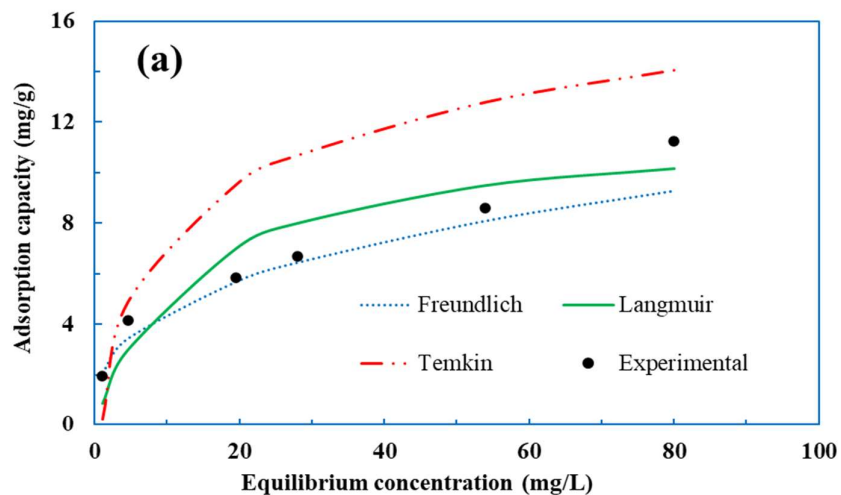
Figure 5-9: Phenol adsorption equilibrium onto $Mg_{0.6}Zn_{0.2}Al_{0.2}$ at various temperatures, (a) 25 °C, (b) 35 °C, (c) 45 °C and (d) 65 °C

92

5.7.4 Phenol adsorption kinetics on $Mg_{0.6}Zn_{0.2}Al_{0.2}$

Phenol adsorption kinetics on $Mg_{0.6}Zn_{0.2}Al_{0.2}$ were found to be best fitted on the pseudo-second order model as shown in Figure 5-10 with the kinetics parameters displayed in Table 5-7. The adsorption rate constants were determined to be 2×10^{-4} g mg^{-1}min^{-1} and 3.3×10^{-3} g mg^{-1}min^{-1} at 25 °C and 65 °C respectively. These results conformed with those observed using Sorbacid 944 clay as indicated in Section 4.7.7. The kinetics data fitted onto the Pseudo-first order and Elovich model are displayed in Appendix H.
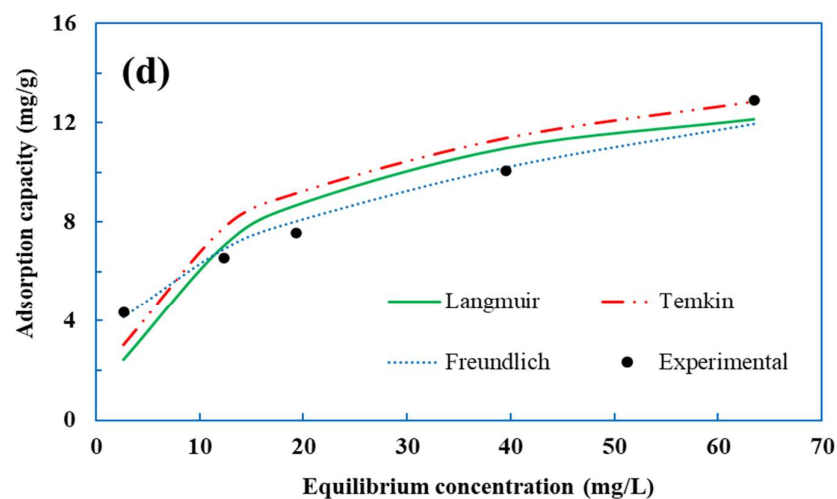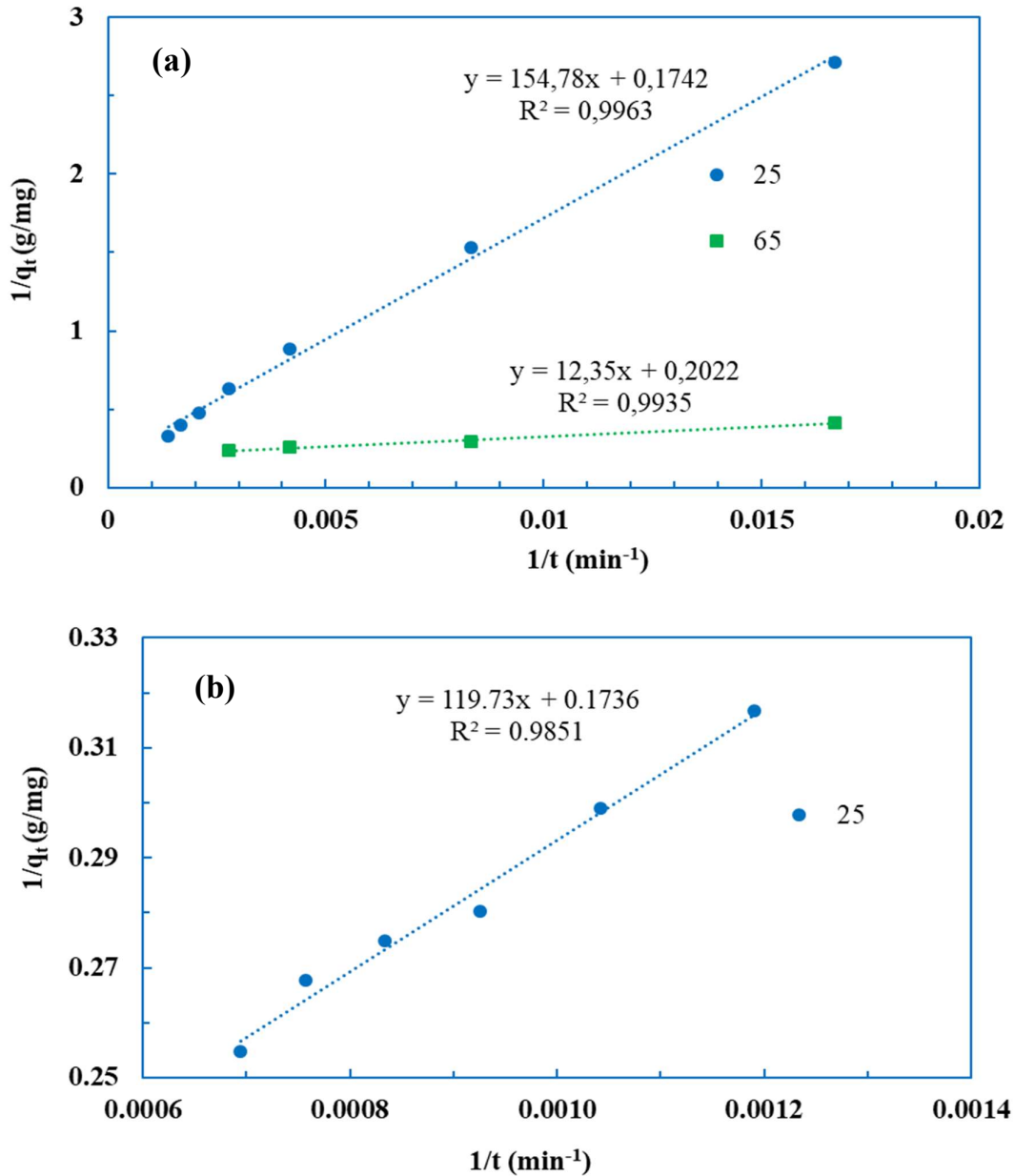

Figure 5-10: Phenol adsorption kinetics on $Mg_{0.6}Zn_{0.2}Al_{0.2}$, (a) Period A (0-12 h) and (b) Period B (12-24 h)

Table 5-7: Phenol kinetics models parameters on $Mg_{0.6}Zn_{0.2}Al_{0.2}$

Temperature (°C)	Period	$q_{e\,(exp)}$ (mg g^{-1})	Pseudo-First Order			Pseudo-Second Order			Elovich		
			$q_{e\,(Cal)}$ (mg g^{-1})	K_1 x 10^{-3} (min^{-1})	R^2	$q_{e\,(Cal)}$ (mg g^{-1})	K_2 x 10^{-3} (g mg^{-1}min^{-1})	R^2	β (g mg^{-1})	α (mg g^{-1}min^{-1})	R^2
25	A		4.26	2.10	0.96	5.74	0.20	1.00	0.93	0.02	0.91
		3.82									
	B		26.88	4.30	0.98	5.99	0.20	0.99	0.74	0.02	0.98
65	A	4.34	2.71	7.40	0.97	4.95	3.30	0.99	1.03	0.22	0.98

5.7.5 Thermodynamics studies of clay $Mg_{0.6}Zn_{0.2}Al_{0.2}$

The Gibbs free energies at all the evaluated temperatures were determined to be less than zero as shown in Table 5-8. These values were closer to each other proving that the spontaneity of the adsorption process is independent of temperature. A linear correlation between ln K_a and inverse of temperature was used to estimate $\Delta H°$ and $\Delta S°$ as depicted in Figure 5-11. The $\Delta H°$ was determined to be 15.02 kJ mol^{-1} signifying an endothermic and physical process. A positive value for $\Delta S°$ at 93.90 J mol^{-1}K^{-1} indicated that there was increased randomness at the solid-solution interface (Farah & Elgendy, 2013; Metwally *et al.*, 2011). The thermodynamics parameters obtained using $Mg_{0.6}Zn_{0.2}Al_{0.2}$ as an adsorbent were comparable with those attained when using Sorbacid 944.

Table 5-8: Thermodynamics parameters for phenol adsorption onto $Mg_{0.6}Zn_{0.2}Al_{0.2}$

Temperature (K)	K_a	$\Delta G°$ (kJ mol^{-1})	$\Delta H°$ (kJ mol^{-1})	$\Delta S°$ (J mol^{-1}K^{-1})
298	190.10	-13.00	15.02	93.90
308	222.10	-13.84		
318	280.45	-14.88		

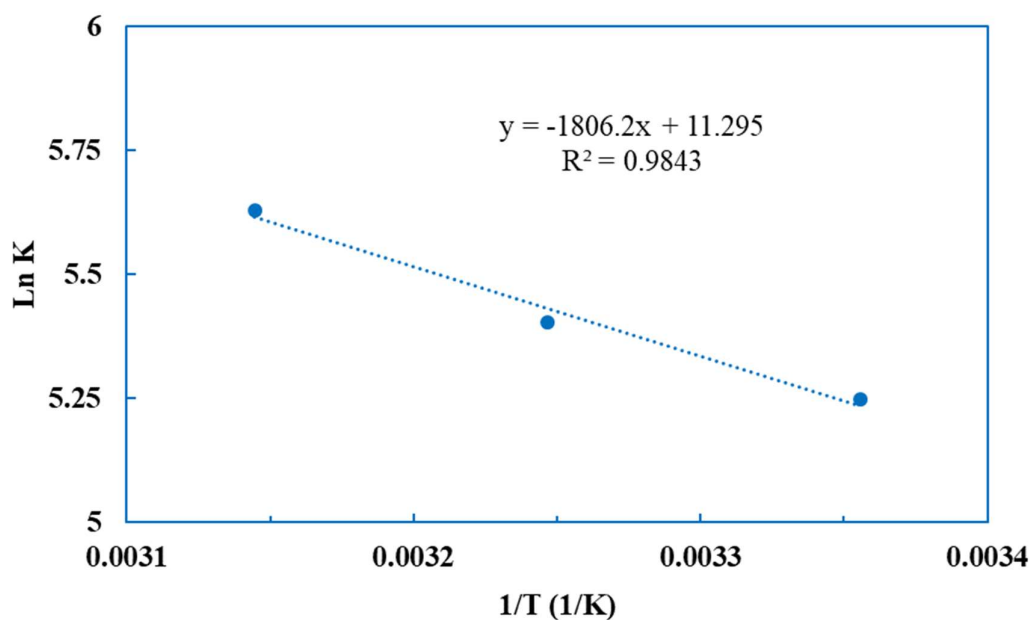*Figure 5-11: Temperature dependence of phenol adsorption onto calcined $Mg_{0.6}Zn_{0.2}Al_{0.2}$*

6   CONCLUSION AND RECOMMENDATIONS

In this study, the potential of commercial layered double hydroxide clays as a low‑cost adsorbents was assessed for the removal of phenol from synthetic wastewater. In order to determine this potential, a number of experiments were carried out, such as the characterisation of the clay, phenol adsorption equilibrium studies and the kinetics studies. This work also involved synthesising of LDH clays based on the metallic composition of the commercial clay to assess the capability of an in-house synthesised clay. Furthermore, the effect of metallic composition of clay on phenol adsorption was evaluated. The optimum calcination temperature was also established.

The X-ray diffraction (XRD) analytical technique was used for phase identification and crystallinity of the commercial clays. The XRD results showed that amongst the assessed commercial clays, Sorbacid 944 was the only clay which contained 100% hydrotalcite as other clays contained impurities, such as calcite, boehmite and silica. The X-ray fluorescence (XRF) analytical technique was used for elemental analysis of the clays. The XRF results on Sorbacid 944 showed that the clay contained ca. 23%, 19% and 16% (wt/wt) of magnesium (Mg), zinc (Zn) and aluminium (Al) respectively.

Calcination of Sorbacid 944 at 500 °C produced mixed metal oxides (MMO), gave promising phenol adsorption efficiencies. Phenol adsorption equilibrium was achieved within 24 h, with equilibrium data being best fitted onto the Freundlich equilibrium isotherm. The maximum adsorption capacity was determined to be ca.17 mg g^{-1}, which is comparable to other low‑cost adsorbents, such as porous clay (14.5 mg g^{-1}) and natural clay (15 mg g^{-1}). Studies on the initial pH of the synthetic contaminated water showed that pH had an inverse proportionality relationship with phenol adsorption for pH greater than 7 (lower pH or acidic media solution was not evaluated). The cause for the inverse proportionality relationship between pH and phenol adsorption was due to elevated pH causing an increase in the concentration of hydroxyl ions (OH^{-}), which increased the reformation rate of CLDH and reduced the adsorption efficiency. A two-stage adsorption mechanism was hypothesised, with both intercalation and surface adsorption taking place from 0 h to12 h, followed by a surface adsorption dominated process. The studies on operational temperature showed an increase in the phenol adsorption rate from 2 x 10^{-4} g mg^{-1}min^{-1} at 25 °C to 3.8 x 10^{-3} g mg^{-1}min^{-1} to at 65 °C. This was attributed to the availability of more adsorption sites for phenol as dissolved

carbon dioxide decreased with an increase in operational temperature. A decrease in CO_2 results in a decrease in carbonate (CO_3^{2-}), which is an interlayer anion, resulting in a low reformation rate. The change in enthalpy of the adsorption process was determined to be ca.20 kJ mol^{-1} indicating an endothermic process dominated by physical adsorption. The changes in Gibbs free energy over the evaluated temperatures ranged between -12 kJ mol^{-1} and -16 kJ mol^{-1}. This showed that the adsorption process was spontaneous irrespective of the operating temperature.

From the clays which were synthesised in-house, a clay which contained molar ratios of Mg (60%), Zn (20%) and Al (20%) ($Mg_{0.6}Zn_{0.2}Al_{0.2}$) was found to possess higher adsorption efficiencies upon calcination at 450 °C for 4 h. Clays which had a Zn/Mg molar ratio greater than 1, showed lower phenol adsorption efficiencies of ca.65% compared to those with a Zn/Mg molar ratio of less than 1 as they gave phenol adsorption efficiencies of more than 80 %. This was due to the presence of Zn^{2+} causing an increase in the concentration of surface acidic sites compared to binary Mg‑Al systems. A higher aluminium content in the clay increased the spinel ($MgAl_2O_4$) upon calcination resulting in a decrease in phenol adsorption. Phenol adsorption equilibrium data and kinetics for clay $Mg_{0.6}Zn_{0.2}Al_{0.2}$ were comparable with those of Sorbacid 944.

Bench-scale studies (equilibrium and kinetic) that were conducted in this research are not enough to demonstrate adsorption capabilities at an industrial scale. Column reactor configurations should be investigated for industrial applications. Furthermore, real wastewater matrices containing multi-contaminants should be used instead of synthetic wastewater with a few pollutants. Since the scope of the current study did not include a techno-economical assessment of the clay; a full economic feasibility of the process should be conducted concurrently with column reactor studies on real wastewater matrices.

REFERENCES

Abas N., Khan N., 2014, Carbon Conundrum, Climate Change, CO_2 Capture and Consumptions, *Journal of CO_2 Utilization,* 8**,** 39-48.

Abdelkader N.B.-H., Bentouami A., Derriche Z., Bettahar N. ,De Menorval L.-C., 2011, Synthesis and Characterization of Mg–Fe Layer Double Hydroxides and Its Application on Adsorption of Orange G from Aqueous Solution, *Chemical Engineering Journal,* 169**,** 231-238.

Adeel Z., Bullock A., Chaudry M., Kuylenstierna J., Qadir M., Schuster-Wallace C., Weitz N. 2014. *Catalyzing Water for Sustainable Development and Growth: Framing Water within the Post 2015 Development Agenda: Options and Considerations: Report*, United Nations University, Institute for Water, Environmental and Health.

Ahmaruzzaman M., 2008, Adsorption of Phenolic Compounds on Low-Cost Adsorbents: A Review, *Advances in Colloid and Interface Science,* 143**,** 48-67.

Ahmaruzzaman M., Sharma D., 2005, Adsorption of Phenols from Wastewater, *Journal of Colloid and Interface Science,* 287**,** 14-24.

Akgerman A., Zardkoohi M., 1996, Adsorption of Phenolic Compounds on Fly Ash, *Journal of Chemical and Engineering Data,* 41**,** 185-187.

Al-Asheh S., Banat F., Abu-Aitah L., 2003, Adsorption of Phenol Using Different Types of Activated Bentonites, *Separation and Purification Technology,* 33**,** 1-10.

Al-Ghouti M.A., Da'ana D.A., 2020, Guidelines for the Use and Interpretation of Adsorption Isotherm Models: A Review, *Journal of Hazardous Materials***,** 122383.

Alcaraz J.J., Arena B.J., Gillespie R.D. ,Holmgren J.S., 1998, Solid Base Catalysts for Mercaptan Oxidation, *Catalysis today,* 43**,** 89-99.

Alexandratos S.D., 2009, Ion-Exchange Resins: A Retrospective from Industrial and Engineering Chemistry Research, *Industrial and Engineering Chemistry Research,* 48**,** 388-398.

Ali, I., Asim, M. & Khan, T. A. 2012. Low cost adsorbents for the removal of organic pollutants from wastewater. *Journal of environmental management,* 113**,** 170-183.

Allen S.J., Gan Q., Matthews R., Johnson P.A., 2005, Kinetic Modeling of the Adsorption of Basic Dyes by Kudzu, *Journal of Colloid and Interface Science,* 286**,** 101-109.

Amor C., Lucas M.S., Garcia J., Dominguez J.R., De Heredia J.B. ,Peres J.A., 2015, Combined Treatment of Olive Mill Wastewater by Fenton's Reagent and Anaerobic Biological Process, *Journal of Environmental Science and Health, Part A,* 50**,** 161-168.

Andreozzi R., Caprio V., Insola A. ,Marotta R., 1999, Advanced Oxidation Processes (AOP) for Water Purification and Recovery, *Catalysis Today,* 53**,** 51-59.

Anku W.W., Mamo M.A., Govender P.P., 2017, Phenolic Compounds in Water: Sources, Reactivity, Toxicity and Treatment Methods, *Phenolic Compounds-Natural Sources. Importance and Applications, First Ed. InTech***,** 419-443.

Arellano-Cárdenas S., Gallardo-Velázquez T., Osorio-Revilla G., López-Cortéz M. ,Gómez-Perea B., 2005, Adsorption of Phenol and Dichlorophenols from Aqueous Solutions by Porous Clay Heterostructure (Pch), *Journal of the Mexican Chemical Society,* 49**,** 287-291.

Audino F., 2019, *Advanced Oxidation Process Models for Optimisation and Decision Making Support in Water Management,* PhD in Chemical Engineering, Universitat Politecnica de Catalunya, Barcelona, Spain.

Auerbach S.M., Carrado K.A., Dutta P.K. 2004. *Handbook of Layered Materials*, CRC press.

Ayawei N., Angaye S.S., Wankasi D., Dikio E.D., 2015, Synthesis, Characterization and Application of Mg/Al Layered Double Hydroxide for the Degradation of Congo Red in Aqueous Solution, *Open Journal of Physical Chemistry,* 5**,** 56.

Ayawei N., Ebelegi A.N., Wankasi D., 2017, Modelling and Interpretation of Adsorption Isotherms, *Journal of Chemistry,* 2017.

Babel S., Kurniawan T.A., 2003, Low-Cost Adsorbents for Heavy Metals Uptake from Contaminated Water: A Review, *Journal of Hazardous Materials,* 97**,** 219-243.

Babikov D., Kendrick B.K., Walker R.B., T Pack R., Fleurat-Lesard P. ,Schinke R., 2003, Formation of Ozone: Metastable States and Anomalous Isotope Effect, *The Journal of Chemical Physics,* 119**,** 2577-2589.

Banat F., Al-Bashir B., Al-Asheh S., Hayajneh O., 2000, Adsorption of Phenol by Bentonite, *Environmental Pollution,* 107**,** 391-398.

Banat F.A., Al-Asheh S., 1999, Biosorption of Phenol by Chicken Feathers, *Environmental Engineering and Policy,* 2**,** 85-90.

Beltran F.J., García-Araya J.F., Acedo B., 1994, Advanced Oxidation of Atrazine in Water—Ii. Ozonation Combined with Ultraviolet Radiation, *Water Research,* 28**,** 2165-2174.

Benito P., Labajos F., Rocha J. ,Rives V., 2006, Influence of Microwave Radiation on the Textural Properties of Layered Double Hydroxides, *Microporous and Mesoporous Materials,* 94**,** 148-158.

Bera P., Rajamathi M., Hegde M. ,Kamath P.V., 2000, Thermal Behaviour of Hydroxides, Hydroxysalts and Hydrotalcites, *Bulletin of Materials Science,* 23**,** 141-145.

Bernardo M.P. ,Ribeiro C., 2018, [Mg-Al]-Ldh and [Zn-Al]-Ldh as Matrices for Removal of High Loadings of Phosphate, *Materials Research,* 21.

Bessaies, H., Iftekhar, S., Asif, M. B., Khriji, J., Necibi, C., Sillanpää, M. & Hamrouni, B. 2021. Characterization and physicochemical aspects of novel cellulose-based layered double hydroxide nanocomposite for removal of antimony and fluoride from aqueous solution. *Journal of Environmental Sciences,* 102**,** 301-315.

Bharali D., Devi R., Bharali P. ,Deka R.C., 2015, Synthesis of High Surface Area Mixed Metal Oxide from the Nimgal Ldh Precursor for Nitro-Aldol Condensation Reaction, *New Journal of Chemistry,* 39**,** 172-178.

Bhattacharyya K.G. ,Sen Gupta S., 2006, Adsorption of Chromium (Vi) from Water by Clays, *Industrial and Engineering Chemistry Research,* 45**,** 7232-7240.

Blanchard G., Maunaye M. ,Martin G., 1984, Removal of Heavy Metals from Waters by Means of Natural Zeolites, *Water Research,* 18**,** 1501-1507.

Böhringer C., 2003, The Kyoto Protocol: A Review and Perspectives, *Oxford Review of Economic Policy,* 19**,** 451-466.

Braslavsky S.E. ,Rubin M.B., 2011, The History of Ozone Part Viii. Photochemical Formation of Ozone, *Photochemical and Photobiological Sciences,* 10**,** 1515-1520.

Braterman P.S., Xu Z.P. ,Yarberry F., 2004, Layered Double Hydroxides (Ldhs), *Handbook of layered materials***,** 373-474.

Bruce R.M., Santodonato J. ,Neal M.W., 1987, Summary Review of the Health Effects Associated with Phenol, *Toxicology and Industrial Health,* 3**,** 535-568.

Cai W., Yu J. ,Jaroniec M., 2010, Template-Free Synthesis of Hierarchical Spindle-Like Γ-Al 2 O 3 Materials and Their Adsorption Affinity Towards Organic and Inorganic Pollutants in Water, *Journal of Materials Chemistry,* 20**,** 4587-4594.

Calace N., Nardi E., Petronio B. ,Pietroletti M., 2002, Adsorption of Phenols by Papermill Sludges, *Environmental Pollution,* 118**,** 315-319.

Cardona Y., Vicente M.A., Korili S.A. ,Gil A., 2020, Progress and Perspectives for the Use of Pillared Clays as Adsorbents for Organic Compounds in Aqueous Solution, *Reviews in Chemical Engineering,* 1.

Cavallaro G., Lazzara G., Rozhina E., Konnova S., Kryuchkova M., Khaertdinov N. ,Fakhrullin R., 2019, Organic-Nanoclay Composite Materials as Removal Agents for Environmental Decontamination, *RSC Advances,* 9**,** 40553-40564.

Cavani F., Trifiro F. ,Vaccari A., 1991, Hydrotalcite-Type Anionic Clays: Preparation, Properties and Applications, *Catalysis Today,* 11**,** 173-301.

Chaillot D., Bennici S. ,Brendlé J., 2020, Layered Double Hydroxides and Ldh-Derived Materials in Chosen Environmental Applications: A Review, *Environmental Science and Pollution Research International*.

Chang H. ,Huang P.J., 1997, Thermal Decomposition of CaC_2O_4 H_2O Studied by Thermo-Raman Spectroscopy with Tga/Dta, *Analytical Chemistry,* 69**,** 1485-1491.

Chao Y.-F., Lee J.-J. ,Wang S.-L., 2009, Preferential Adsorption of 2, 4- Dichlorophenoxyacetate from Associated Binary-Solute Aqueous Systems by Mg/Al-No3 Layered Double Hydroxides with Different Nitrate Orientations, *Journal of Hazardous materials,* 165**,** 846-852.

Chen C., Gunawan P. ,Xu R., 2011, Self-Assembled Fe_3O_4-Layered Double Hydroxide Colloidal Nanohybrids with Excellent Performance for Treatment of Organic Dyes in Water, *Journal of Materials Chemistry,* 21**,** 1218-1225.

Chen H., Hu L., Chen M., Yan Y. ,Wu L., 2014, Nickel–Cobalt Layered Double Hydroxide Nanosheets for High-Performance Supercapacitor Electrode Materials, *Advanced Functional Materials,* 24**,** 934-942.

Chen L., Li C., Wei Y., Zhou G., Pan A., Wei W. ,Huang B., 2016, Hollow Ldh Nanowires as Excellent Adsorbents for Organic Dye, *Journal of Alloys and Compounds,* 687**,** 499-505.

Chen S., Xu Z.P., Zhang Q., Lu G.M., Hao Z.P. ,Liu S., 2009, Studies on Adsorption of Phenol and 4-Nitrophenol on Mgal-Mixed Oxide Derived from Mgal-Layered Double Hydroxide, *Separation and Purification Technology,* 67**,** 194-200.

Cheung C.W., Porter J.F. ,McKay G., 2000, Elovich Equation and Modified Second-Order Equation for Sorption of Cadmium Ions onto Bone Char, *Journal of Chemical Technology and Biotechnology,* 75**,** 963-970.

Chingombe P., Saha B. ,Wakeman R., 2006, Sorption of Atrazine on Conventional and Surface Modified Activated Carbons, *Journal of Colloid and Interface science,* 302**,** 408-416.

Chiou C.T. 2003. *Partition and Adsorption of Organic Contaminants in Environmental Systems*, John Wiley & Sons.

Choudary B.M., Madhi S., Chowdari N.S., Kantam M.L. ,Sreedhar B., 2002, Layered Double Hydroxide Supported Nanopalladium Catalyst for Heck-, Suzuki-, Sonogashira-, and Stille-Type Coupling Reactions of Chloroarenes, *Journal of the American Chemical Society,* 124**,** 14127-14136.

Chu K. ,Hashim M., 2003, Modeling Batch Equilibrium and Kinetics of Copper Removal by Crab Shell, *Separation Science and Technology,* 38**,** 3927-3950.

Chuang Y.H., Tzou Y.M., Wang M.K., Liu C.H. ,Chiang P.N., 2008, Removal of 2-Chlorophenol from Aqueous Solution by Mg/Al Layered Double Hydroxide (Ldh) and Modified Ldh, *Industrial and Engineering Chemistry Research,* 47**,** 3813-3819.

Constantino V.R. ,Pinnavaia T.J., 1995, Basic Properties of Mg2+ 1-Xal3+ X Layered Double Hydroxides Intercalated by Carbonate, Hydroxide, Chloride, and Sulfate Anions, *Inorganic Chemistry,* 34**,** 883-892.

Cormenzana U., Pavlovic I., Barriga C., Hermosín M. ,Cornejo J., 2001, Adsorption of Anionic Species on Hydrotalcite-Like Compounds: Effect of Interlayer Anion and Crystallinity.

Costa F.R., Leuteritz A., Wagenknecht U., Jehnichen D., Haeussler L. ,Heinrich G., 2008, Intercalation of Mg–Al Layered Double Hydroxide by Anionic Surfactants: Preparation and Characterization, *Applied Clay Science,* 38**,** 153-164.

Crini G., 2006, Non-Conventional Low-Cost Adsorbents for Dye Removal: A Review, *Bioresource technology,* 97**,** 1061-1085.

Crini G. ,Lichtfouse E. 2018. *Green Adsorbents for Pollutant Removal: Fundamentals and Design*, Springer.

Dada A., Olalekan A., Olatunya A. ,Dada O., 2012, Langmuir, Freundlich, Temkin and Dubinin–Radushkevich Isotherms Studies of Equilibrium Sorption of Zn^{2+} Unto Phosphoric Acid Modified Rice Husk, *IOSR Journal of Applied Chemistry,* 3**,** 38-45.

Daud M., Hai A., Banat F., Wazir M.B., Habib M., Bharath G. ,Al-Harthi M.A., 2019, A Review on the Recent Advances, Challenges and Future Aspect of Layered Double Hydroxides (Ldh)–Containing Hybrids as Promising Adsorbents for Dyes Removal, *Journal of Molecular Liquids***,** 110989.

Delle Site A., 2001, Factors Affecting Sorption of Organic Compounds in Natural Sorbent/Water Systems and Sorption Coefficients for Selected Pollutants. A Review, *Journal of Physical and Chemical Reference Data,* 30**,** 187-439.

Demarche P., Junghanns C., Nair R.R. ,Agathos S.N., 2012, Harnessing the Power of Enzymes for Environmental Stewardship, *Biotechnology Advances,* 30**,** 933-953.

Derbyshire F., Jagtoyen M., Andrews R., Rao A., Martin-Gullon I. ,Grulke E.A., 2001, Carbon Materials in Environmental Applications, *Chemistry and Physics of Carbon***,** 1-66.

Dichiara A.B., Weinstein S.J. ,Rogers R.E., 2015, On the Choice of Batch or Fixed Bed Adsorption Processes for Wastewater Treatment, *Industrial and Engineering Chemistry Research,* 54**,** 8579-8586.

Djebbar M., Djafri F., Bouchekara M. ,Djafri A., 2012, Adsorption of Phenol on Natural Clay, *Applied Water Science,* 2**,** 77-86.

Doğan M., Abak H. ,Alkan M., 2009, Adsorption of Methylene Blue onto Hazelnut Shell: Kinetics, Mechanism and Activation Parameters, *Journal of Hazardous Materials,* 164**,** 172-181.

dos Santos R.M.M., Gonçalves R.G.L., Constantino V.R.L., Santilli C.V., Borges P.D., Tronto J. ,Pinto F.G., 2017, Adsorption of Acid Yellow 42 Dye on Calcined Layered Double Hydroxide: Effect of Time, Concentration, Ph and Temperature, *Applied Clay Science,* 140**,** 132-139.

Dubey D., Pardasani D., Gupta A., Palit M., Kanaujia P.K. ,Tak V., 2006, Hollow Fiber-Mediated Liquid-Phase Microextraction of Chemical Warfare Agents from Water, *Journal of Chromatography A,* 1107**,** 29-35.

Dursun G., Çiçek H. ,Dursun A.Y., 2005, Adsorption of Phenol from Aqueous Solution by Using Carbonised Beet Pulp, *Journal of Hazardous Materials,* 125**,** 175-182.

El-Khaiary M.I., 2008, Least-Squares Regression of Adsorption Equilibrium Data: Comparing the Options, *Journal of Hazardous Materials,* 158**,** 73-87.

Elmoubarki R., Mahjoubi F.Z., Elhalil A., Tounsadi H., Abdennouri M., Sadiq M.h., Qourzal S., Zouhri A. ,Barka N., 2017, Ni/Fe and Mg/Fe Layered Double Hydroxides and Their Calcined Derivatives: Preparation, Characterization and Application on Textile Dyes Removal, *Journal of Materials Research and Technology,* 6**,** 271-283.

Evans D.G. ,Duan X., 2006, Preparation of Layered Double Hydroxides and Their Applications as Additives in Polymers, as Precursors to Magnetic Materials and in Biology and Medicine, *Chemical Communications***,** 485-496.

Fang H., Liu Y., Ke S. ,Zhang T., 2004, Anaerobic Degradation of Phenol in Wastewater at Ambient Temperature, *Water Science and Technology,* 49**,** 95-102.

Farah J.Y. ,Elgendy N., 2013, Performance, Kinetics and Equilibrium in Biosorption of Anionic Dye Acid Red 14 by the Waste Biomass of Saccharomyces Cerevisiae as a Low-Cost Biosorbent, *Turkish Journal of Engineering and Environmental Sciences,* 37**,** 146-161.

Feng J., He Y., Liu Y., Du Y. ,Li D., 2015, Supported Catalysts Based on Layered Double Hydroxides for Catalytic Oxidation and Hydrogenation: General Functionality and Promising Application Prospects, *Chemical Society Reviews,* 44**,** 5291-5319.

Forano C., Costantino U., Prévot V. ,Gueho C.T. 2013. Layered Double Hydroxides (Ldh). *Developments in Clay Science.* Elsevier.

Forano C., Hibino T., Leroux F. ,Taviot-Guého C., 2006, .1 Layered Double Hydroxides, *Developments in Clay Science,* 1**,** 1021-1095.

Fost S. ,Aly M. 1981. Adsorption Processes for Water Treatment. Betterworth Publications, Stoneharm, Massachusetts, Mass, USA.

Gao H., Cao R., Xu X., Xue J., Zhang S., Hayat T., Alharbi N.S. ,Li J., 2018, Surface Area- and Structure-Dependent Effects of Ldh for Highly Efficient Dye Removal, *ACS Sustainable Chemistry and Engineering,* 7**,** 905-915.

Gao Z., Du B., Zhang G., Gao Y., Li Z., Zhang H. ,Duan X., 2011, Adsorption of Pentachlorophenol from Aqueous Solution on Dodecylbenzenesulfonate Modified Nickel−

Titanium Layered Double Hydroxide Nanocomposites, *Industrial and Engineering Chemistry Research,* 50**,** 5334-5345.

Gardziella A., Pilato L.A. ,Knop A. 2013. *Phenolic Resins: Chemistry, Applications, Standardization, Safety and Ecology*, Springer Science and Business Media.

Garg V.K., Amita M., Kumar R. ,Gupta R., 2004, Basic Dye (Methylene Blue) Removal from Simulated Wastewater by Adsorption Using Indian Rosewood Sawdust: A Timber Industry Waste, *Dyes and pigments,* 63**,** 243-250.

Gasser M., Mohsen H. ,Aly H., 2008, Humic Acid Adsorption onto Mg/Fe Layered Double Hydroxide, *Colloids and Surfaces A: Physicochemical and Engineering Aspects,* 331**,** 195-201.

Gevers B.R., Naseem S., Leuteritz A. ,Labuschagné F.J., 2019, Comparison of Nano-Structured Transition Metal Modified Tri-Metal Mgmal–Ldhs (M= Fe, Zn, Cu, Ni, Co) Prepared Using Co‑Precipitation, *RSC advances,* 9**,** 28262-28275.

Geyikci F. ,Coruh S., 2013, Adsorptive Removal of Aromatic Compound by Montmorillonite: Application of Factorial Design Analysis, *Acta Geodynamica et Geromaterialia,* 10**,** 335-341.

Glassman J.A., 2009, The Acquittal of Carbon Dioxide, *Online: http://www.rocketscientistsjournal. com/2006/10/co2_acquittal. htm l.*

Gong J., Liu T., Wang X., Hu X. ,Zhang L., 2011, Efficient Removal of Heavy Metal Ions from Aqueous Systems with the Assembly of Anisotropic Layered Double Hydroxide Nanocrystals@ Carbon Nanosphere, *Environmental Science and Technology,* 45**,** 6181-6187.

Gong M., Li Y., Wang H., Liang Y., Wu J.Z., Zhou J., Wang J., Regier T., Wei F. ,Dai H., 2013, An Advanced Ni–Fe Layered Double Hydroxide Electrocatalyst for Water Oxidation, *Journal of the American Chemical Society,* 135**,** 8452-8455.

Gross K.C. ,Seybold P.G., 2001, Substituent Effects on the Physical Properties and Pka of Phenol, *International Journal of Quantum Chemistry,* 85**,** 569-579.

Grover A., Mohiuddin I., Malik A.K., Aulakh J.S. ,Kim K.-H., 2019, Zn-Al Layered Double Hydroxides Intercalated with Surfactant: Synthesis and Applications for Efficient Removal of Organic Dyes, *Journal of Cleaner Production,* 240**,** 118090.

Gu Z., Wu A., Li L. ,Xu Z.P., 2014, Influence of Hydrothermal Treatment on Physicochemical Properties and Drug Release of Anti-Inflammatory Drugs of Intercalated Layered Double Hydroxide Nanoparticles, *Pharmaceutics,* 6**,** 235-248.

Günay A., Arslankaya E. ,Tosun I., 2007, Lead Removal from Aqueous Solution by Natural and Pretreated Clinoptilolite: Adsorption Equilibrium and Kinetics, *Journal of Hazardous Materials,* 146**,** 362-371.

Harizi I., Chebli D., Bouguettoucha A., Rohani S. ,Amrane A., 2019, A New Mg–Al–Cu–Fe-Ldh Composite to Enhance the Adsorption of Acid Red 66 Dye: Characterization, Kinetics and Isotherm Analysis, *Arabian Journal for Science and Engineering,* 44**,** 5245-5261.

He H., Ma Y., Zhu J., Yuan P. ,Qing Y., 2010, Organoclays Prepared from Montmorillonites with Different Cation Exchange Capacity and Surfactant Configuration, *Applied clay science,* 48**,** 67-72.

Hernández W.Y., Aliç F., Verberckmoes A. ,Van Der Voort P., 2017, Tuning the Acidic–Basic Properties by Zn-Substitution in Mg–Al Hydrotalcites as Optimal Catalysts for the Aldol Condensation Reaction, *Journal of Materials Science,* 52**,** 628-642.

Hernández W.Y., Lauwaert J., Van Der Voort P. ,Verberckmoes A., 2017, Recent Advances on the Utilization of Layered Double Hydroxides (Ldhs) and Related Heterogeneous Catalysts in a Lignocellulosic-Feedstock Biorefinery Scheme, *Green Chemistry,* 19**,** 5269-5302.

Hibino T., 2018, Anion Selectivity of Layered Double Hydroxides: Effects of Crystallinity and Charge Density, *European Journal of Inorganic Chemistry,* 2018**,** 722-730.

Ho Y., Ng J. ,McKay G., 2000, Kinetics of Pollutant Sorption by Biosorbents, *Separation and purification methods,* 29**,** 189-232.

Hu C., He Y., Liu D., Sun S., Li D., Zhu Q. ,Yu J., 2019, Advances in Mineral Processing Technologies Related to Iron, Magnesium, and Lithium, *Reviews in Chemical Engineering,* 36**,** 107-146.

Hu G., Wang N., O'Hare D. ,Davis J., 2007, Synthesis of Magnesium Aluminium Layered Double Hydroxides in Reverse Microemulsions, *Journal of Materials Chemistry,* 17**,** 2257-2266.

Hu J., Song Z., Chen L., Yang H., Li J. ,Richards R., 2010, Adsorption Properties of Mgo (111) Nanoplates for the Dye Pollutants from Wastewater, *Journal of Chemical and Engineering Data,* 55**,** 3742-3748.

Hu M., Yan X., Hu X., Feng R. ,Zhou M., 2018a, High-Capacity Adsorption of Benzotriazole from Aqueous Solution by Calcined Zn-Al Layered Double Hydroxides, *Colloids and Surfaces A: Physicochemical and Engineering Aspects,* 540**,** 207-214.

Hu Z.-P., Gao Z.-M., Liu X. ,Yuan Z.-Y., 2018b, High-Surface-Area Activated Red Mud for Efficient Removal of Methylene Blue from Wastewater, *Adsorption Science and Technology,* 36**,** 62-79.

Hussein M.Z.B., Zainal Z. ,Choong E.M., 2001, Structure and Surface Transformations of Humic-Adsorbed Synthetic Hydrotalcite-Like Materials, *Journal of Porous Materials,* 8**,** 219- 226.

Ibrahim M.B. ,Jimoh W.L., 2012, Thermodynamics and Adsorption Isotherms for the Biosorption of Cr (Vi), Ni (II) and Cd (II) onto Maize Cob, *ChemSearch Journal,* 3**,** 7-12.

Iftekhar, S., Srivastava, V., Hammouda, S. B. & Sillanpää, M. 2018. Fabrication of novel metal ion imprinted xanthan gum-layered double hydroxide nanocomposite for adsorption of rare earth elements. *Carbohydrate polymers,* 194**,** 274-284.

Iqbal M.A. ,Fedel M., 2018, The Effect of the Surface Morphologies on the Corrosion Resistance of *in Situ* Growth Mgal-Ldh Based Conversion Film on Aa6082, *Surface and Coatings Technology,* 352**,** 166-174.

Iyi N. ,Sasaki T., 2008, Deintercalation of Carbonate Ions and Anion Exchange of an Al-Rich Mgal-Ldh (Layered Double Hydroxide), *Applied Clay Science,* 42**,** 246-251.

Jang H.J., Lee C.H., Kim S., Kim S.H. ,Lee K.B., 2014, Hydrothermal Synthesis of K_2CO_3 Promoted Hydrotalcite from Hydroxide-Form Precursors for Novel High-Temperature CO_2 Sorbent, *ACS Applied Materials and Interfaces,* 6**,** 6914-6919.

Jayabalakrishnan R. ,Raja S.M., 2007, Vermiculite Clay Mineral Barrier Treatment System for Chrome Tannery Effluent, *Journal of Applied Sciences,* 7**,** 1547-1550.

Jiao F.-p., Fu Z.-d., Shuai L. ,Chen X.-q., 2012, Removal of Phenylalanine from Water with Calcined Cuznal-CO_3 Layered Double Hydroxides, *Transactions of Nonferrous Metals Society of China,* 22**,** 476-482.

Juang R.-S. ,Chen M.-L., 1997, Application of the Elovich Equation to the Kinetics of Metal Sorption with Solvent-Impregnated Resins, *Industrial and Engineering Chemistry Research,* 36**,** 813-820.

Kalló D., 2001, Applications of Natural Zeolites in Water and Wastewater Treatment, *Reviews in Mineralogy and Geochemistry,* 45**,** 519-550.

Kameda T., Yamazaki T. ,Yoshioka T., 2010, Preparation of Mg–Al Layered Double Hydroxides Intercalated with 1, 3, 6-Naphthalenetrisulfonate and 3-Amino-2, 7-Naphthalenedisulfonate and Assessment of Their Selective Uptake of Aromatic Compounds from Aqueous Solutions, *Solid state sciences,* 12**,** 946-951.

Kamenev I., Munter R., Pikkov L. ,Kekisheva L., 2003, Wastewater Treatment in Oil Shale Chemical Industry, *Oil Shale,* 20**,** 443-458.

Kanekar P., Sarnaik S. ,Kelkar A., 1998, Bioremediation of Phenol by Alkaliphilic Bacteria Isolated from Alkaline Lake of Lonar, India, *Journal of Applied Microbiology,* 85**,** 128S-133S.

Karci A., Arslan-Alaton I., Olmez-Hanci T. ,Bekbolet M., 2013, Degradation and Detoxification of Industrially Important Phenol Derivatives in Water by Direct Uv-C Photolysis and H2o2/Uv-C Process: A Comparative Study, *Chemical Engineering Journal,* 224**,** 4-9.

Kerchiche S., Chebout R., Barama A. ,Bachari K., 2017, New Way for Iron Introduction in Ldh Matrix Used as Catalysts for Friedel–Crafts Reactions, *Arabian Journal of Chemistry,* 10**,** S328-S333.

Khalfaoui M., Knani S., Hachicha M. ,Lamine A.B., 2003, New Theoretical Expressions for the Five Adsorption Type Isotherms Classified by Bet Based on Statistical Physics Treatment, *Journal of Colloid and Interface Science,* 263**,** 350-356.

Khenifi A., Derriche Z., Mousty C., Prévot V. ,Forano C., 2010, Adsorption of Glyphosate and Glufosinate by Ni2alno3 Layered Double Hydroxide, *Applied Clay Science,* 47**,** 362-371.

Khitous M., Salem Z. ,Halliche D., 2016, Removal of Phosphate from Industrial Wastewater Using Uncalcined Mgal-No3 Layered Double Hydroxide: Batch Study and Modeling, *Desalination and Water Treatment,* 57**,** 15920-15931.

Kim Y.M., Park D., Lee D.S., Jung K.A. ,Park J.M., 2009, Sudden Failure of Biological Nitrogen and Carbon Removal in the Full-Scale Pre-Denitrification Process Treating Cokes Wastewater, *Bioresource Technology,* 100**,** 4340-4347.

Kinloch A.J. 2012. *Adhesion and Adhesives: Science and Technology*, Springer Science and Business Media.

Klemkaite K., Prosycevas I., Taraskevicius R., Khinsky A. ,Kareiva A., 2011, Synthesis and Characterization of Layered Double Hydroxides with Different Cations (Mg, Co, Ni, Al), Decomposition and Reformation of Mixed Metal Oxides to Layered Structures, *Central European Journal of Chemistry,* 9**,** 275-282.

Kloprogge J.T., Wharton D., Hickey L. ,Frost R.L., 2002, Infrared and Raman Study of Interlayer Anions CO_3^{2-}, NO_3^-, SO_4^{2-} and ClO_4^- in Mg/Al-Hydrotalcite, *American Mineralogist,* 87**,** 623-629.

Kovanda F., Grygar T., Dorničák V., Rojka T., Bezdička P. ,Jirátová K., 2005, Thermal Behaviour of Cu–Mg–Mn and Ni–Mg–Mn Layered Double Hydroxides and Characterization of Formed Oxides, *Applied Clay Science,* 28**,** 121-136.

Kukadiya A., 2016, Study of Removal of Phenol by Biological Treatment Methods—with Ref-Erence to Moving Bed Biofilm Reactor and Activated Sludge Process, *International Journal of Engineering Research and Technology,* 5**,** 400-403.

Kumar P., 2010, *Remediation of High Phenol Concentration Using Chemical and Biological Technologies*, University of Saskatchewan.

Kuosa M., Kallas J. ,Häkkinen A., 2015, Ozonation of P-Nitrophenol at Different Ph Values of Water and the Influence of Radicals at Acidic Conditions, *Journal of Environmental Chemical Engineering,* 3**,** 325-332.

Labuschagne F.J.W.J., Wiid A., Venter H., Gevers B. ,Leuteritz A., 2018, Green Synthesis of Hydrotalcite from Untreated Magnesium Oxide and Aluminum Hydroxide, *Green Chemistry Letters and Reviews,* 11**,** 18-28.

Laipan M., Fu H., Zhu R., Sun L., Steel R.M., Ye S., Zhu J. ,He H., 2018, Calcined Mg/Al-Ldh for Acidic Wastewater Treatment: Simultaneous Neutralization and Contaminant Removal, *Applied Clay Science,* 153**,** 46-53.

Lakherwal D., 2014, Adsorption of Heavy Metals: A Review, *International journal of environmental research and development,* 4**,** 41-48.

Lanas J. ,Alvarez J.I., 2004, Dolomitic Lime: Thermal Decomposition of Nesquehonite, *Thermochimica Acta,* 421**,** 123-132.

Laoufi N., Tassalit D. ,Bentahar F., 2008, The Degradation of Phenol in Water Solution by Tio2 Photocatalysis in a Helical Reactor, *Global NEST Journal,* 10**,** 404-418.

Largitte L. ,Pasquier R., 2016, A Review of the Kinetics Adsorption Models and Their Application to the Adsorption of Lead by an Activated Carbon, *Chemical Engineering Research and Design,* 109**,** 495-504.

Lavrich D.J., Wetterer S.M., Bernasek S.L. ,Scoles G., 1998, Physisorption and Chemisorption of Alkanethiols and Alkyl Sulfides on Au (111), *The Journal of Physical Chemistry B,* 102**,** 3456-3465.

Leechart P., Nakbanpote W. ,Thiravetyan P., 2009, Application of 'Waste'wood-Shaving Bottom Ash for Adsorption of Azo Reactive Dye, *Journal of environmental management,* 90**,** 912-920.

Lei X., Jin M. ,Williams G.R., 2014, Layered Double Hydroxides in the Remediation and Prevention of Water Pollution, *Energy and Environment Focus,* 3**,** 4-22.

Li Y., Bi H.-Y. ,Zang Y.-B., 2013, Single and Simultaneous Sorption of Copper Ions and P-Cresol into Surfactant-Modified Hydrotalcite-Like Compound with Chelating Ligand, *Separation and Purification Technology,* 116**,** 448-453.

Liang X., Zang Y., Xu Y., Tan X., Hou W., Wang L. ,Sun Y., 2013, Sorption of Metal Cations on Layered Double Hydroxides, *Colloids and Surfaces A: physicochemical and engineering aspects,* 433**,** 122-131.

Lin Y.-J., Li D.-Q., Evans D.G. ,Duan X., 2005, Modulating Effect of Mg–Al–CO_3 Layered Double Hydroxides on the Thermal Stability of Pvc Resin, *Polymer Degradation and Stability,* 88**,** 286-293.

Lipczynska-Kochany E., 1991, Degradation of Aqueous Nitrophenols and Nitrobenzene by Means of the Fenton Reaction, *Chemosphere,* 22**,** 529-536.

Liu Y., 2009, Is the Free Energy Change of Adsorption Correctly Calculated?, *Journal of Chemical and Engineering Data,* 54**,** 1981-1985.

Liu Y. ,Xu H., 2007, Equilibrium, Thermodynamics and Mechanisms of Ni2+ Biosorption by Aerobic Granules, *Biochemical Engineering Journal,* 35**,** 174-182.

Luo Z., Gao M., Yang S.,Yang Q., 2015, Adsorption of Phenols on Reduced-Charge Montmorillonites Modified by Bispyridinium Dibromides: Mechanism, Kinetics and Thermodynamics Studies, *Colloids and Surfaces A: Physicochemical and Engineering Aspects,* 482**,** 222-230.

Lupa L., Cocheci L., Pode R., Hulka I., 2018, Phenol Adsorption Using Aliquat 336 Functionalized Zn-Al Layered Double Hydroxide, *Separation and Purification Technology,* 196**,** 82-95.

Lv L., He J., Wei M., Evans D., Duan X., 2006, Factors Influencing the Removal of Fluoride from Aqueous Solution by Calcined Mg–Al–CO_3 Layered Double Hydroxides, *Journal of Hazardous Materials,* 133**,** 119-128.

Ma M. ,Cantwell F.F., 1998, Solvent Microextraction with Simultaneous Back-Extraction for Sample Cleanup and Preconcentration: Quantitative Extraction, *Analytical Chemistry,* 70**,** 3912-3919.

Mallakpour, S. & Hatami, M. 2019. An effective, low-cost and recyclable bio-adsorbent having amino acid intercalated LDH@ Fe3O4/PVA magnetic nanocomposites for removal of methyl orange from aqueous solution. *Applied Clay Science,* 174**,** 127-137.

McBain A., Senior E., Paterson A., Du Plessis C. ,Watson-Craik I., 1996, Bioremediation of Soil Contaminated with 4-Chloro-2-Methylphenoxyacetic Acid(Mcpa): Essential Laboratory Studies, *South African Journal of Science,* 92**,** 426-430.

McCoy M. ,Liapis A., 1991, Evaluation of Kinetic Models for Biospecific Adsorption and Its Implications for Finite Bath and Column Performance, *Journal of Chromatography A,* 548**,** 25- 60.

McKay G. ,Ho Y., 1999, The Sorption of Pb (Ii) on Peat, *Water Res,* 33**,** 578-584.

Meenakshisundaram S., 2017, Environmental Photocatalysis/Photocatalytic Decontamination, *Handbook of Eco Materials***,** 1-16.

Metwally S., El-Gammal B., Aly H. ,Abo-El-Enein S., 2011, Removal and Separation of Some Radionuclides by Poly-Acrylamide Based Ce (Iv) Phosphate from Radioactive Waste Solutions, *Separation Science and Technology,* 46**,** 1808-1821.

Michałowicz J. ,Duda W., 2007, Phenols--Sources and Toxicity, *Polish Journal of Environmental Studies,* 16.

Milanovic N., 2016, *Synthesis, Structural and Magnetic Properties of Layered Double Hydroxides,* Master of Materials Science and Nanotechnology, University of Oslo, Oslo, Norway.

Mitran G., Cacciaguerra T., Loridant S., Tichit D. ,Marcu I.-C., 2012, Oxidative Dehydrogenation of Propane over Cobalt-Containing Mixed Oxides Obtained from Ldh Precursors, *Applied Catalysis A: General,* 417**,** 153-162.

Mohammadi S., Kargari A., Sanaeepur H., Abbassian K., Najafi A. ,Mofarrah E., 2015, Phenol Removal from Industrial Wastewaters: A Short Review, *Desalination and Water Treatment,* 53**,** 2215-2234.

Mohan S.V., Rao N.C. ,Karthikeyan J., 2002, Adsorptive Removal of Direct Azo Dye from Aqueous Phase onto Coal Based Sorbents: A Kinetic and Mechanistic Study, *Journal of Hazardous Materials,* 90**,** 189-204.

Mohapatra L. ,Parida K., 2016, A Review on the Recent Progress, Challenges and Perspective of Layered Double Hydroxides as Promising Photocatalysts, *Journal of Materials Chemistry A,* 4**,** 10744-10766.

Müller R. ,Babel W., 1994, Phenol and Its Derivatives as Heterotrophic Substrates for Microbial Growth—an Energetic Comparison, *Applied microbiology and biotechnology,* 42**,** 446-451.

Mulligan C.N., Yong R.N. ,Gibbs B.F., 2001, Heavy Metal Removal from Sediments by Biosurfactants, *Journal of Hazardous Materials,* 85**,** 111-125.

Myers A.L. ,Monson P.A., 2014, Physical Adsorption of Gases: The Case for Absolute Adsorption as the Basis for Thermodynamic Analysis, *Adsorption,* 20**,** 591-622.

Naguib D.M. ,Badawy N.M., 2020, Phenol Removal from Wastewater Using Waste Products, *Journal of Environmental Chemical Engineering,* 8**,** 103592.

Narayanan S. ,Krishna K., 1998, Hydrotalcite-Supported Palladium Catalysts: Part I: Preparation, Characterization of Hydrotalcites and Palladium on Uncalcined Hydrotalcites for Co Chemisorption and Phenol Hydrogenation, *Applied Catalysis A: General,* 174**,** 221-229.

Naseer W.A., 2018, *Adsorption of Rare Earth Elements on Novel "Mg-Al Layered Double Hydroxide with Gum Arabic",* Lappeenranta University of Technology, Lappeenranta, Finland.

National Centre for Biotechnology Information N.C.f.B.I. 2021. *Pubchem Compound Summary for Cid 966, Phenol;Phenoxide.* (Accessed 30 January 2021).

Nethaji S., Sivasamy A. ,Mandal A., 2013, Adsorption Isotherms, Kinetics and Mechanism for the Adsorption of Cationic and Anionic Dyes onto Carbonaceous Particles Prepared from Juglans Regia Shell Biomass, *International Journal of Environmental Science and Technology,* 10**,** 231-242.

Ni Z.-M., Xia S.-J., Wang L.-G., Xing F.-F. ,Pan G.-X., 2007, Treatment of Methyl Orange by Calcined Layered Double Hydroxides in Aqueous Solution: Adsorption Property and Kinetic Studies, *Journal of Colloid and Interface Science,* 316**,** 284-291.

Nundkumar N., 2017, *A Comparative Investigation of Transgene Expression and Gene Silencing of Non-Functionalized Layered Double Hydroxides Versus Amino-Acid Functionalized Hydrotalcites,* Doctor of Philosophy, University of Kwazulu Natal, Durban, South Africa.

Ogawa M. ,Asai S., 2000, Hydrothermal Synthesis of Layered Double Hydroxide− Deoxycholate Intercalation Compounds, *Chemistry of materials,* 12**,** 3253-3255.

Orthman J., Zhu H. ,Lu G., 2003, Use of Anion Clay Hydrotalcite to Remove Coloured Organics from Aqueous Solutions, *Separation and Purification Technology,* 31**,** 53-59.

Otero M., Rozada F., Calvo L., Garcıa A. ,Moran A., 2003, Elimination of Organic Water Pollutants Using Adsorbents Obtained from Sewage Sludge, *Dyes and Pigments,* 57**,** 55-65.

Paasivirta J., Heinola K., Humppi T., Karjalainen A., Knuutinen J., Mäntykoski K., Paukku R., Piilola T., Surma-Aho K. ,Tarhanen J., 1985, Polychlorinated Phenols, Guaiacols and Catechols in Environment, *Chemosphere,* 14**,** 469-491.

Paller G., Hommel R.K. ,Kleber H.P., 1995, Phenol Degradation by Acinetobacter Calcoaceticus Ncib 8250, *Journal of Basic Microbiology,* 35**,** 325-335.

Pandey P., Sambi S., Sharma S. ,Singh S. Batch Adsorption Studies for the Removal of Cu (Ii) Ions by Zeolitenax from Aqueous Stream. Proceedings of the world congress on Engineering and computer science, 2009. 20-22.

Paredes S.P., Valenzuela M.A., Fetter G. ,Flores S.O., 2011, Tio2/Mgal Layered Double Hydroxides Mechanical Mixtures as Efficient Photocatalysts in Phenol Degradation, *Journal of physics and Chemistry of solids,* 72**,** 914-919.

Pedersen, O., Colmer, T. D. & Sand-Jensen, K. 2013. Underwater photosynthesis of submerged plants–recent advances and methods. *Frontiers in Plant Science,* 4**,** 140.

Peings V., Frayret J. ,Pigot T., 2015, Mechanism for the Oxidation of Phenol by Sulfatoferrate (Vi): Comparison with Various Oxidants, *Journal of Environmental Management,* 157**,** 287-296.

Peng S., Ma M., Jin S. ,Chen T., 2009, Kinetics of P-Nitrophenol Adsorption by Layered Double Oxides During Its Hydration, *Water Environment Research,* 81**,** 91-96.

Perez-Moya M., Graells M., del Valle L.J., Centelles E. ,Mansilla H.D., 2007, Fenton and Photo-Fenton Degradation of 2-Chlorophenol: Multivariate Analysis and Toxicity Monitoring, *Catalysis Today,* 124**,** 163-171.

Pérez-Barrado E., 2015, *Layered Double Hydroxides for Applications in Catalysis and Electroluminescent Devices*, Universitat Rovira i Virgili, Tarragona, Spain.

Piccin J., Dotto G. ,Pinto L., 2011, Adsorption Isotherms and Thermochemical Data of Fd and C Red N 40 Binding by Chitosan, *Brazilian Journal of Chemical Engineering,* 28**,** 295-304.

Pignatello J.J., 1998, Soil Organic Matter as a Nanoporous Sorbent of Organic Pollutants, *Advances in Colloid and Interface Science,* 76**,** 445-467.

Pilato L. 2010. *Phenolic Resins: A Century of Progress*, Springer.

Pillai I.M.S. ,Gupta A.K., 2015, Batch and Continuous Flow Anodic Oxidation of 2, 4-Dinitrophenol: Modeling, Degradation Pathway and Toxicity, *Journal of Electroanalytical Chemistry,* 756**,** 108-117.

Plazinski W., Rudzinski W. ,Plazinska A., 2009, Theoretical Models of Sorption Kinetics Including a Surface Reaction Mechanism: A Review, *Advances in Colloid and Interface Science,* 152**,** 2-13.

Polat H., Molva M. ,Polat M., 2006, Capacity and Mechanism of Phenol Adsorption on Lignite, *International Journal of Mineral Processing,* 79**,** 264-273.

Prince J., Montoya A., Ferrat G. ,Valente J.S., 2009, Proposed General Sol− Gel Method to Prepare Multimetallic Layered Double Hydroxides: Synthesis, Characterization, and Envisaged Application, *Chemistry of Materials,* 21**,** 5826-5835.

Rabaaoui N., Saad M.E.K., Moussaoui Y., Allagui M.S., Bedoui A. ,Elaloui E., 2013, Anodic Oxidation of O-Nitrophenol on Bdd Electrode: Variable Effects and Mechanisms of Degradation, *Journal of Hazardous Materials,* 250**,** 447-453.

Raj K. ,Viswanathan B., 2009, Effect of Surface Area, Pore Volume and Particle Size of P25 Titania on the Phase Transformation of Anatase to Rutile.

Ramírez E.E.P., Asunción M., Rivalcoba V.S., Hernández A.L.M. ,Santos C.V., 2017, Removal of Phenolic Compounds from Water by Adsorption and Photocatalysis, *Phenolic compounds-Natural Sources, Importance and Applications*.

Rao N., Singh J.R., Misra R. ,Nandy T., 2009, Liquid–Liquid Extraction of Phenol from Simulated Sebacic Acid Wastewater.

Rashed M.N., 2013, Adsorption Technique for the Removal of Organic Pollutants from Water and Wastewater, *Organic Pollutants-Monitoring, Risk and Treatment***,** 167-194.

Redaoui D., Sahnoune F., Heraiz M. ,Raghdi A., 2017, Mechanism and Kinetic Parameters of the Thermal Decomposition of Gibbsite Al (Oh) 3 by Thermogravimetric Analysis, *Acta Phys. Pol. Ser. A,* 131**,** 562-565.

Ribeiro A.R., Nunes O.C., Pereira M.F. ,Silva A.M., 2015, An Overview on the Advanced Oxidation Processes Applied for the Treatment of Water Pollutants Defined in the Recently Launched Directive 2013/39/Eu, *Environment International,* 75**,** 33-51.

Ringot D., Lerzy B., Chaplain K., Bonhoure J.-P., Auclair E. ,Larondelle Y., 2007, In Vitro Biosorption of Ochratoxin a on the Yeast Industry by-Products: Comparison of Isotherm Models, *Bioresource Technology,* 98**,** 1812-1821.

Rives V. 2001. *Layered Double Hydroxides: Present and Future*, Nova Publishers.

Rizescu, C. E., Vasile, D. A., Minea, D. A., Stirbescu, R.M., Marin, L., Atkinson, I., Predoana, L. & Ion, R.M. 2020. Layered Double Hydroxides as Consolidants and Anion Absorbents for Heritage Conservation. *Multidisciplinary Digital Publishing Institute Proceedings,* 57**,** 84.

Rodgher V.S., 2012, *Photocalytic Degradation of Malic Acid under Thin Coated TiO$_2$*, University of Western Ontario, Ontario, Canada.

Roelofs J., Lensveld D., Van Dillen A. ,De Jong K., 2001, On the Structure of Activated Hydrotalcites as Solid Base Catalysts for Liquid-Phase Aldol Condensation, *Journal of Catalysis,* 203**,** 184-191.

Ruan X., Huang S., Chen H. ,Qian G., 2013, Sorption of Aqueous Organic Contaminants onto Dodecyl Sulfate Intercalated Magnesium Iron Layered Double Hydroxide, *Applied Clay Science,* 72**,** 96-103.

Russell J. ,Wilson M., 1987, A Hand Book of Determinative Methods in Clay Mineralogy, *Blackie and Son Ltd., New York***,** 301-320.

Sahoo M., Singha S. ,Parida K., 2011, Amine Functionalized Layered Double Hydroxide: A Reusable Catalyst for Aldol Condensation, *New Journal of Chemistry,* 35**,** 2503-2509.

Salih A.M., 2018, *The Purification of Industrial Wastewater to Remove Heavy Metals and Investigation into the Use of Zeolite as a Remediation Tool*, University of Wolverhampton, Wolverhampton, England.

Samiey B., 2015, A New Approach for Analysis of Adsorption from Liquid Phase: A Critical Review, *Journal of Pollution Effects and Control***,** 1-9.

Santos R., Tronto J., Briois V. ,Santilli C., 2017, Thermal Decomposition and Recovery Properties of Znal–Co 3 Layered Double Hydroxide for Anionic Dye Adsorption: Insight into the Aggregative Nucleation and Growth Mechanism of the Ldh Memory Effect, *Journal of Materials Chemistry A,* 5**,** 9998-10009.

Sattler J.J., Ruiz-Martinez J., Santillan-Jimenez E. ,Weckhuysen B.M., 2014, Catalytic Dehydrogenation of Light Alkanes on Metals and Metal Oxides, *Chemical Reviews,* 114**,** 10613-10653.

Schouten N., Van der Ham L.G., Euverink G.-J.W. ,De Haan A.B., 2007, Optimization of Layered Double Hydroxide Stability and Adsorption Capacity for Anionic Surfactants, *Adsorption,* 13**,** 523-532.

Schweigert N., Zehnder A.J. ,Eggen R.I., 2001, Chemical Properties of Catechols and Their Molecular Modes of Toxic Action in Cells, from Microorganisms to Mammals: Minireview, *Environmental Microbiology,* 3**,** 81-91.

Senturk H.B., Ozdes D., Gundogdu A., Duran C. ,Soylak M., 2009, Removal of Phenol from Aqueous Solutions by Adsorption onto Organomodified Tirebolu Bentonite: Equilibrium, Kinetic and Thermodynamic Study, *Journal of Hazardous Materials,* 172**,** 353-362.

Sepehr M.N., Al-Musawi T.J., Ghahramani E., Kazemian H. ,Zarrabi M., 2017, Adsorption Performance of Magnesium/Aluminum Layered Double Hydroxide Nanoparticles for Metronidazole from Aqueous Solution, *Arabian Journal of Chemistry,* 10**,** 611-623.

Setti N.D., Jouini N. ,Derriche Z., 2010, Sorption Study of an Anionic Dye–Benzopurpurine 4b–on Calcined and Uncalcined Mg–Al Layered Double Hydroxides, *Journal of Physics and Chemistry of Solids,* 71**,** 556-559.

Shahbeig H., Bagheri N., Ghorbanian S.A., Hallajisani A. ,Poorkarimi S., 2013, A New Adsorption Isotherm Model of Aqueous Solutions on Granular Activated Carbon, *World Journal of Modelling and Simulation,* 9**,** 243-254.

Sharma S.K., Kushwaha P.K., Srivastava V.K., Bhatt S.D. ,Jasra R.V., 2007, Effect of Hydrothermal Conditions on Structural and Textural Properties of Synthetic Hydrotalcites of Varying Mg/Al Ratio, *Industrial & Engineering Chemistry Research,* 46**,** 4856-4865.

Shimada H. ,Ogoshi T., 2005, Catalysis by Calcined Zn2+/Al3+ Layered Double Hydroxides in Friedel–Crafts Alkylation of Benzene with Benzyl Chloride, *Bulletin of the Chemical Society of Japan,* 78**,** 937-939.

Shooto N., Ayawei N., Wankasi D., Sikhwivhilu L. ,Dikio E., 2016, Study on Cobalt Metal Organic Framework Material as Adsorbent for Lead Ions Removal in Aqueous Solution, *Asian Journal of Chemistry,* 28**,** 277.

Silvério F., Dos Reis M.J., Tronto J. ,Valim J.B., 2013, Sorption of Aspartic and Glutamic Aminoacids on Calcined Hydrotalcite, *SpringerPlus,* 2**,** 211.

Sokol D., Salak A.N., Ferreira M.G., Beganskiene A. ,Kareiva A., 2018, Bi-Substituted Mg 3 Al–Co 3 Layered Double Hydroxides, *Journal of Sol‑Gel Science and Technology,* 85**,** 221-230.

Stoytcheva M. 2011. *Pesticides: Formulations, Effects, Fate*, BoD–Books on Demand.

Streat M., Patrick J. ,Perez M.C., 1995, Sorption of Phenol and Para-Chlorophenol from Water Using Conventional and Novel Activated Carbons, *Water Research,* 29**,** 467-472.

Suzum E., Okamoto M. ,Ono Y., 1990, Catalysis by Synthetic Hydrotalcite-Like Materials in Halide Exchange between Alkyl Halides, *Journal of Molecular Catalysis,* 61**,** 283-294.

Swearingen L.E., 2002, Some Physical Properties of Phenol in Benzene, *The Journal of Physical Chemistry,* 32**,** 1346-1353.

Takehira K., 2017, Recent Development of Layered Double Hydroxide-Derived Catalysts−Rehydration, Reconstitution, and Supporting, Aiming at Commercial Application−, *Applied Clay Science,* 136**,** 112-141.

Tasic Z., Gupta V. ,Antonijevic M., 2014, The Mechanism and Kinetics of Degradation of Phenolics in Wastewaters Using Electrochemical Oxidation, *Int. J. Electrochem. Sci,* 9**,** 3473-3490.

Thawornchaisit U. ,Pakulanon K., 2007, Application of Dried Sewage Sludge as Phenol Biosorbent, *Bioresource technology,* 98**,** 140-144.

Theiss F.L., 2012, *Synthesis and Characterisation of Layered Double Hydroxides and Their Application for Water Purification*, Queensland University of Technology, Australia.

Tian R., Liang R., Wei M., Evans D.G. ,Duan X. 2016. Applications of Layered Double Hydroxide Materials: Recent Advances and Perspective. *50 Years of Structure and Bonding–the Anniversary Volume.* Springer.

Tor A., Cengeloglu Y., Aydin M.E. ,Ersoz M., 2006, Removal of Phenol from Aqueous Phase by Using Neutralized Red Mud, *Journal of Colloid and Interface Science,* 300**,** 498-503.

Ugurlu M., Gurses A., Yalcin M. ,Dogar C., 2005, Removal of Phenolic and Lignin Compounds from Bleached Kraft Mill Effluent by Fly Ash and Sepiolite, *Adsorption,* 11**,** 87-97.

Vandenberg L.N., Hauser R., Marcus M., Olea N. ,Welshons W.V., 2007, Human Exposure to Bisphenol a (Bpa), *Reproductive Toxicology,* 24**,** 139-177.

Varadwaj G.B.B., Oyetade O.A., Rana S., Martincigh B.S., Jonnalagadda S.B. ,Nyamori V.O., 2017, Facile Synthesis of Three-Dimensional Mg–Al Layered Double Hydroxide/Partially Reduced Graphene Oxide Nanocomposites for the Effective Removal of Pb2+ from Aqueous Solution, *ACS applied Materials and Interfaces,* 9**,** 17290-17305.

Velu S. ,Swamy C., 1997, Effect of Substitution of Fe3+ Cr3+ on the Alkylation of Phenol with Methanol over Magnesium-Aluminium Calcined Hydrotalcite, *Applied Catalysis A: General,* 162**,** 81-91.

Villegas L.G.C., Mashhadi N., Chen M., Mukherjee D., Taylor K.E. ,Biswas N., 2016, A Short Review of Techniques for Phenol Removal from Wastewater, *Current Pollution Reports,* 2**,** 157-167.

Vreysen S. ,Maes A., 2008, Adsorption Mechanism of Humic and Fulvic Acid onto Mg/Al Layered Double Hydroxides, *Applied Clay Science,* 38**,** 237-249.

Weber Jr W.J., McGinley P.M. ,Katz L.E., 1991, Sorption Phenomena in Subsurface Systems: Concepts, Models and Effects on Contaminant Fate and Transport, *Water research,* 25**,** 499-528.

World Health Organization (W.H.O.) 1994. Phenol: Health and Safety Guide. Geneva, Switzerland.

World Health Organization (W.H.O.) 1996. Cresols: Health and Safety Guide. Geneva, Switzerland.

Yang Z., Choi K.-M., Jiang N. ,Park S.-E., 2007, Microwave Synthesis of Hydrotalcite by Urea Hydrolysis, *Bulletin of the Korean Chemical Society,* 28**,** 2029-2033.

Yang Z., Wang F., Zhang C., Zeng G., Tan X., Yu Z., Zhong Y., Wang H. ,Cui F., 2016, Utilization of Ldh-Based Materials as Potential Adsorbents and Photocatalysts for the Decontamination of Dyes Wastewater: A Review, *RSC Advances,* 6**,** 79415-79436.

You Y., Zhao H. ,Vance G.F., 2002, Hybrid Organic–Inorganic Derivatives of Layered Double Hydroxides and Dodecylbenzenesulfonate: Preparation and Adsorption Characteristics, *Journal of Materials Chemistry,* 12**,** 907-912.

Zaghouane-Boudiaf H., Boutahala M. ,Arab L., 2012, Removal of Methyl Orange from Aqueous Solution by Uncalcined and Calcined Mgnial Layered Double Hydroxides (Ldhs), *Chemical Engineering Journal,* 187**,** 142-149.

Zaghouane-Boudiaf H., Boutahala M., Tiar C., Arab L. ,Garin F., 2011, Treatment of 2, 4, 5-Trichlorophenol by Mgal–Sdbs Organo-Layered Double Hydroxides: Kinetic and Equilibrium Studies, *Chemical Engineering Journal,* 173**,** 36-41.

Zhang B., Dong Z., Sun D., Wu T. ,Li Y., 2017, Enhanced Adsorption Capacity of Dyes by Surfactant-Modified Layered Double Hydroxides from Aqueous Solution, *Journal of Industrial and Engineering Chemistry,* 49**,** 208-218.

Zhang F., Ni Z., Xia S., Liu X. ,Wang Q., 2009, Removal of Naphthol Green B from Aqueous Solution by Calcined Layered Double Hydroxides: Adsorption Property and Mechanism Studies, *Chinese Journal of Chemistry,* 27**,** 1767-1772.

Zhang J., Sun B. ,Guan X., 2013, Oxidative Removal of Bisphenol a by Permanganate: Kinetics, Pathways and Influences of Co-Existing Chemicals, *Separation and Purification Technology,* 107**,** 48-53.

Zhao X., Zhang F., Xu S., Evans D.G. ,Duan X., 2010, From Layered Double Hydroxides to Zno-Based Mixed Metal Oxides by Thermal Decomposition: Transformation Mechanism and Uv-Blocking Properties of the Product, *Chemistry of Materials,* 22**,** 3933-3942.

Zhao Y., Jia X., Waterhouse G.I., Wu L.Z., Tung C.H., O'Hare D. ,Zhang T., 2016, Layered Double Hydroxide Nanostructured Photocatalysts for Renewable Energy Production, *Advanced Energy Materials,* 6**,** 1501974.

Zhao Y., Li F., Zhang R., Evans D.G. ,Duan X., 2002, Preparation of Layered Double-Hydroxide Nanomaterials with a Uniform Crystallite Size Using a New Method Involving Separate Nucleation and Aging Steps, *Chemistry of Materials,* 14**,** 4286-4291.

Zhu K.-Z., Liu C.-B., Ye X.-K. ,Wu Y., 1997, Catalysis of Copper-Containing Transition Metal Hydrotalcite-Like Compounds in the Phenol Hydroxylation with Hydrogen Peroxide, *Chemical Journal of Chinese Universities-Chinese Edition-,* 18**,** 1533-1535.

Zhu M.-X., Li Y.-P., Xie M. ,Xin H.-Z., 2005, Sorption of an Anionic Dye by Uncalcined and Calcined Layered Double Hydroxides: A Case Study, *Journal of Hazardous Materials,* 120**,** 163-171.

Zhu X., Ma J., Wang Y., Tao J., Zhou J., Zhao Z., Xie L. ,Tian H., 2006, Fabrication of Indium Sulfide Nanofibers Via a Hydrothermal Method Assisted by Aao Template, *Materials Research Bulletin,* 41**,** 1584-1588.

Zubair M., Daud M., McKay G., Shehzad F. ,Al-Harthi M.A., 2017, Recent Progress in Layered Double Hydroxides (Ldh)-Containing Hybrids as Adsorbents for Water Remediation, *Applied Clay Science,* 143**,** 279-292.

APPENDICES

Appendix A: Phenol Calibration Curve (HPLC)

Empower2 software

Untitled

Processing Method:	080720 PROCESS
Processing Method ID:	8099
Channel:	W2489 ChA
Proc. Chnl. Descr.:	****
Date Calibrated:	2020/07/08 11:52:53 AM SAST

Project Name:	Defaults\SHANE HLOGI
System:	Alliance UV
Calibration ID:	8105

A   -4.197615e+003
B   1.431678e+004
C   0.000000e+000
D   0.000000e+000
R^2 0.999665

Calibration Plot
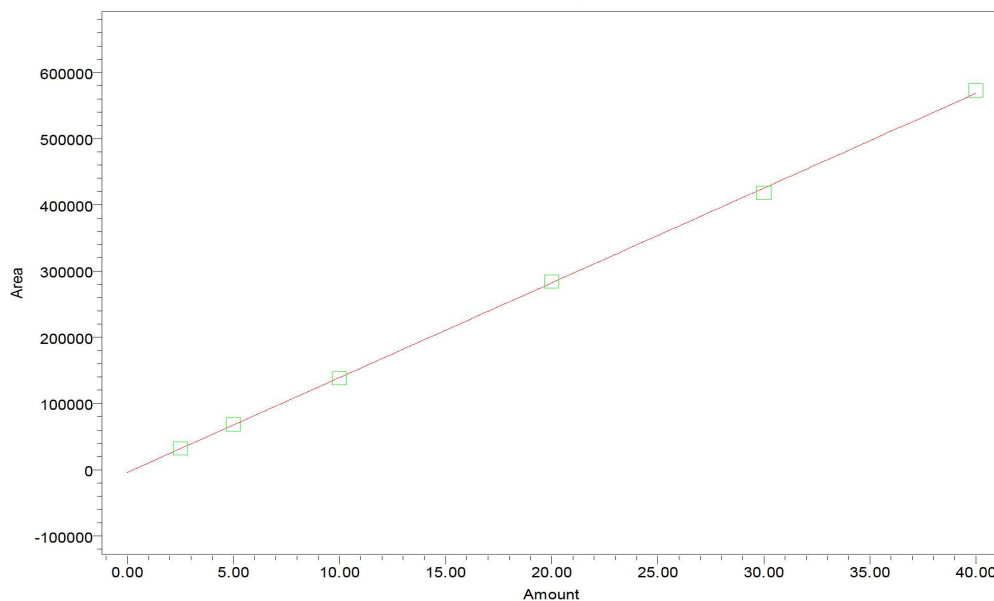
Peak: PHENOL

	Name	Level	X Value	Response	Calc. Value	% Deviation	Manual	Ignore
1	PHENOL	Level 1	2.500000	31995.534847	2.528023	1.121	No	No
2	PHENOL	Level 2	5.000000	68310.379940	5.064546	1.291	No	No
3	PHENOL	Level 3	10.000000	138341.844697	9.956112	-0.439	No	No
4	PHENOL	Level 4	20.000000	284293.499132	20.150559	0.753	No	No
5	PHENOL	Level 5	30.000000	418140.946339	29.499550	-1.668	No	No

Reported by User: Student
Report Method: Untitled
Report Method ID: 100
Page: 1 of 2

Project Name: Defaults\SHANE HLOGI
Date Printed:
2020/07/19
01:16:57 PM Africa/Johannesburg

Appendix B: XRD Spectra for commercial clays
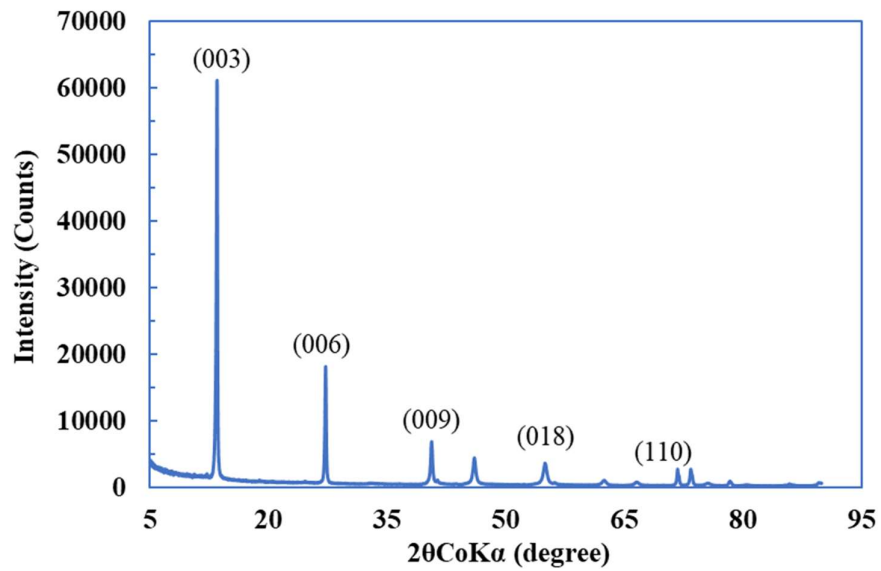
Figure B- 1: XRD spectra for neat Sorbacid 944
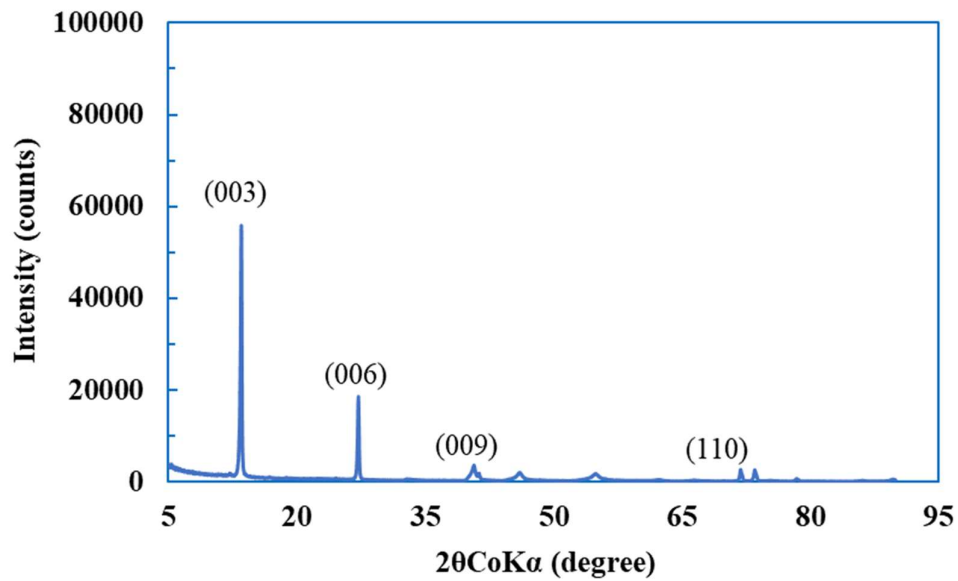
Figure B- 2: XRD patterns for DHT-4A

122
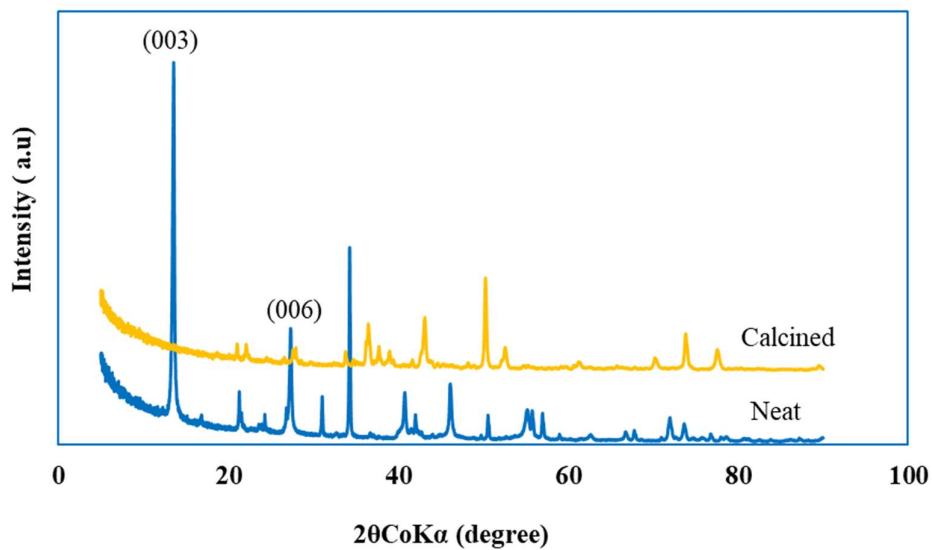
Figure B- 3: XRD peaks for GF‑450
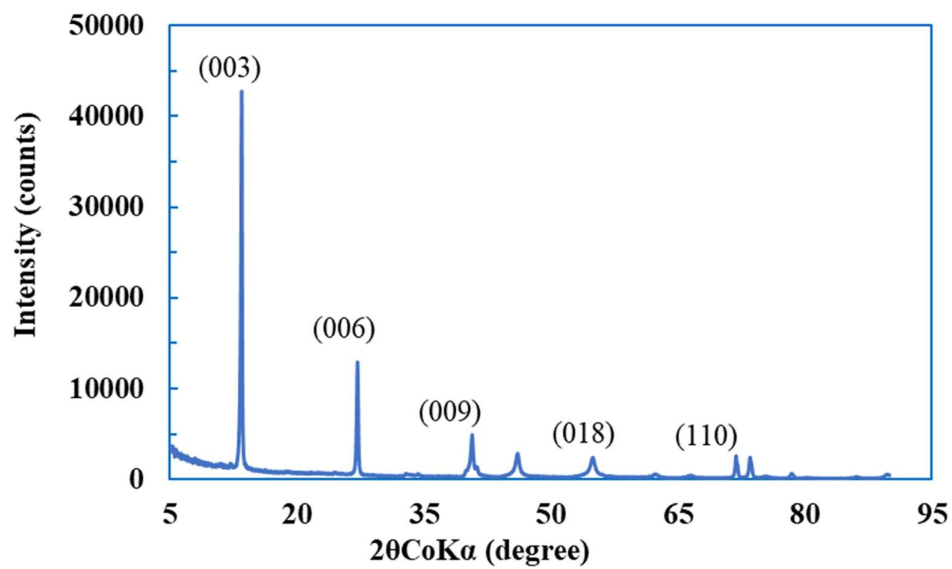
Figure B- 4: XRD peaks for Sorbacid 911
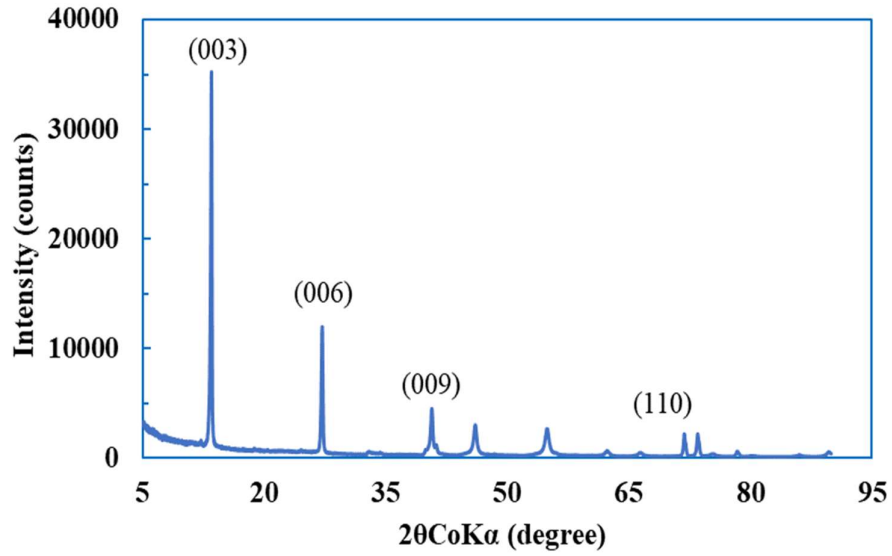
Figure B- 5: XRD peaks for Hycite 713
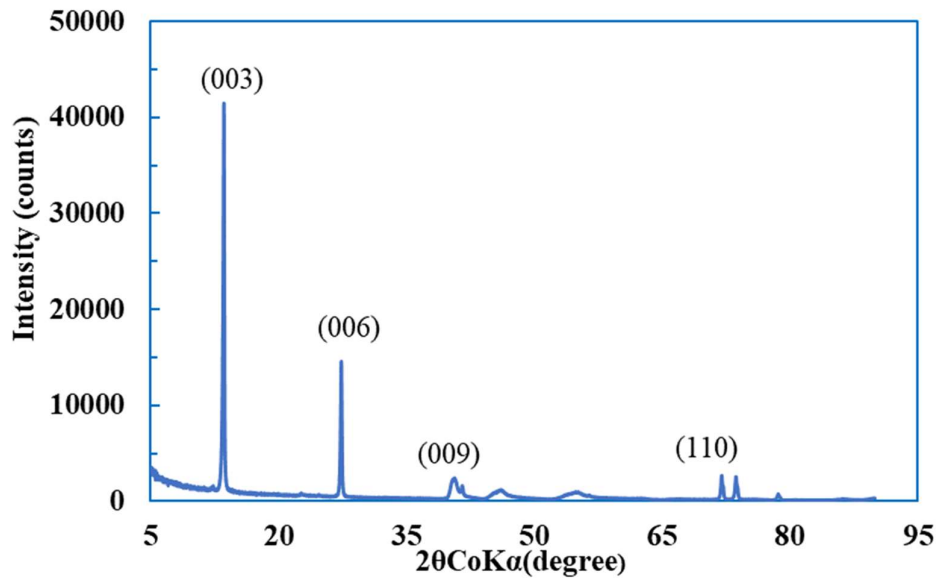
Figure B- 6: XRD peaks for Alcamizer 1

Appendix C: Thermal stability of Sorbacid 911, Alcamizer 1 and Hycite 713.
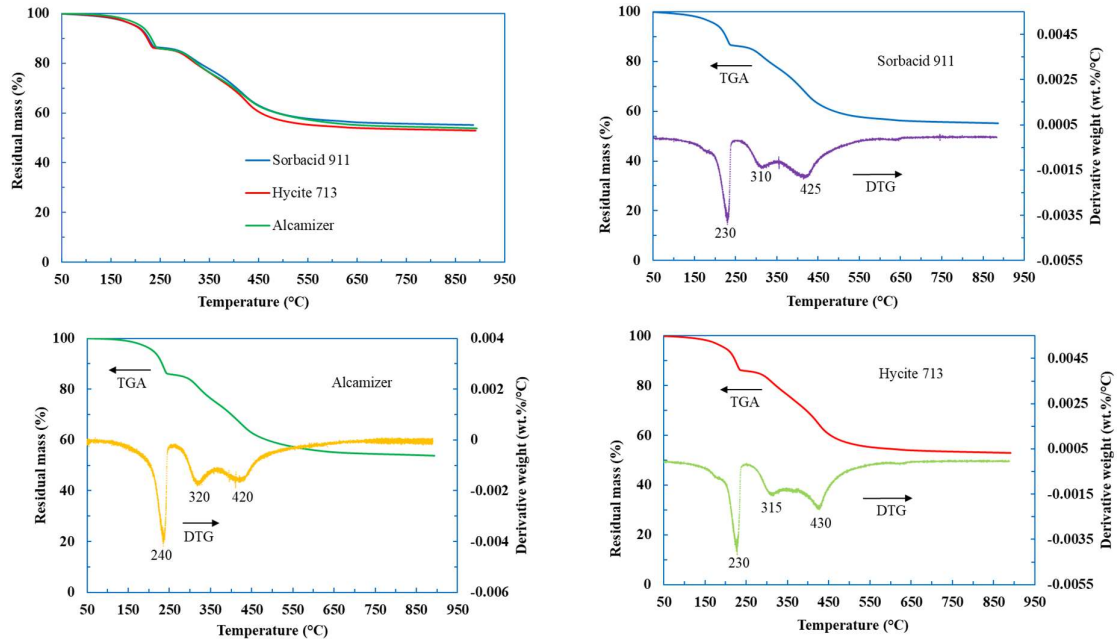
Figure C- 1: Thermal analysis for Sorbacid 911, Hycite 713 and Alcamizer 1

Appendix D: Fourier transform infrared spectroscopy for Sorbacid 911, Alcamizer 1 and Hycite 713.
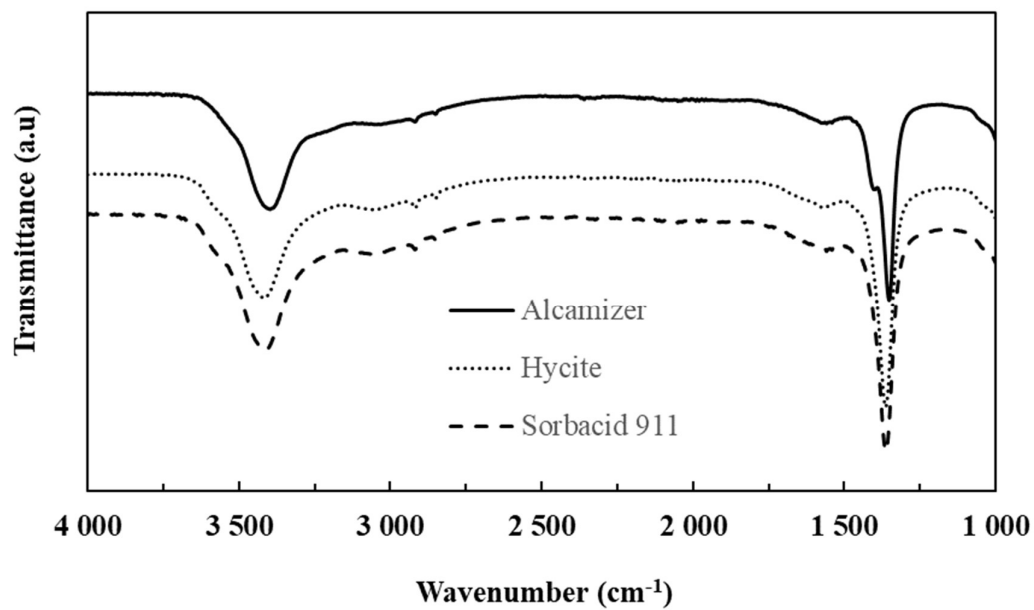
Figure D- 1:FTIR peaks for Alcamizer, Hycite and Sorbacid 911

Appendix E: Phenol adsorption efficiencies for calcined commercial clays
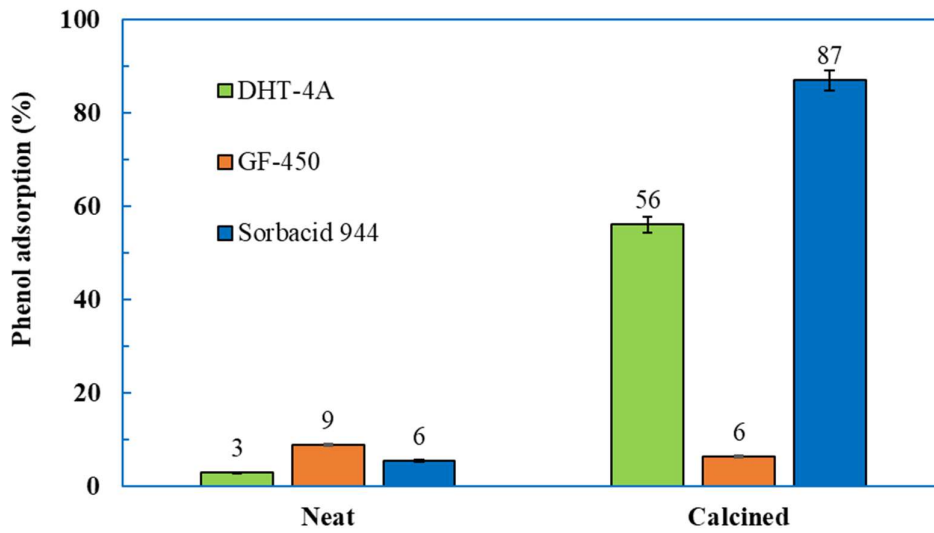
Figure E- 1: Phenol adsorption efficiencies on neat and calcined clays
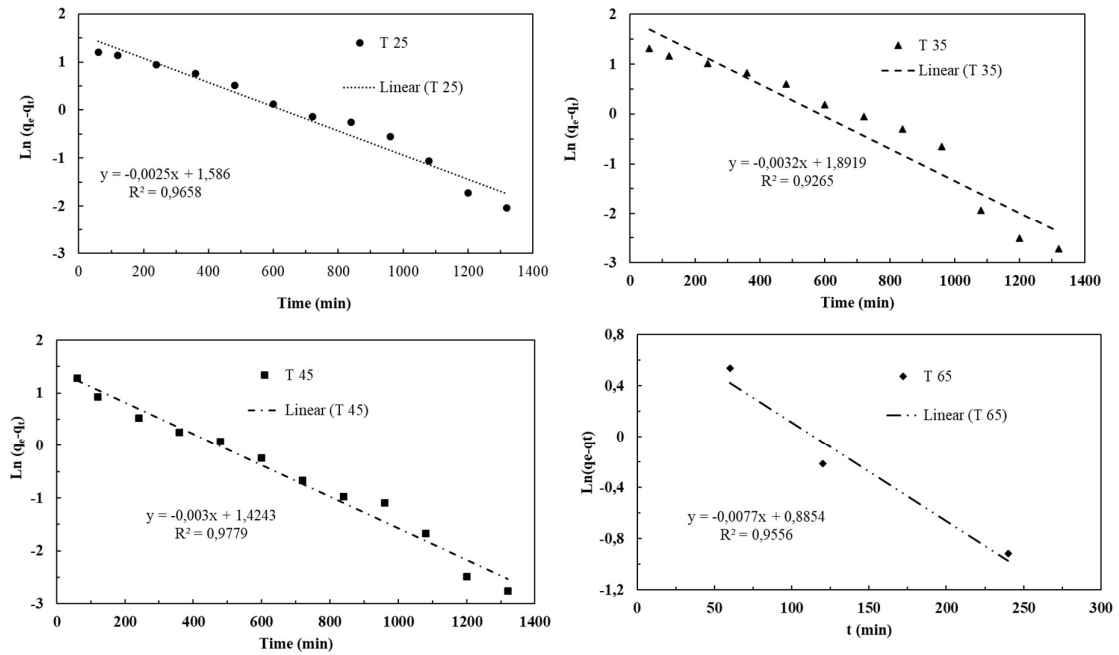
Figure E- 2: Pseudo-first order kinetics data
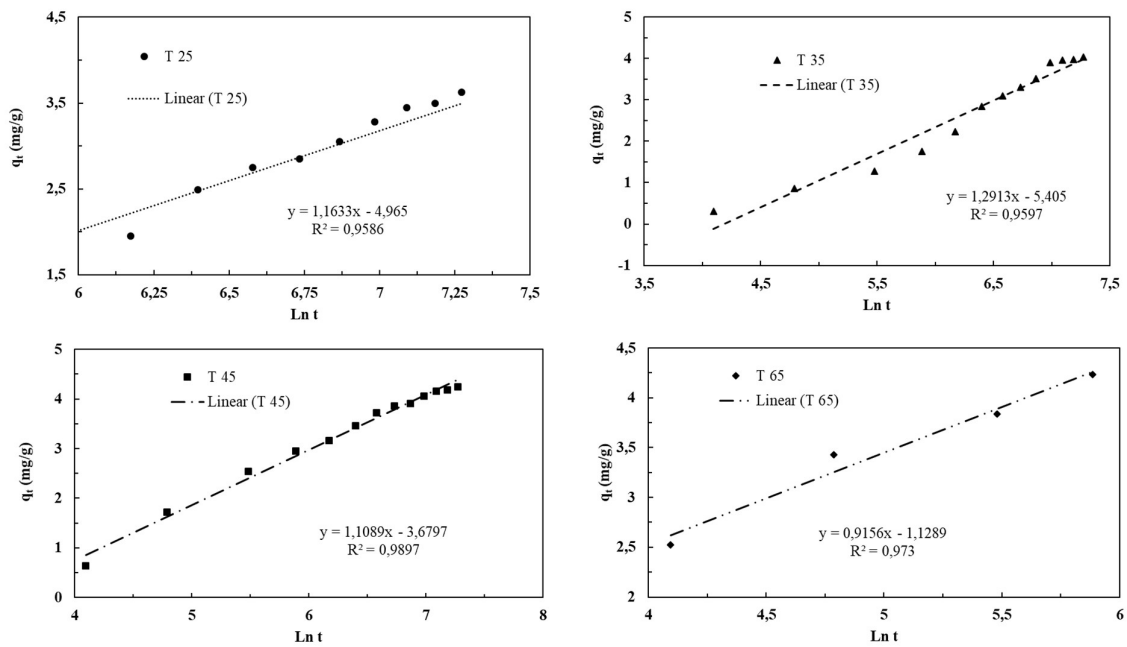
Figure E- 3: Elovich kinetics data
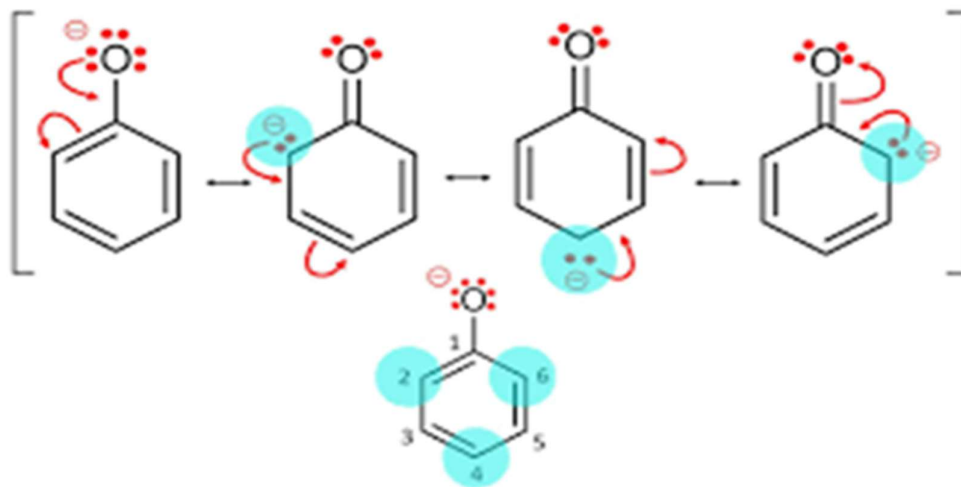
Figure E-4: Resonance structures of phenoxide ion
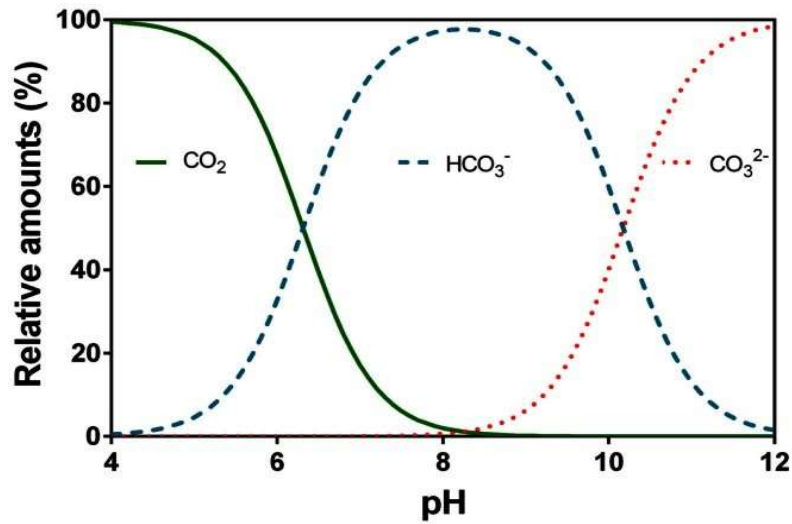
Figure E-5: Relative speciation (%) of carbon dioxide bicarbonate and carbonate in water as a function of pH (Pedersen *et al*., 2013)
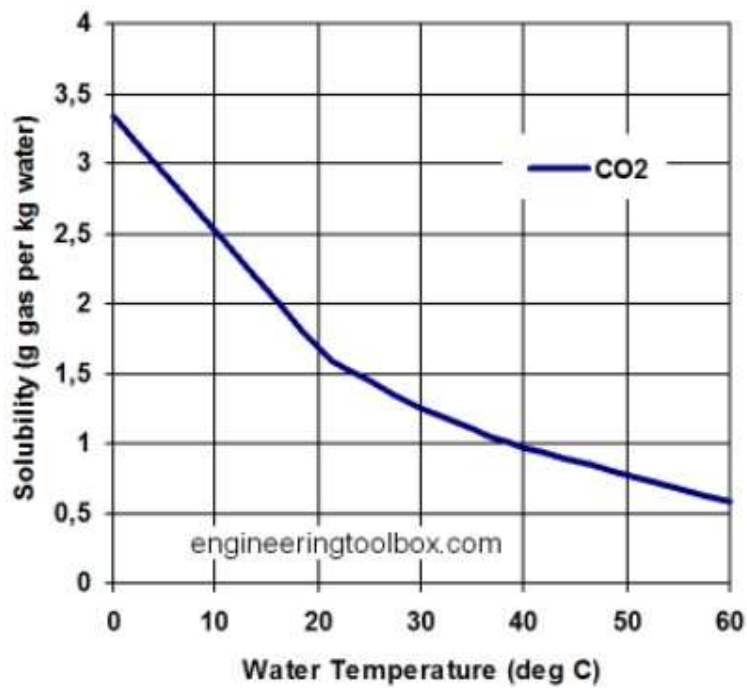
Figure E- 6: Carbon dioxide solubility against temperature (Glassman, 2009)

Appendix F: XRD patterns for synthesised clays
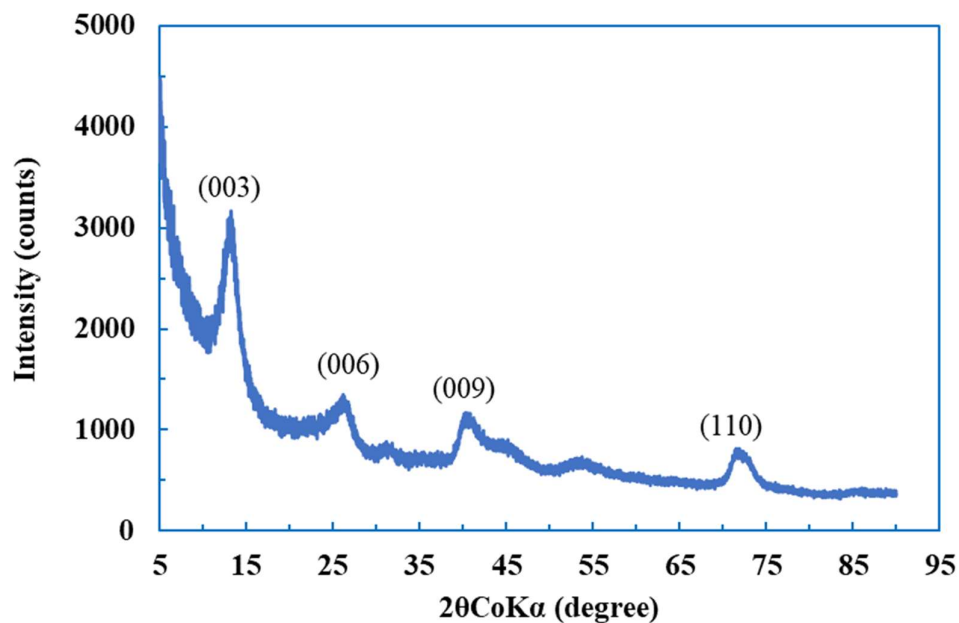
Figure F- 1: X-ray diffraction peaks for Mg$_{0.6}$Zn$_{0.2}$Al$_{0.2}$
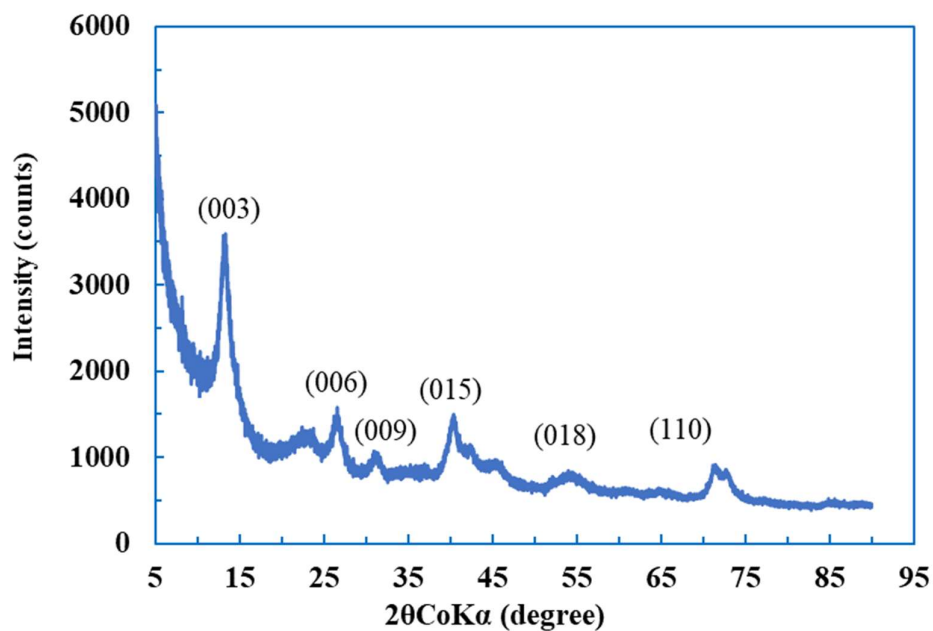
Figure F- 2: X-ray diffraction peaks for Mg$_{0.4}$Zn$_{0.4}$Al$_{0.2}$
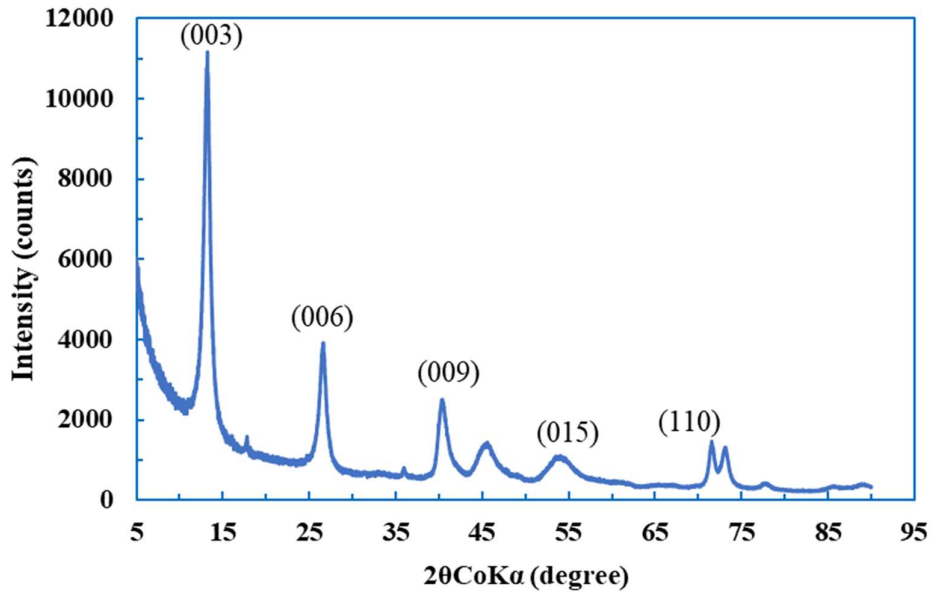
Figure F- 3: X-ray diffraction peaks for Mg$_{0.75}$Al$_{0.25}$
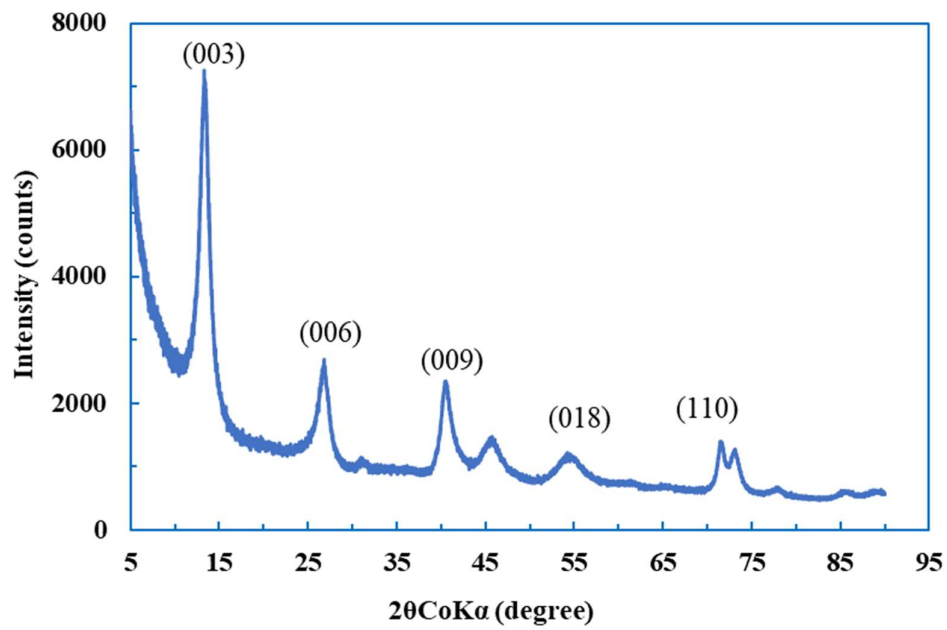
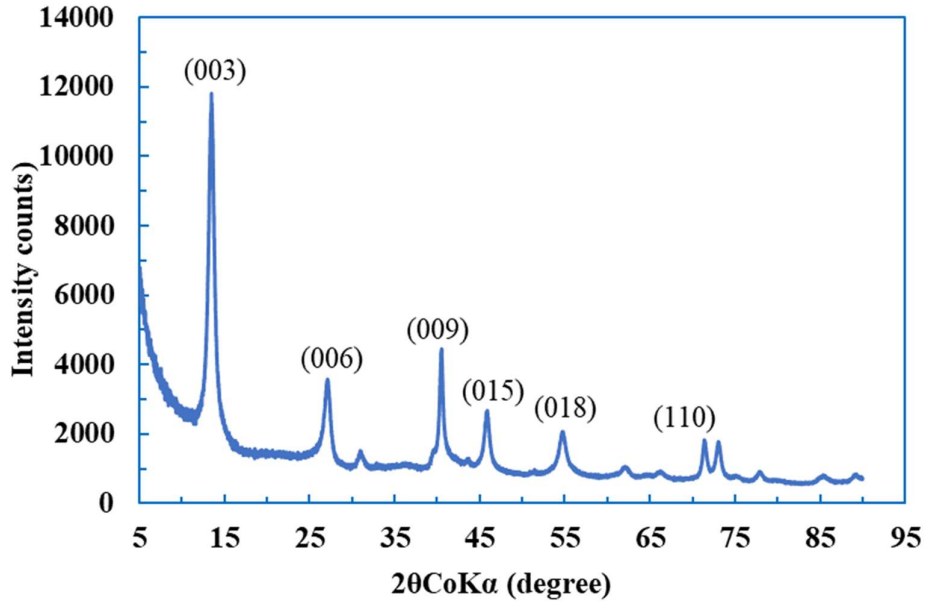*Figure F- 4: X-ray diffraction peaks for Mg$_{0.5}$Zn$_{0.25}$Al$_{0.25}$*

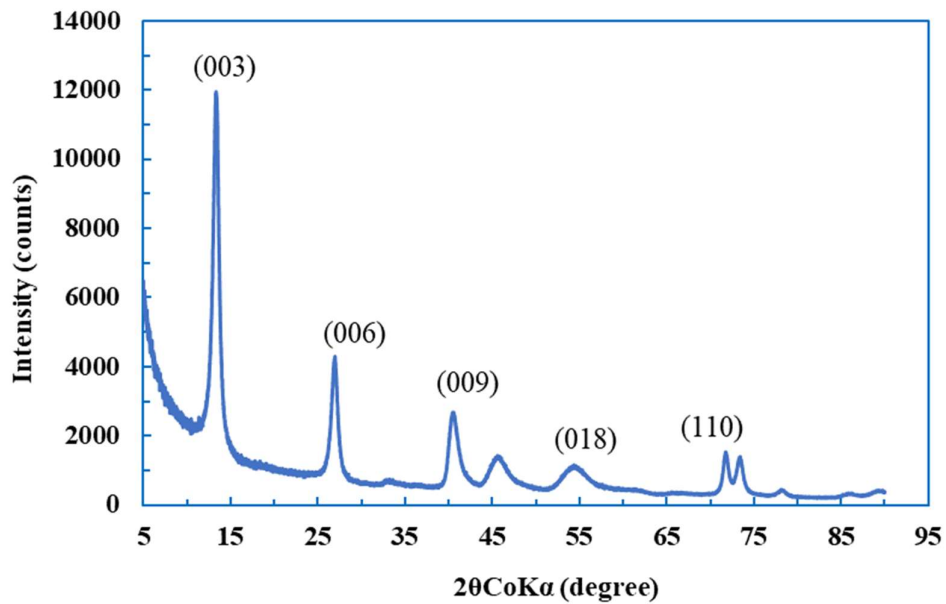*Figure F- 5: X-ray diffraction patterns for $Mg_{0.25}Zn_{0.5}Al_{0.25}$*

Figure F- 6: X-ray diffraction patterns for $Mg_{0.67}Al_{0.33}$

Appendix G: Thermal stability of synthesised clays
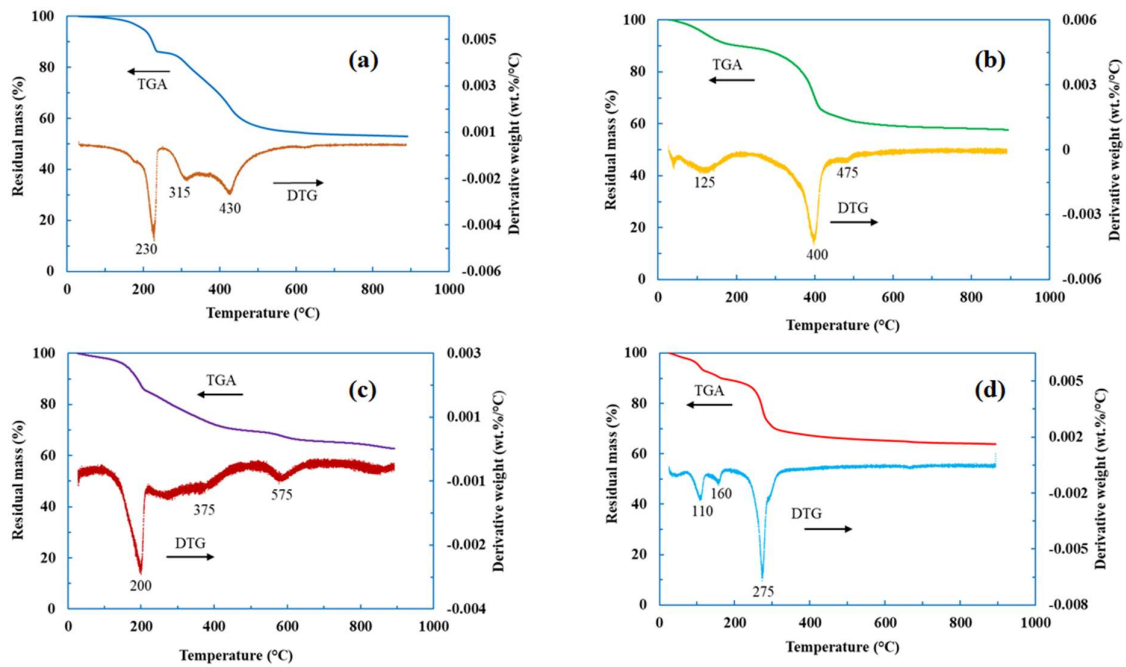

Figure G-1: Thermal analysis on synthesized clay (a) $Mg_{0.4}Zn_{0.4}Al_{0.2}$ (b) $Mg_{0.6}Zn_{0.2}Al_{0.2}$ (c) clay $Mg_{0.75}Al_{0.25}$ and (d) $Zn_{0.75}Al_{0.25}$

133

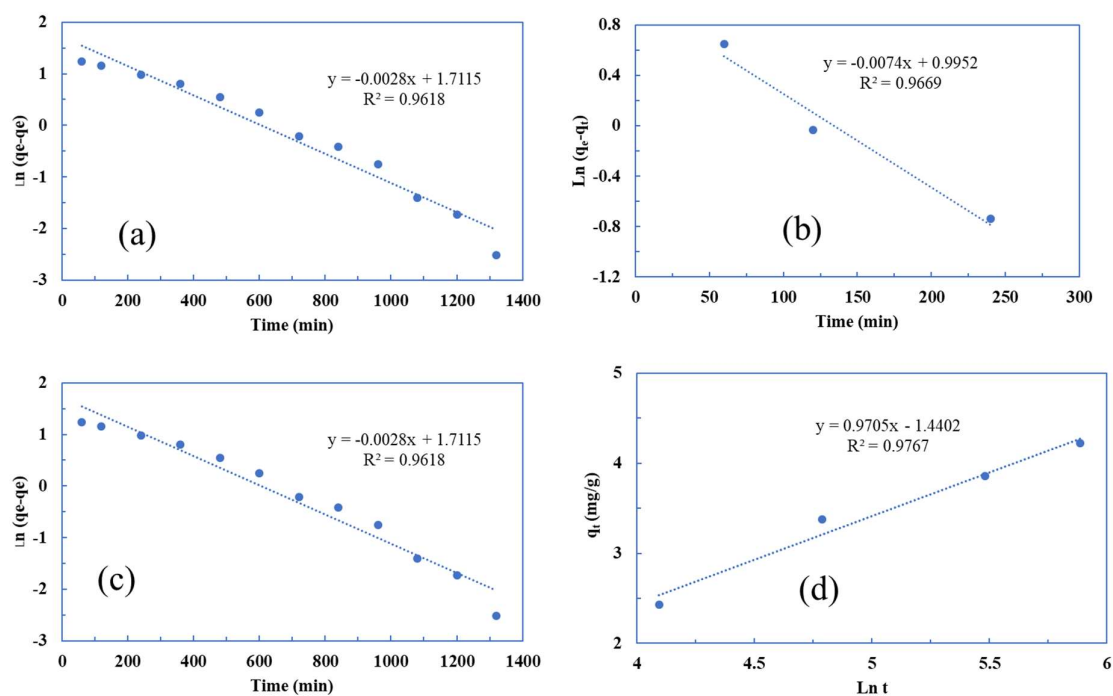**Appendix H: Phenol adsorption kinetics on clay Mg$_{0.6}$Zn$_{0.2}$Al$_0$.**

Figure H: Phenol adsorption kinetics on clay Mg$_{0.6}$Zn$_{0.2}$Al$_{0.2}$, (a) Pseudo-first order at 24 °C, (b) Pseudo-first order at 65 °C, (c) Elovich kinetics model at 25 °C and (d) Elovich kinetics model at 65 °C